# 論文 / 著書情報
# Article / Book Information

| | |
|---|---|
| 題目(和文) | |
| Title(English) | Revealing Decadal Glacial Changes and Lake Evolution in the Cordillera Real, Bolivia, based on Satellite Data Analysis |
| 著者(和文) | HUANGYilin |
| Author(English) | Yilin Huang |
| 出典(和文) | 学位:博士(工学),<br>学位授与機関:東京工業大学,<br>報告番号:甲第12888号,<br>授与年月日:2024年9月20日,<br>学位の種別:課程博士,<br>審査員:木内 豪,髙木 泰士,中村 恭志,中村 隆志,VARQUEZ ALVIN CHRIST |
| Citation(English) | Degree:Doctor (Engineering),<br>Conferring organization: Tokyo Institute of Technology,<br>Report number:甲第12888号,<br>Conferred date:2024/9/20,<br>Degree Type:Course doctor,<br>Examiner:,,,, |
| 学位種別(和文) | 博士論文 |
| Type(English) | Doctoral Thesis |

# Revealing Decadal Glacial Changes and Lake Evolution in the Cordillera Real, Bolivia, based on Satellite Data Analysis

by

HUANG Yilin

A thesis submitted in partial fulfillment of the requirements for the
degree of Doctor of Engineering in
Global Engineering for Development, Environment and Society (GEDES)

Examination Committee: Prof. Tsuyoshi Kinouchi (Chairperson)
Prof. Hiroshi Takagi
Assoc. Prof. Takashi Nakamura (Suzukakedai)
Assoc. Prof. Takashi Nakamura (Ookayama)
Assoc. Prof. Alvin C.G. Varquez

Tokyo Institute of Technology
School of Environment and Society

Japan
September 2024

This page is intentionally left blank.

# Acknowledgments

I would like to express my deepest and most sincere gratitude to my research supervisor for both my master's and PhD programs, Prof. Kinouchi Tsuyoshi. His continuous encouragement and invaluable guidance have been instrumental in my exploration of and dedication to this topic. Without his patient and kind mentorship, neither my first paper nor this dissertation would have been possible.

My heartfelt thanks go to my committee members: Prof. Hiroshi Takagi, Assoc. Prof. Takashi Nakamura (Suzukakedai), Assoc. Prof. Takashi Nakamura (Ookayama), and Assoc. Prof. Alvin C.G. Varquez. Their insightful feedback and valuable opinions have significantly enhanced this dissertation.

I am profoundly grateful to the Tokyo Tech Academy for Leadership (ToTAL) program and the Cross the border! Tokyo-Tech pioneering doctoral research project not only for their financial support but also for their thoughtful career guidance. The communication platform they provided allowed me to forge meaningful friendships and gain exposure to research in diverse fields.

Words cannot express my immense gratitude to my parents for their unconditional love, unwavering understanding, and countless sacrifices. Their support throughout my PhD journey has been a constant source of strength and inspiration.

I would like to express my heartfelt thanks to my dearest friend Tokine and the world’s cutest Gogogo, who have kept me company during the drafting of both of my papers. My deepest gratitude also goes to my long-time bestie Lin Sihan, who has encouraged me to persist in my PhD journey by setting a role model through her continued medical school studies. I wish the world’s luckiest Shrimp Dumpling a life filled with health and safety. The 7kg little Russian kitten Yuzai has provided me with immense mental support, and I would like to extend my thanks to his owner, Gezi, for consistently sharing photos and videos every day. Though I live alone now, I would like to extend my sincere thanks to my two-year roommates, Wanuji and Vicheka. I will always cherish the memories of the time we spent together.

My gratitude also goes to my lab mates who have been with me throughout my long journey in this lab. A special thanks to Zhao Yakun, who has been by my side for

almost my entire time in Japan, and to my senior Lv Yanping, who was my student mentor and warmly welcomed me when I first arrived Japan. I would also like to thank Zhou Chuanqiao and Sun Qunyan for their invaluable help with my papers, I will always remember the time we spent together in the library. Special thanks to Tonoyama san, who spent the same length of years in the lab with me and was always so helpful with all the technical daily issues. Thanks to Davin, the only person in the lab using GEE and coding, with whom I could discuss programming issues. And thanks to Hira, who always patiently listened to my immature explanations of my study. I wish you all the best with your PhD journey. Thanks to my master fellows, Tadahira, Matsumoto and Sakaki, I forgot to include an acknowledgment in my master's thesis, so thank you for taking care of me when I didn’t know Japanese. And thanks to my PhD fellows, Abhishek and Raksmey, who graduated earlier than me—I appreciate being able to use your graduate materials as references. Thanks to Tsai Yizhen and her boyfriend Zhang Tingwei, who will graduate together with me—your mental support throughout the graduation process has been so important to me. Last but not least, I would like to thank my boyfriend, Li Minhui, without whom I could not have survived the PhD journey.

Finally, I extend my sincere appreciation to all those who have supported me, directly or indirectly, in completing this research work. Your contributions, however small they may have seemed, have been integral to my success.

# Abstract

Glaciers serve as invaluable natural freshwater reservoirs for downstream regions worldwide, with glacial meltwater playing a significant role in various functions, including domestic use, agriculture, hydropower generation, and environmental health. As global warming persists and precipitation patterns become more variable, the accelerated melting and retreat of glaciers, dramatically reshape the hydrological systems and ecological landscapes. This is of particular importance for tropical glaciers, especially in the tropical Andes where more than 99% of tropical glaciers are located, due to the vulnerability of glaciers to climate change and the significant cumulative specific mass reductions they have experienced since the 1960s, with even more pronounced retreat observed in small glaciers at lower elevations. This further leads to the emergence of new lakes and wetlands, profoundly affecting water availability, ecosystems, and the susceptibility to disasters in the region.

While numerous studies related to tropical glaciers primarily focus on the glacier dynamics, glacial runoff, and the risk of glacial lake outburst floods (GLOF), there remains a substantial deficiency in the comprehensive understanding of lake evolution in this region. Moreover, the analysis of spatiotemporal changes in the multitude of glacial lakes and their potential implications for water resources is notably lacking, although obtaining continuous lake dynamics records would help explore the relationship between key hydrological factors, including precipitation and supply of meltwater from glaciers, and lake evolution patterns.

Yet, current methodologies in glacier mapping still encounter challenges, including incorrectly mapping seasonal snow and misclassifying cloud cover and shadows cast by the steep terrain as glaciers. Similar defects exist in the mapping of glacial lakes, where these methods confront issues such as misclassifying shadows as lakes and being unable to capture spatial information such as pixel proximity and the geometric characteristics of classes, which is crucial for effective water classification. This highlights the critical need for a precise and rapid method to effectively capture changes in glaciers and lakes and their interactions. Such an approach is essential to conduct comprehensive research

aimed at understanding the dynamic nature of these water bodies and the intricate interplay of critical climate change factors impacting them.

This study presents a semi-automated methodology developed on the cloud platforms Google Earth Engine and Google Colab to effectively detect dynamic changes in the glaciers as well as glacial and non-glacial lakes of the Cordillera Real, Bolivia, using over 200 Landsat images from 1984 to 2021. Through the calculation of streams and catchments, we establish hydrological connections between glaciers and lakes, enabling an analysis of the correlation between glacier-fed lakes and their source glaciers while considering the influence of multiple climate factors, including temperature, precipitation, and evaporation.

The study updated the glacier area data in the Cordillera Real and clarified the trend in glacier melting with a uniform five-year interval. Over the study period, glaciers reduced their total area by 42%, a significant portion of glaciers shrank before 2010, especially those situated below 5400 m.a.s.l. However, as the distribution of glaciers is more concentrated at high elevations, and thus more resilient to the rising temperature of recent years, the rate of glacier recession has slowed down in recent years.

Similarly, after a consistent increase since 1985, the area of natural glacier-fed lakes stabilized after 2010. A strong correlation between glacier area and the extent of natural glacier-fed lakes highlights the significant downstream impact of glacier recession on water bodies. Even though the overall area of lakes shows a continuous increase over the years, the increase almost entirely comes from the contribution of human-affected lakes, aligning with the recent stabilization observed in the area of natural glacier-fed lakes. Despite these overall trends, many smaller lakes, especially non-glacier-fed ones, decreased in size, attributed to seasonal and inter-annual variations in lake inflow caused by climate variability.

Catchment level analysis shows that lakes in close proximity to glaciers exhibit a higher correlation with glacier retreat, indicating a direct impact of glacier melt on these water bodies. In contrast, lakes farther from glaciers were more influenced by non-glacial factors. The spatiotemporal analysis revealed significant warming, especially at higher elevations, and contrasting evaporation rates, with higher rates on the eastern

side. Although overall precipitation increased, it was insufficient to sustain downstream lakes due to the combined effects of temperature rise and enhanced evaporation. The accelerated melting of glaciers, coupled with changes in precipitation patterns, threatens the stability of water supplies in the region.

This study reveals the response of glaciers and lakes to climate variations, including the contribution of human-constructed water reservoirs, providing valuable insights into crucial aspects of future water resources in the Cordillera Real. This enhances our understanding of the impact of climate change on glaciers and lakes within the Cordillera Real region and its potential implications for downstream water resources and future water management strategies. The findings in this study suggest the potential decline of natural lakes amid ongoing climate changes, prompting alterations in natural landscapes and local water resources. Our research underscores the urgent need for comprehensive monitoring and sustainable water management strategies to mitigate the adverse effects of climate change on glacial and hydrological systems in the Andean region.

# Table of Contents

# List of Tables

# List of Figures

# List of Abbreviations

| | |
|---|---|
| GEE | Google Earth Engine |
| CFMask | the C Function of Mask algorithm |
| CHIRPS | Climate Hazards group Infrared Precipitation with Stations |
| CRS | coordinate reference system |
| CV | coefficient of variation |
| FLDAS | Famine Early Warning Systems Network Land Data Assimilation System |
| GLIMS | Global Land Ice Measurements From Space |
| ICESat | laser altimetry satellites |
| IQR | Interquartile Range |
| JRC | JRC Global Surface Water Mapping |
| MAE | mean absolute error |
| NDSI | Normalized Difference Snow Index |
| NDWI | Normalized Difference Water Index |
| NSE | Nash–Sutcliffe efficiency |
| OSM | OpenStreetMap |
| PBIAS | percent bias |
| QA band | quality assessment band |
| RMSE | root mean square error |
| ROI | region of interest |
| RSR | RMSE-observations standard deviation ratio |
| SNIC | simple non-iterative clustering segmentation |
| SRTM DEM | Shuttle Radar Topography Mission digital elevation data |
| TOA | top-of-atmosphere |
| WBD | water body data |

# Chapter 1 Introduction

This chapter explains the importance of this research by introducing the background, motivations, and detailed objectives. It then describes the overall framework which aims to fulfill the above-mentioned objectives and provides an outline of the thesis.

## 1.1. Background and research motivation

Glaciers serve as invaluable natural freshwater reservoirs for downstream regions worldwide, with glacial meltwater playing a significant role in various functions, including domestic use, agriculture, hydropower generation, and environmental health (Immerzeel et al., 2010; Vergara et al., 2007). As global warming persists and precipitation patterns become more variable, the accelerated melting and retreat of glaciers, dramatically reshape the hydrological systems and ecological landscapes. This is of particular importance for tropical glaciers, especially in the tropical Andes where more than 99% of tropical glaciers are located (Kaser, 1999), due to the vulnerability of glaciers to climate change and the significant cumulative specific mass reductions they have experienced since the 1960s (Bradley et al., 2006; Zemp et al., 2019), with even more pronounced retreat observed in small glaciers at lower elevations (Rabatel et al., 2013). This further leads to the emergence of new lakes and wetlands, profoundly affecting water availability, ecosystems, and the susceptibility to disasters in the region.

While numerous studies related to tropical glaciers primarily focus on the glacier dynamics, glacial runoff, and the risk of glacial lake outburst floods (GLOF) (Carey, 2005; Cook et al., 2016; Dussaillant et al., 2019; Kinouchi et al., 2019; Kougkoulos, 2019; Liu et al., 2013; Rabatel et al., 2013; Seehaus et al., 2020; Sicart et al., 2011; Soruco et al., 2009; Veettil et al., 2018; Veettil and Kamp, 2021; Vuille et al., 2018), there remains a substantial deficiency in the comprehensive understanding of lake evolution in this region (Drenkhan et al., 2018). Moreover, the analysis of spatiotemporal changes in the multitude of glacial lakes and their potential implications for water resources is notably lacking, although obtaining continuous lake dynamics records would help explore the relationship between key hydrological factors, including

precipitation and supply of meltwater from glaciers, and lake evolution patterns (Song and Sheng, 2016). This highlights the critical need for a precise and rapid method to effectively capture changes in glaciers and lakes and their interactions. Such an approach is essential to conduct comprehensive research aimed at understanding the dynamic nature of these water bodies and the intricate interplay of critical climate change factors impacting them.

## 1.2. Study region

The Cordillera Real is a glacierized mountain range located in Northwest Bolivia, South America. This mountain range separates the cold arid Altiplano Plateau from the wet warm Amazon Basin. The runoff from glacierized basins, flowing into large lakes like Lake Tuni and Lake Milluni, significantly contributes to the drinking water systems that cater to the needs of La Paz and El Alto, two major cities in Bolivia (Kinouchi et al., 2019). Under the influence of high solar radiation and low glacier albedo, meltwater discharge reaches its peak annual values in November–December (Sicart et al., 2011).

Consistent with the previous study (Jordan, 1991), smaller glacierized areas to the further south, Mururata, and Illimani are included in this study. As lakes supplied by glacier meltwaters can have a certain distance from the glacier margins (Yao et al., 2018), this study considered the region above 4300 m.a.s.l. to encompass the major lakes in the study region, including Lake Tuni and Lake Milluni. The region that was investigated in this study is shown in Figure 1.1.

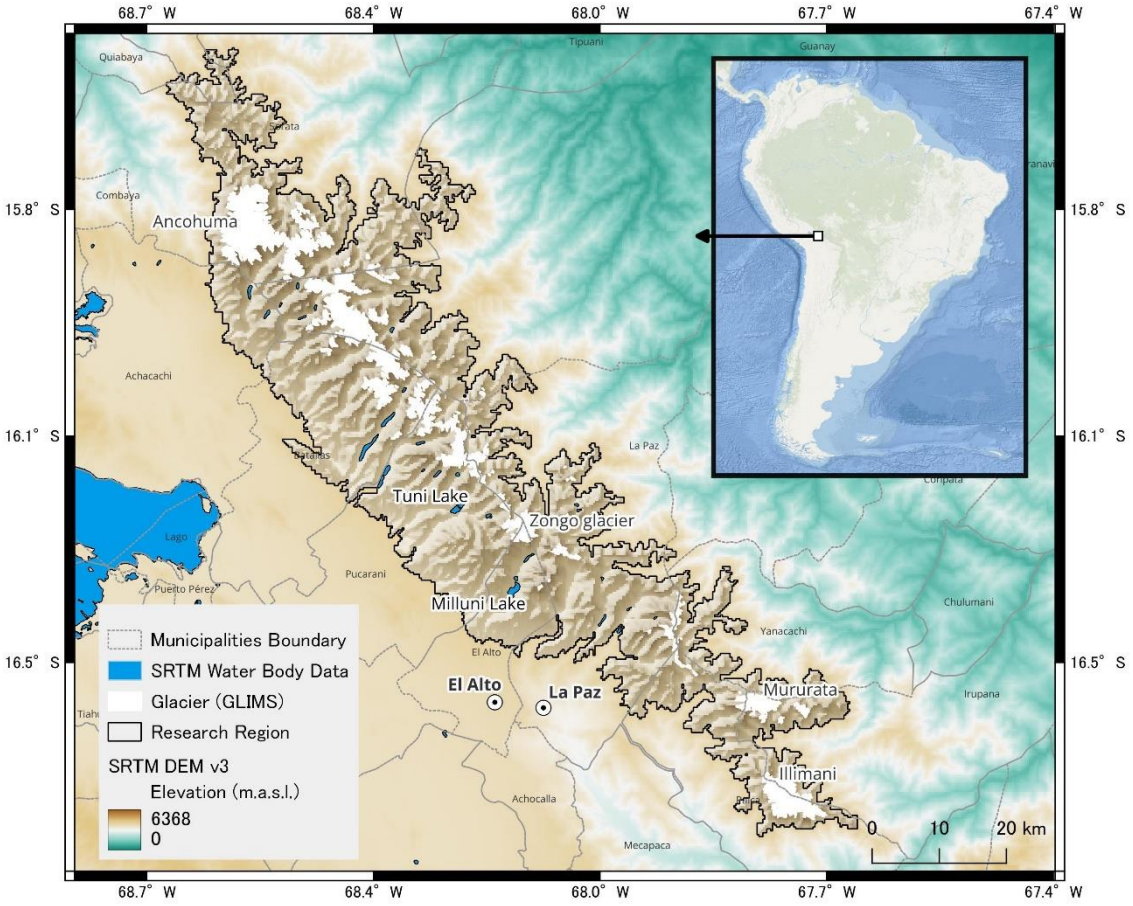


**Figure 1.1** Study region.

## 1.3. Research objectives

This study primarily focuses on unveiling the spatiotemporal changes in glaciers and lakes, encompassing approximately four decades from 1984 to 2021 within the tropical Andes and specifically focusing on the Cordillera Real region of Bolivia. In addition to comprehending the dynamic nature and interconnectedness of glaciers and glacial lakes, our investigation aims to explore the influence of critical climate change factors, including temperature, precipitation and evaporation, in conjunction with human activities, on the observed transformations in these water bodies. Through this comprehensive analysis, our goal is to bridge the gap in understanding the changes of lakes in the tropical Andes and elucidate the implications of these evolutions on the region's water resources and environment for the future.

## 1.4. Research framework

The research framework is designed to achieve the research objectives through a comprehensive methodological approach.

The process begins with data preparation, which involves filtering cloud-free satellite images and pre-processing supporting datasets. This includes reprojecting all datasets to a common coordinate reference system (CRS) and standardizing the temporal resolution of time series datasets.

For glacier mapping, the methodology is developed based on a thorough literature review, selecting appropriate indexes for automated glacier pixel identification. Temporal composition is applied to mitigate seasonal variations and snow cover issues, which were noted in previous mapping efforts. Glacier area changes are then analyzed over uniform five-year periods and across different altitude classes.

Lake mapping follows a similar initial approach, applying satellite image filtering techniques with more relaxed cloud cover requirements. After reviewing existing datasets and mapping methodologies, an object-based algorithm is chosen over pixel-based identification methods to better capture temporal and seasonal variations in lake area. The lake mapping process is divided into three steps: locating lake objects within the study region, capturing area changes for each object over the study period, and summarizing regional water surface changes. To investigate the effects of glaciers and human activity, lakes are further classified using information gathered from open datasets, literature reviews, and calculations based on regional stream maps.

To understand climate influences, in the absence of comprehensive observed data, reanalysis data is used to acquire temperature, precipitation, and evaporation information. The selection of reliable data is based on comparisons with on-site observations. Climate data is then compared against the observed glacier and lake area changes. The relationship between glacial lakes and their source glaciers is assessed through the delineation of lake catchments. Additionally, information on human construction of water reservoirs is collected from various sources and confirmed against observed lake area changes to evaluate potential impacts on water resources.

Scripts used in this study to achieve the objectives of (1) cloud cover rate filtering, (2) glacier mapping, (3) image composition, and (4) lake mapping are available at

https://github.com/Elain26/CordilleraReal_Glacial_Changes_Lake_Evolution (access requires permission from the author). The data that support the findings of this study are available from the author upon request.

## 1.5. Outline

There are a total of 5 chapters in this thesis. Each chapter is briefly described below. Chapter 2 to 4 present the main research findings of this study.

Chapter 1 establishes the foundation of this research by presenting its significance, background, and motivations, along with a concise overview of the study region. It then outlines the detailed objectives and introduces the research framework, delineating the technical approach for achieving these goals. The chapter concludes with a comprehensive outline of the thesis structure, providing readers with a clear roadmap of the study.

Chapter 2 begins with a literature review of previous research on glacier changes in the study region and commonly used glacier mapping methodologies. It then introduces the mapping technique developed in this study and presents the results of glacier area changes observed during the study period.

Chapter 3 start with brief introduction on available water surface datasets and a literature review on lake mapping methodologies. It then describes the mapping technique developed in this study and reports the lake inventory and lake area changes observed during the study period.

Chapter 4 focuses on the climate factors influencing glaciers and lakes and their potential impact on water resources. It begins with the selection of climate datasets on temperature and precipitation, then describes the impact of these factors on glaciers and glacial lakes. It also explores the connection between glacier melting and lake area changes under the changing climate, and finally, discusses the potential influence on water resources.

Chapter 5 gives the conclusions of this research, together with its limitations and future perspectives.

# Chapter 2 Decadal changes in glacier coverage in the Cordillera Real

Chapter 2 starts with a literature review of previous research on glacier changes in the study region and commonly used methodologies in glacier mapping. It then introduces the mapping technique developed in this study and analyzes the glacier area changes observed during the study period.

## 2.1. Literature review on glacier changes and methodology

Tropical glaciers have been experiencing rapid shrinkage throughout the past decade. Table 2.1 has summarized previous studies that related to the glaciers mass and area changes in the Cordillera Real. Studies confirm that the glacier retreat follows a non-uniform trend over time (Soruco et al., 2009), strongly linked to rising air temperature (Soruco et al., 2009). Under the influence of global warming, it is predicted that glacier recession in the tropical Andes will persist (Vuille et al., 2008), possibly leading to complete disappearance in mid-2050s under the RCP8.5 scenario (Yarleque et al., 2018). However, research suggests that unlike glaciers in the inner tropics, which are notably susceptible to impending warming, glaciers in the drier outer tropics may exhibit greater resilience (Vuille et al., 2018).

Due to the difficulty in reaching high-altitude regions (Veettil and Kamp, 2021) and the low availability and high cost of field measurement, satellite images are more frequently used for the analysis of glaciers and observing their long-term variations in the Andes (Liu et al., 2013). The traditional methods for mapping glaciers in mountainous regions involve using the band ratio method (Paul et al., 2002) and Normalized Difference Snow Index (NDSI) (Hall et al., 2002) images with manually selected thresholds.

In the Cordillera Real, except for the very early study by Jorden (1991) which used geodetic methods on aerial photographs, all other studies employed optical satellite images with manually selected thresholds. Liu et al. (2013) applied the band ratio between the near-infrared band and shortwave infrared band, while Cook et al. (2016)

and Kougkoulos (2019) used the band ratio between the red band and shortwave infrared band. Vettile et al. (2018) employed the NDSI method. Seehaus et al. (2020) combined the band ratio method and NDSI method.

Yet, current methodologies in glacier mapping still encounter challenges, including incorrectly mapping seasonal snow and misclassifying cloud cover and shadows cast by the steep terrain as glaciers (Paul and Rastner, 2023).

Table 2.1 Previous studies related to glacier mass and area changes in the Cordillera Real

| **Reference** | **Stuey region** | **Observation related to Cordilleras Real** | **Period** | **Coverage (Years)** | **Type** | **Method** |
|---|---|---|---|---|---|---|
| Veettil et al. (2018) | South American Andes | Estimated glacial area reduction between 1975 and 2016 in Cordilleras Real 50.7% | 1975-2016 | 41 | Area | NDSI |
| Dussaillant et al. (2019) | Outer tropics | Larger glaciers in Bolivia presented negative mass balance rates of $-0.42 \pm 0.23$ m w.e.yr$^{-1}$ | 2001-2017 | 16 | Mass | |
| Liu et al. (2013) | Cordillera Real | More than 30% of glacier area loss between 1987 and 2010 | 1987-2010 | 23 | Area | Band ratio (TM4 / TM5) |
| Cook et al. (2016) | Cordillera Real | 41.9 % across the Cordillera Real (315.2±31.5 to 183.1±18.3 km$^2$), Rates of ice loss appear to vary across the study period, with an initially rapid shrinkage between 1986 and1992 (14.5 km$^2$a$^{-1}$), relatively modest losses between 1992and 1999 (5.1 km$^2$a$^{-1}$), strong ice shrinkage between 1999and 2010 (8.1 km$^2$a$^{-1}$), and modest losses between 2010 and2014 (4.0 km$^2$a$^{-1}$) | 1986-2014 | 28 | Area | Band ratio (TM3 / TM5) |
| Kugkoulos (2019) | Cordillera Real | In the Cordillera Real, glaciers have shrunk by 7 % from 183.1 ± 18.3 km$^2$ to 170 ± 17 km$^2$. The east-facing Cordillera Real shrunk from 136 km$^2$ to 69 km$^2$, or 49 % shrinkage, which is around 5 % greater loss than the west-facing side (179 km$^2$ to 101 km$^2$, or 44 %). | 1986-2018 | 32 | Area | Band ratio (TM3 / TM5) |

(continued on next page)

Table 2.2 (continued)

| Reference | Stuey region | Observation related to Cordilleras Real | Period | Coverage (Years) | Type | Method |
|---|---|---|---|---|---|---|
| Seehaus et al. (2019) | Cordillera Real | In the Cordillera Real, the glacier area shrunk from 244 $km^2$ in 2000 to 175 $km^2$ in2016 (−28%) An increased area change rate of $-15 \pm 5\ km^2a^{-1}$ is revealed for 2013–2016 | 2000-2016 | 16 | Area | Combination of NDSI and Band Ratio |
| Soruco et al. (2009) | 21 glaciers in the Cordillera Real | Glaciers lost 43% of their volume between 1963 and 2006, essentially over the 1975–2006 period and 48% of their surface area between 1975 and 2006 | 1963-2006 | 43 | Mass | |
| Veettil et al. (2019) | Cerro Tilata | The loss of glacier coverage was high (more than 45% between 2002 and 2017), which is similar to the observed trends in the entire eastern mountain ranges of Peru and Bolivia | 2002-2017 | 15 | Area | NDSI |
| Francou et al. (2000) | Chacaltaya | From 1940 to 1983, the glacier has lost 62% of its mass, with the recession increasing dramatically during the past 2 decades. In 1998, Chacaltaya was reduced to 7% of the 1940s ice volume | 1940-1998 | 58 | Mass | |
| Morizawa et al. (2013) | Condoriri | The areal change between 1988 and 2010 of the Condoriri glacier in Bolivia and found that the area decreased by 41% | 1988-2010 | 22 | Area | NDSI |

## 2.2. Methodology of mapping glacier area changes

### 2.2.1. Preprocess of Landsat images

This study utilizing the cloud platforms Google Earth Engine (GEE) and Google Colab for precisely and rapidly captured the changes in glaciers and lakes.

The cloud-based geospatial processing platform offers several advantages. It provides easy access to extensive public data catalogs, including the Landsat series. Its fast performance is driven by Google's computational infrastructure, which is optimized for parallel processing of geospatial data. Additionally, the platform features a variety of built-in functions, enhancing its versatility and utility.

Landsat 5 and Landsat 8 Collection 2 Tier 1 calibrated top-of-atmosphere (TOA) reflectance data from 1984 to 2021 were accessed from the GEE platform (https://developers.google.com/earth-engine/datasets/catalog/landsat, accessed on 1 June 2022). The cloud cover rate in the study region was determined using the quality assessment band (QA band) in the Landsat images, calculated through the C Function of Mask (CFMask) algorithm (Foga et al., 2017). In the QA band, the bit 0 to 4 are used to identify cloud and cloud-effected pixels (Table 2.2). In this study, any pixel that has 1 among bits 0 to 4 is classified as a cloud pixel, then calculate cloud cover rate of the study region.

Table 2.3 QA Band bit description (Partial) (U.S. Geological Survey, 2020)

| Bit | Flag Description | Values |
|---|---|---|
| 0 | Fill | 0 for image data<br>1 for fill data |
| 1 | Dilated Cloud | 0 for cloud is not dilated or no cloud<br>1 for cloud dilation |
| 2 | Cirrus | 0 for Cirrus Confidence: no confidence level set or Low Confidence<br>1 for high confidence cirrus |
| 3 | Cloud | 0 for cloud confidence is not high<br>1 for high confidence cloud |
| 4 | Cloud Shadow | 0 for Cloud Shadow Confidence is not high<br>1 for high confidence cloud shadow |

To mitigate cloud interference, a cloud cover threshold of 15% is applied to assure a relatively clear scene for the mapping of glaciers in the whole study region. A total of 51 images (34 Landsat-5 images and 17 Landsat-8 images) (Figure 2.1 and Table A1) were filtered out. Covers 34 years, an average of 1.5 images per year with a time gap of no longer than 2 years. All available images were taken between April and October.

The Cordillera Real, located in the outer tropical Andes, experiences a dry season from May to September and a wet season from October to March, with significant snow accumulation occurring only during the wet season (Veettil et al., 2017). Consequently, snow/ice cover in the region typically peaks in April/May and gradually decreases until reaching a minimum in September/October, a trend also observed in our satellite images. The use of images from April to October, particularly those taken in August or later, can significantly reduce overestimation from temporary snow cover and minimize obstruction from rainy season clouds.

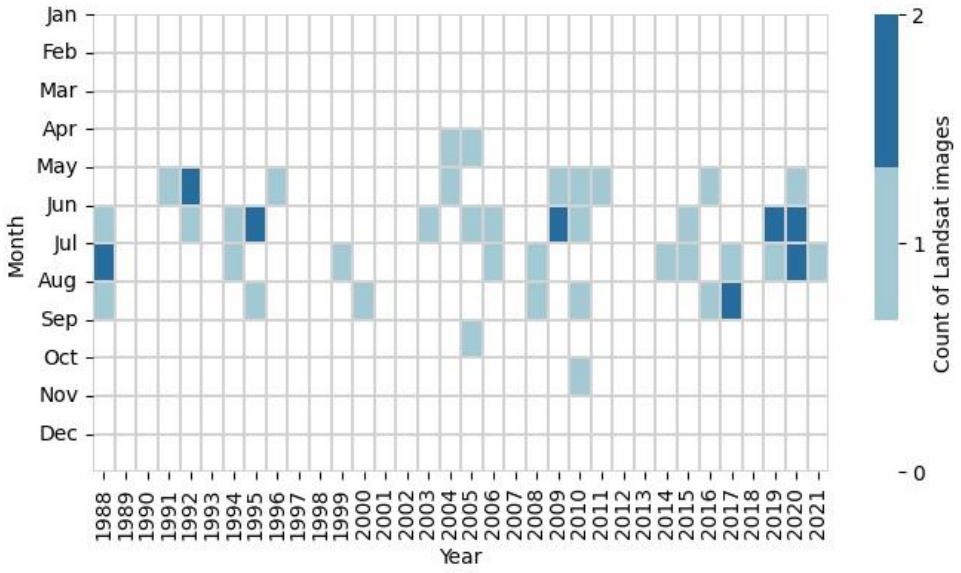


**Figure 2.1** Temporal distribution of Landsat images with cloud cover threshold less than 15%.

Additionally, this study utilized the following datasets for the glacier mapping as follows: (1) SRTM DEM obtained from the GEE platform (https://developers.google.com/earth-engine/datasets/catalog/USGS_SRTMGL1_003, accessed on 1 June 2022), employed for generating slope maps; (2) GLIMS data acquired from the GEE platform (https://developers.google.com/earth-

engine/datasets/catalog/GLIMS_current, accessed on 1 June 2022), used as a reference area to determine suitable thresholds for glacier mapping; Detailed information about the datasets used is summarized in Table 2.3.

For consistency with the Landsat images, SRTM DEM was then reprojected to EPSG:32619 with a scale of 30 m. This data defined an area above 4300 m a.s.l.as the study region.

### 2.2.2. Selection of DEM data

In this study, the SRTM DEM v3 was selected as the preferred digital elevation model (DEM) over other available free DEM data, including (1) the Terra Advanced Spaceborne Thermal Emission and Reflection Radiometer (ASTER) Global Digital Elevation Model (GDEM) Version 3 (ASTGTM) and (2) ALOS Global Digital Surface Model Version 3.2. All three DEMs have a relatively high spatial resolution of 1 arc-second (approximately 30 m). Their performance, particularly over large water surfaces, was evaluated against an RGB composite Landsat image of Lake Tuni, the largest lake in the study region (Figure 2.2).

In terms of absolute elevation values, there was little difference between the three datasets. However, when hillshades were calculated, noticeable differences emerged. The ALOS DEM did not perform well on the flat water surface of Lake Tuni, with inconsistent elevations across half of the lake. The ASTER DEM showed the water surface more clearly, but the boundary between the lake and land was not smooth. Liu et al. (2024) investigated the vertical accuracy of the SRTM DEM against 395,000 laser altimetry satellites (ICESat) footprints across 9,800 lakes, finding a mean absolute error (MAE) of 2.52 m for pixels with slope values <1°.

The average elevation of the four major lakes in the study region (Tuni, Incachaca, Milluni, and Ajuankhota) was calculated using SRTM DEM and compared with the observed water levels from February 2000, when the SRTM DEM was collected. For Lake Milluni, which lacked water level data for 2000, the February 2001 level was used. Although there was a difference of about 10 meters in absolute elevation values, the correlation between the observed water levels and SRTM DEM elevations was very high, with an $r^2$ of 0.9994 (Figure 2.3). Overall, the SRTM DEM provided the best performance and was thus selected as the DEM for this study.

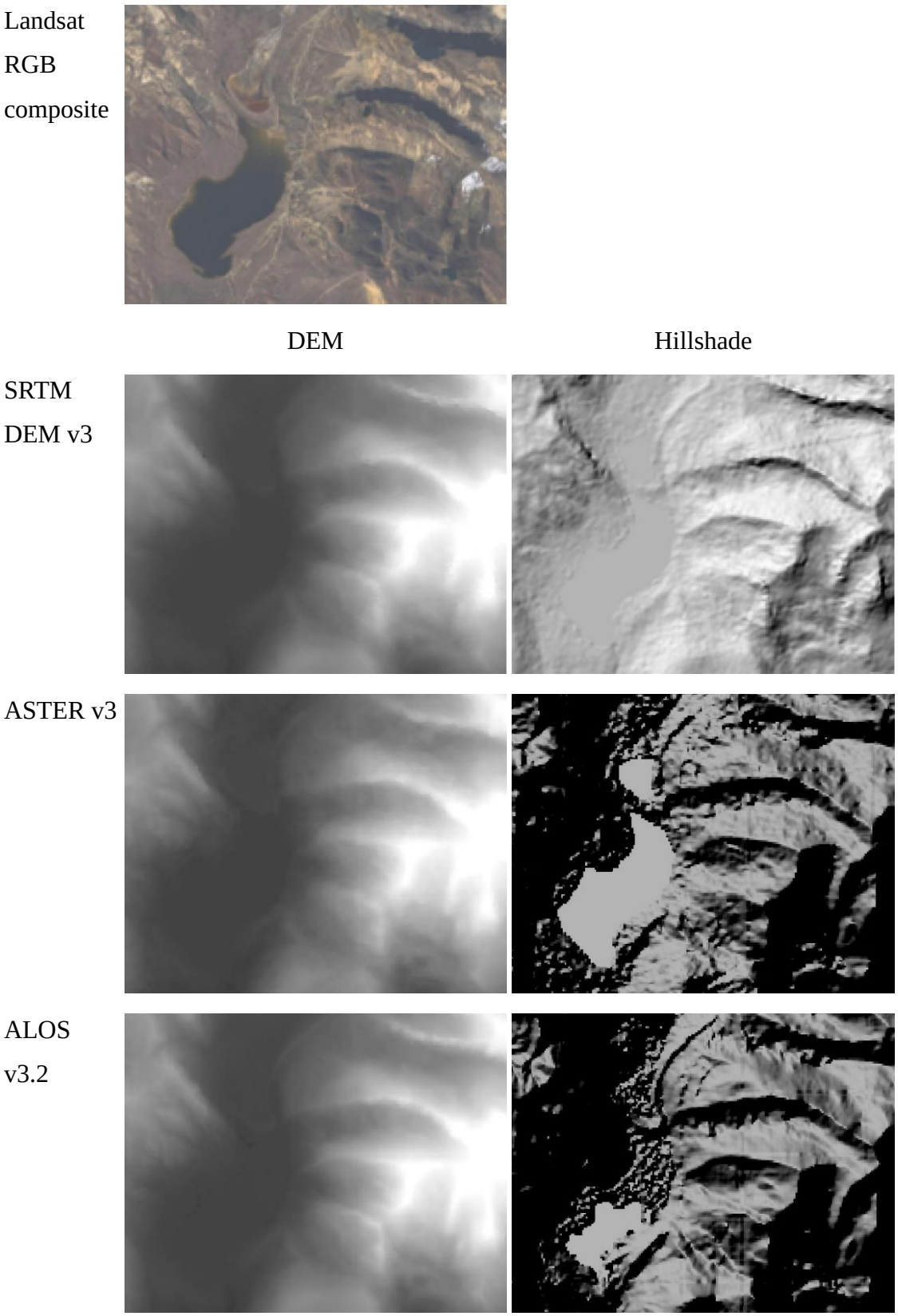


**Figure 2.2** Comparison of three DEM datasets (Display setting DEM: Min: 4300, Max: 5200; Hillshade: Min:0, Max:255)

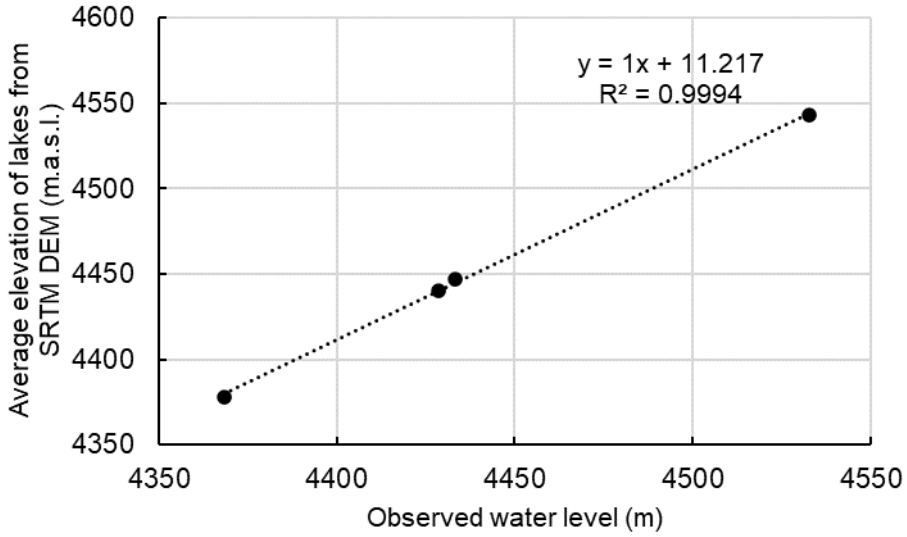


**Figure 2.3** Comparison between observed water level and average elevation from SRTM DEM in four lakes (Tuni, Incachaca, Milluni, and Ajuankhota)

Table 2.4 Detailed information on the datasets used in glacier mapping

| Full Name | Abbreviate | Temporal Domain | Temporal Resolution | Spatial Resolution | Institutional Sources | Reference | Data access |
|---|---|---|---|---|---|---|---|
| Landsat 5 TM Collection 2 Tier 1 TOA Reflectance | Landsat 5 | 1984-2011 | - | 30 m | USGS/Google | - | https://developers.google.com/earth-engine/datasets/catalog/LANDSAT_LT05_C02_T1_TOA |
| Landsat 8 Collection 2 Tier 1 TOA Reflectance | Landsat 8 | 2013-present | - | 30 m | USGS/Google | - | https://developers.google.com/earth-engine/datasets/catalog/LANDSAT_LC08_C02_T1_TOA |
| Shuttle Radar Topography Mission (SRTM) digital elevation data V3 product (SRTM Plus) | SRTM DEM | 2000 | - | 1 arc-second (approximately 30m) | NASA / USGS / JPL-Caltech | (Farr et al. 2007) | https://developers.google.com/earth-engine/datasets/catalog/USGS_SRTMGL1_003 |
| Global Land Ice Measurements From Space | GLIMS | 1999-2000 | - | - | National Snow and Ice Data Center (NSDIC) | (Raup et al. 2007) | https://developers.google.com/earth-engine/datasets/catalog/GLIMS_current |

### 2.2.3. Mapping glacier area

To begin, Landsat 5 and Landsat 8 images free from cloud interference were carefully filtered out and utilized in glacier mapping. The NDSI for each image was calculated using the following equation:

$$\mathrm{NDSI} = \frac{\mathrm{Green} - \mathrm{SWIR1}}{\mathrm{Green} + \mathrm{SWIR1}} \tag{2.1}$$

where the Green band and SWIR1 band correspond to Band 2 and Band 5, respectively, for Landsat 5, and the Green band and SWIR1 band correspond to Band 3 and Band 6, respectively, for Landsat 8.

Unlike previous glacier mapping studies in this region, which manually selected the NDSI threshold, our study, covering a longer time period and necessitating the processing of a substantial volume of Landsat images, employed the Otsu thresholding method (Otsu, 1979) within the sample region.

The Otsu method (Otsu, 1979) is a commonly used algorithm for image thresholding, which is the process of segmenting an image into regions based on the intensity of the pixels. The method maximizes the between-class variance and finds the threshold value that maximizes the separation between the foreground and background regions in the image. The area within 500 m of the glaciers recorded in the GLMIS dataset was selected as the sample region for calculating the proper NDSI threshold. Pixels within the sample regions should be separated into glacier and land class. The algorithm iteratively searches for the minimum within-class variance $\sigma^2(T)$, the corresponding threshold $T$ is the Otsu threshold.

$$\sigma^2(T) = \omega_G(T)\sigma_G^2(T) + \omega_L(T)\sigma_L^2(T) \tag{2.2}$$

where $\omega_G(T)$ and $\omega_L(T)$ is the probability of number of pixels for glacier and land at threshold $T$, calculated from equation (2.3) and (2.4); $\sigma_G^2(T)$ and $\sigma_L^2(T)$ is the variance of glacier and land at threshold $T$, calculated from equation (2.5) and (2.6).

$$\omega_G(T) = \frac{P_G(T)}{P_{all}} \tag{2.3}$$

$$\omega_L(T) = \frac{P_L(T)}{P_{all}} \tag{2.4}$$

where $P_{all}$ is the total pixel count of the whole sample regions, $P_G(T)$ and $P_L(T)$ is the count of glacier or land pixels at threshold T.

$$\sigma_G^2(T) = \frac{\sum(x_G - \bar{x}_G)^2}{P_G - 1} \tag{2.5}$$

$$\sigma_L^2(T) = \frac{\sum(x_L - \bar{x}_L)^2}{P_L - 1} \tag{2.6}$$

where $x_G$ and $x_L$ is the value of pixels in the glacier or land class, $\bar{x}_G$ and $\bar{x}_L$ is the means of pixel values in the glacier or land class.

This automated approach efficiently determined the optimal NDSI threshold for each Landsat image with a minimum of 0.25 and a maximum of 0.32, subsequently applied across the entire study region to delineate glacier areas.

Furthermore, a shadow cast correction was implemented using the blue band (Mölg et al., 2018; Paul et al., 2011). A TOA value below 0.1 in the blue band was considered indicative of shadow presence. Additionally, the regions identified as lakes in the subsequent section were omitted from the glacier mapping.

To minimize the potential overestimation of glacier area caused by seasonal snow cover, Landsat images from 1985 to 2021 were divided into eight segments, each covering a five-year period, except for the final period from 2020 to 2021. A pixel can only be classified as a glacier pixel if it is classified as such throughout the designated time segment, as illustrated in the “Five-year composite” step in Figure 2.4. If a pixel was once identified as a non-glacier pixel (green pixel) during the 5-year stack, the pixel will be identified as a non-glacier pixel. Subsequently, the area of each glacier fragment was calculated. Fragments smaller than 5400 $m^2$ (equivalent to 6 Landsat pixels) were excluded following previous research (Bolch et al., 2010; Drenkhan et al., 2018), as these are more likely to represent snow patches. Additionally, the elevation distribution was calculated using the SRTM DEM to augment our understanding of glacier changes.

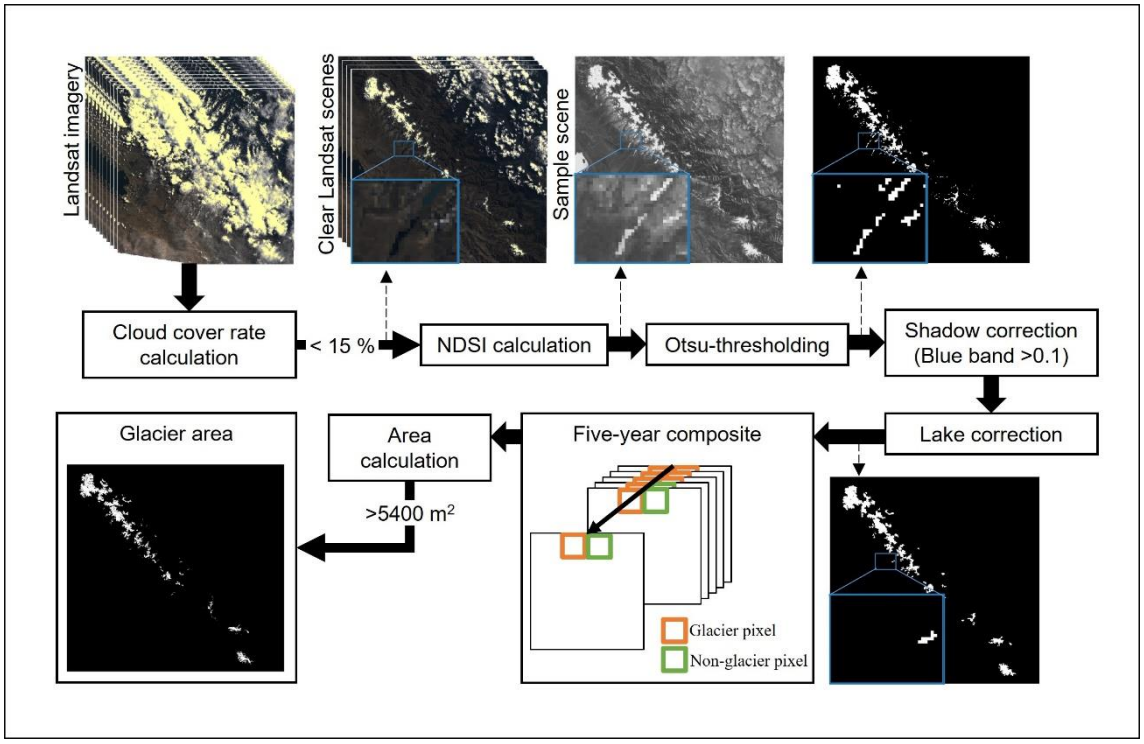


**Figure 2.4** Flow chart of glacier mapping.

### 2.2.4. Error estimation

The error in glacier area mapping can result from various factors such as clouds and temporal snow cover. In this study, we use images with low cloud cover rates to minimize interference from clouds and composite multiple images to reduce overestimation caused by temporary snow. Nevertheless, accurately mapping glaciers remains challenging in the absence of suitable ground truth data (Paul et al., 2011). Therefore, the uncertainties of glacier mapping in this study were determined using the equation proposed by Hanshaw and Bookhagen (2014), which assumes that the error associated with area measurements follows a normal or Gaussian distribution.

$$\mathrm{Error}(1\sigma) = \left(\frac{\mathrm{P}}{\mathrm{G}}\right) * 0.6872 * \frac{\mathrm{G}^2}{2} \tag{2.7}$$

where P is the perimeter of glaciers, and G is the spatial resolution of the images, which in this case is 30 m. The calculated uncertainties during the study period are approximately 5%.

## 2.3. Glacier area change

As illustrated in Figure 2.5, the glacier area was 277.17 km$^2$ in 1985–1989. Over subsequent years, it experienced a significant loss, decreasing by 42% by 2021. The rate of recession was not consistent throughout the study period, with the fastest recession occurring between 1985–1989 and 1990–1994 when the glaciers diminished at a rate of 8.19 km$^2$/year. From 2000 to 2009, the glaciers continued retreating at a high reduction rate of 6.86 km$^2$/year. However, after 2010, the decrease notably slowed down. In the most recent period, 2020–2021, the total glacier area measured 164.33 km$^2$, nearly the same as the area in 2015–2019, which was 160.32 km$^2$. It is worth noting that all available satellite images during 2020–2021 were taken before August, which might lead to a slight overestimation of glacier area due to the temporal snow cover at the beginning of the dry season.

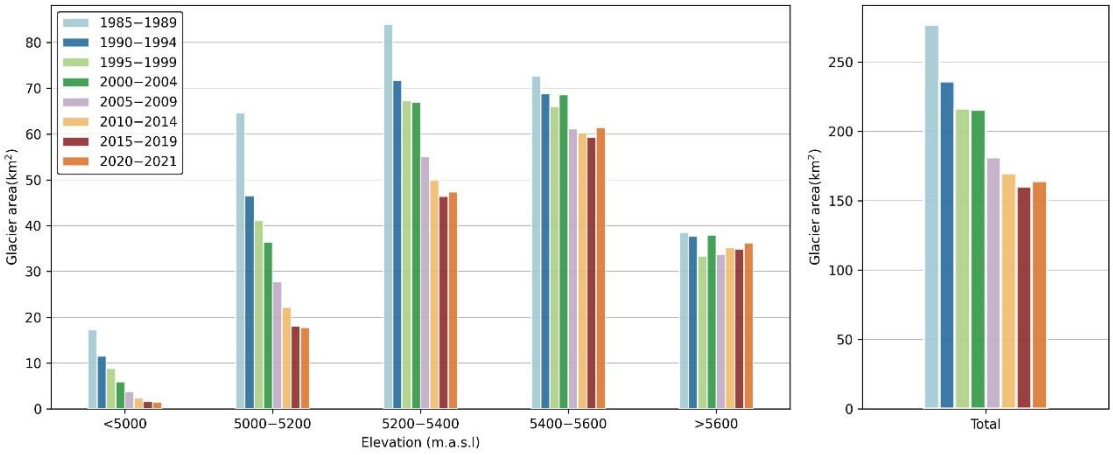


**Figure 2.5** Glacier area along different elevations.

As predicted in previous research (Bradley et al., 2006), an assessment based on elevation reveals that the most vulnerable glaciers are those situated below 5400 m.a.s.l. The most severe area loss is observed in relatively lower elevations, with glaciers below 5000 m.a.s.l. nearly disappearing. Notably, 73.9% of the area loss occurred within the 5000–5400 m range, while only 2.1% of the loss occurred above 5600 m. Glaciers below 5200 m exhibit a continuous decrease over time, especially those between 5000 and 5200 m.a.s.l. After a sharp decrease before 1990, the glaciers in this elevation range lost around 2–4% of their area per year until 2019, leaving only 17.79 km$^2$, around one-fourth of their area from 1985–1989. Glaciers between 5200 and 5400 m.a.s.l. also

show a continuous downward trend since 1985, except for a slight increase observed during 2020–2021. Generally, glaciers at higher elevations experienced comparatively less area loss during the same period than those at lower elevations. Furthermore, glaciers above 5400 m.a.s.l. experienced slight area increases, particularly in 2000–2004 and 2020–2021, resulting in a higher average elevation for the remaining glaciers. In the latest period, 2020–2021, 59.4% of the glaciers were above 5400 m.a.s.l.

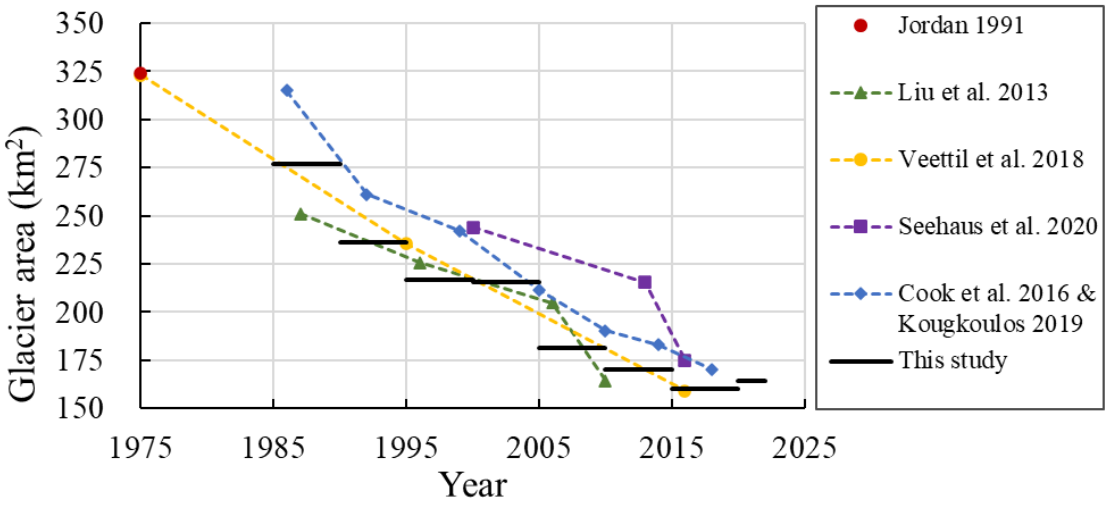


**Figure 2.6** The glacier area from this study compared with previous research (Cook et al., 2016; Kougkoulos, 2019; Liu et al., 2013; Seehaus et al., 2020; Soruco et al., 2009).

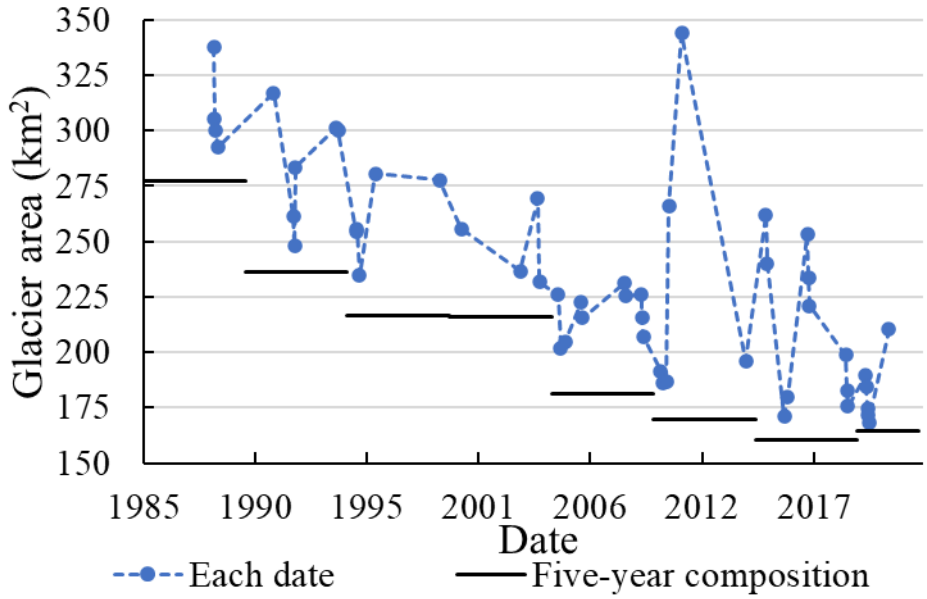


**Figure 2.7** The glacier area of five-year composition compared with the area on each specific date.

Tropical glaciers have been experiencing rapid shrinkage throughout the past decade, with this study observing over a 40% loss in glacier area within the Cordillera Real from 1985 to 2021. Figure 2.6 depicts a significant loss in glacier surface area during the study period, consistent with previous research (Cook et al., 2016; Kougkoulos, 2019; Liu et al., 2013; Seehaus et al., 2020; Soruco et al., 2009). However, our latest glacier mapping results reveal a notable decline in the rate of glacier recession over the last ten years. This reduction in glacier melting is believed to be a consequence of the altered distribution of glaciers concerning elevation. Assuming an estimated temperature sensitivity of the ELA at 150 ± 30 m °C−1 by Lejeune (2009) and extrapolating Zongo glacier's characteristics to the entire Cordillera Real, the rise in ELA due to recent temperature increases in the last 15 years is anticipated to be less than 100 m. Consequently, approximately 75% of current glaciers are located above 5300 m.a.s.l., the elevation where ELA is positioned. This insight may explain the observed process of glacier melting over recent decades.

In this study, glaciers were assumed to exist consistently throughout each five-year period. While there is a possibility of glacier decline within these periods, the same methodology was applied across all periods. Therefore, the observed trend in glacier area change remains reliable.

When comparing glaciers mapped from individual images, the five-year composite glacier area appears smaller than that from any single image within the same period (Figure 2.7). And our findings are within the lower range of previous studies. However, using single images for glacier mapping can lead to overestimation due to the potential inclusion of seasonal snow, which varies depending on the month the image was taken. The five-year composite method significantly reduces this risk of overestimation.

## 2.4. Summary

In this chapter, 51 Landsat images on the cloud platform GEE were utilized to develop an automated method for detailed mapping of glacier changes. This method is efficient and significantly reduces manual work. A significant loss in glacier surface area was observed during the study period, consistent with previous research. Our latest glacier mapping results reveal a notable decline in the rate of glacier recession over the

last ten years. Glaciers below 5000 m.a.s.l. are nearly disappearing. Most area loss occurred within the 5000–5400 m.a.s.l range. Glaciers above 5600 m.a.s.l are relatively stable.

# Chapter 3 Lake inventory and lake area changes in the Cordillera Real

Chapter 3 begins with a brief introduction to some available global water surface datasets and a literature review on lake mapping methodologies. It then describes the mapping methodology developed in this study and reports on the lake inventory and the lake area changes observed during the study period.

## 3.1. Literature review on global water surface datasets and methodology of mapping lake area changes

There are many existing models and datasets for water surface on a global scale, including Landsat Global Inland Water (GLCF), Landsat Level-3 Dynamic Surface Water Extent (DSWE), etc. Among them, two datasets have relatively good performance in mapping lakes in the Cordillera Real. One of the datasets is the JRC Global Surface Water Mapping Layers v1.3 (Pekel et al., 2016), which contains maps of the location and temporal distribution of surface water from 1984 to 2020. It provides statistics on the extent and changes of those water surfaces. This dataset was generated using 4,453,989 scenes from Landsat 5, 7, and 8. Each pixel was individually classified into non-water, permanent water, and non-permanent water using an expert system.

Another dataset is OpenStreetMap (OSM) (OpenStreetMap contributors, 2017), an open-source and collaborative mapping platform that aims to create a free and editable map of the world. OSM allows anyone to contribute by adding, updating, and correcting geographic data, including roads, buildings, landmarks, and natural features. The project started in 2004 and has grown into a global community of millions of volunteers who use GPS devices, satellite imagery, and local knowledge to create accurate and up-to-date maps.

However, both datasets still lack the necessary accuracy to fully capture the seasonal changes in lake areas. The misidentification of mountain shadows as lakes or glaciers, remains a significant challenge for most water surface models, including the

JRC model. Additionally, the JRC model's algorithm is susceptible to errors that result in mapped areas being influenced by data from neighboring years.

For the method that were used for mapping water surface, there are mainly 7 indexes that were often used in identifying water surface. To meet the requirement of distinguishing complicated landcover situation in the Cordillera Real, these indexes were calculated using the 2019/06/07 Landsat-8 image in the study region, on which the cloud cover rate of the target area is less than 1%. The differences among lake, glacier, and mountain shadow were manually inspected (Table 3.1).

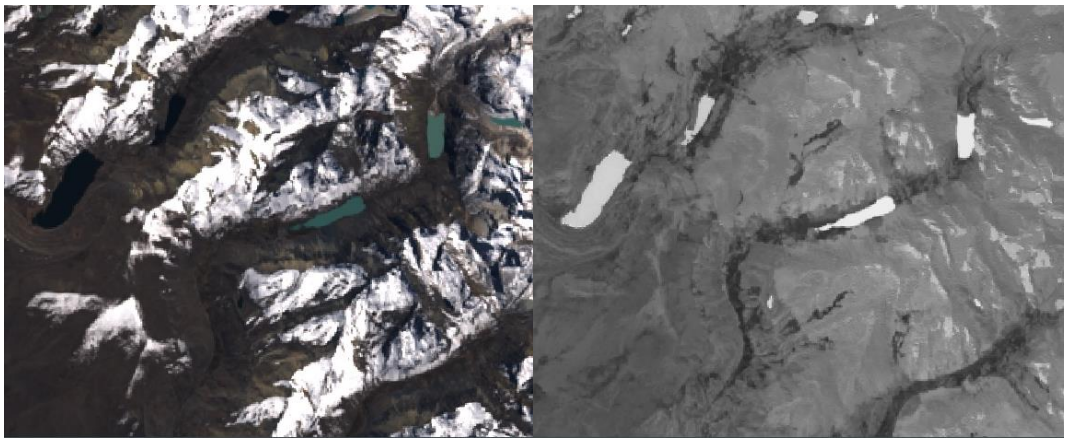

(a) (b)

**Figure 3.1** (a) Landsat-8 images in the study region in 2019/06/07 (Partial, RGB) (b) NDWI (green) images calculated using Landsat image

As it was compared in Table 3.1 and shown in Figure 3.1, the NDWI by McFEETERS (1996) is the most proper index for delineating glacial lakes in the Cordillera Real. This index can not only enhance the presence of water surface but also depress soil and terrestrial vegetation features. It is often used for mapping glaciers and glacial lakes in mountainous regions with manually selected thresholds. Lately, pixel-wised classification utilizing machine learning methods has relieved the burden of manual operation (Pekel et al., 2016; Veh et al., 2018; Zhao et al., 2018). Yet, defects exist in the mapping of glacial lakes, where these methods confront issues such as misclassifying shadows as lakes and being unable to capture spatial information such as pixel proximity and the geometric characteristics of classes, which is crucial for effective water classification.

Table 3.1 Information of often used indexes in identifying water surface

| **Name** | **Abbreviate** | **Equation** | **Differentiate water/snow** | **Differentiate water/shadow** | **Reference** |
|---|---|---|---|---|---|
| Normalized Difference Water Index | NDWI_Green | $\frac{\text{Green} - \text{NIR}}{\text{Green} + \text{NIR}}$ | Good | Medium | (McFeeters, 1996) |
| Normalized Difference Water Index | NDWI_SWIR | $\frac{\text{NIR} - \text{SWIR}}{\text{NIR} + \text{SWIR}}$ | Bad | Good | (Gao, 1996) |
| Modified Normalized Difference Water Index | MNDWI | $\frac{\text{Green} - \text{MIR}}{\text{Green} + \text{MIR}}$ | Bad | Medium | (Xu, 2006) |
| Normalized Difference Water Index | NDWI_Blue | $\frac{\text{Blue} - \text{NIR}}{\text{Blue} + \text{NIR}}$ | Good | Bad | (Huggel et al., 2002) |
| Water Ratio Index | WRI | $\frac{\text{Green} + \text{Red}}{\text{NIR} + \text{MIR}}$ | Bad | Bad | (Shen and Li, 2010) |
| Normalized Difference Vegetation Index | NDVI | $\frac{\text{NIR} - \text{Red}}{\text{NIR} + \text{Red}}$ | Good | Medium | (Rouse et al., 1974) |
| Automated Water Extraction Index | AWEI | $4 * (\text{Green} - \text{MIR}) - (0.25 * \text{NIR} + 2.75 * \text{SWIR})$ | Bad | Bad | (Feyisa et al., 2014) |

## 3.2. Methodology of lake detection and mapping lake area changes

Except for Landsat images and SRTM DEM which were introduced in the previous chapter, this study utilized the following datasets for the Lake mapping: (1) the SRTM Water Body Dataset (SRTM WBD) from the National Geospatial-Intelligence Agency (NGA) (https://earthexplorer.usgs.gov/, accessed on 28 April 2022), /). This dataset depicts lakes that are greater than 600 m × 183 m in Feb 2000, it covers a water surface of about 16 $km^2$ in the study region. The SRTM WBD was used as a reference area for establishing suitable thresholds for glacial lake mapping; (2) Sentinel-2 MSI: MultiSpectral Instrument, Level-1C data acquired from The Copernicus Data Space Ecosystem (https://dataspace.copernicus.eu/explore-data/data-collections/sentinel-data/sentinel-2, accessed on 19 June 2023), employed to validate the results of lake delineation. These high-resolution images, with a spatial resolution of 10 meters, cover the period from 2015 to the present, enabling accurate manual visual validation.

The primary methodology employed in this study for mapping glacial lakes involves two main technical components: (1) glacial lake inventory: identifying the position of lakes that emerged during the research period (Figure 3.2a); (2) lake delineation: analyzing the area changes of each lake, followed by post-processing (Figure 3.2b)

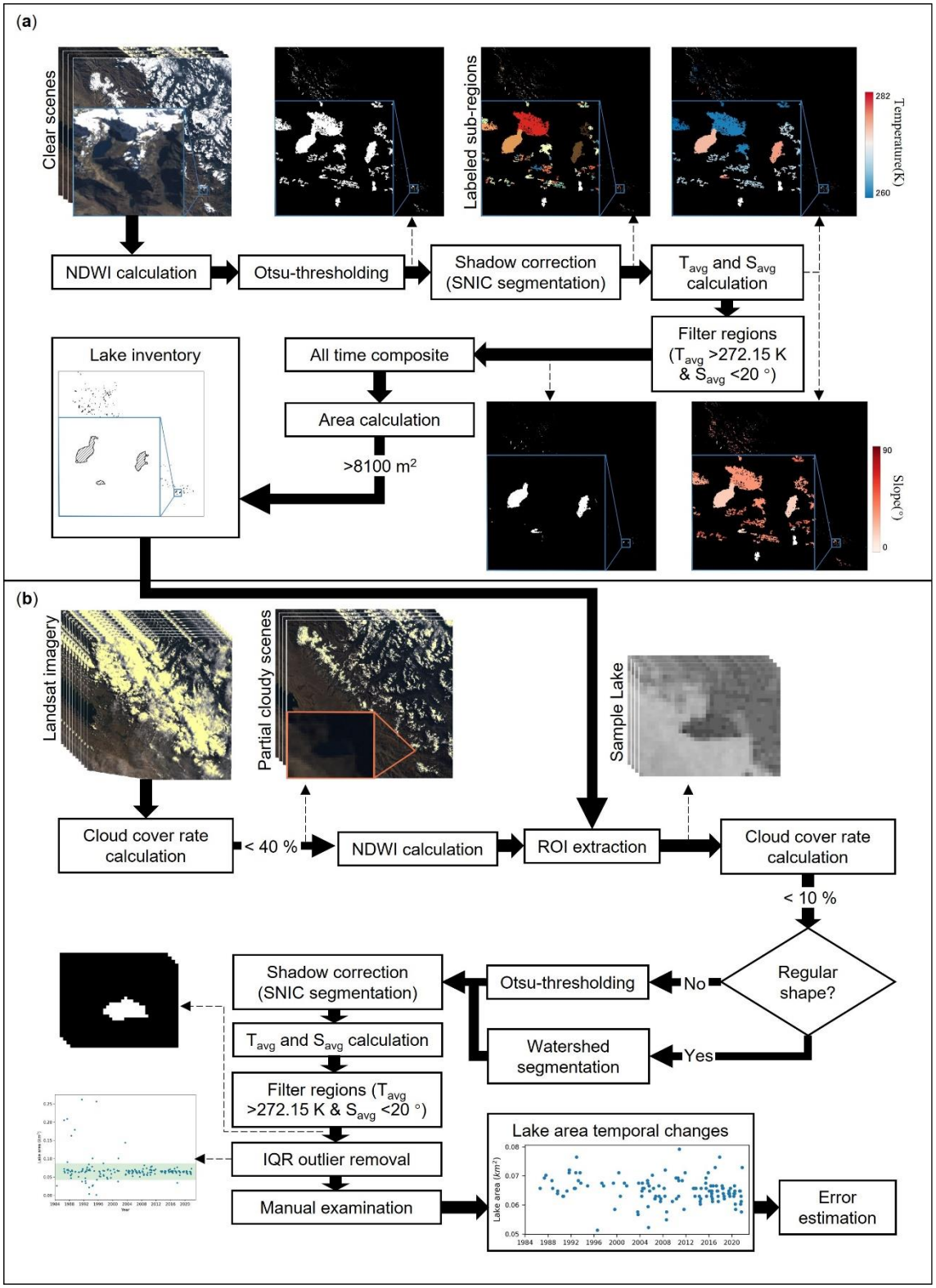


**Figure 3.2** Flow chart of (a) lake inventory mapping, and (b) lake area change detection. ($T_{avg}$: average temperature of each sub-region; $S_{avg}$: average slope of each sub-region).

### 3.2.1. Lake inventory mapping

This study used NDWI, a commonly used index in mountainous regions like the Himalayas (Jiang et al., 2018; Li and Sheng, 2012; Wang et al., 2020) and Andes (Cook et al., 2016) for mapping glacial lakes. This index not only enhances the identification of water surfaces but also reduces the impact of soil and terrestrial vegetation properties (McFEETERS, 1996). The NDWI is defined as follows:

$$\mathrm{NDWI} = \frac{\mathrm{Green} - \mathrm{NIR}}{\mathrm{Green} + \mathrm{NIR}} \tag{3.1}$$

For Landsat 5, the Green band and NIR band correspond to Band 2 and Band 3, respectively. For Landsat 8, the Green band and NIR band correspond to Band 3 and Band 4, respectively.

Similar to the glacier mapping process, the sample region for determining the suitable NDWI threshold using the Otsu method was selected within 150 m of the waterbodies' edge (excluding cloud pixels and those with a slope higher than 30°) in the SRTM WBD of each Landsat image. To account for potential errors from glaciers and mountain shadows, 0.1 was added to the calculated Otsu threshold, which was then applied to the entire study region in order to extract waterbodies.

In Figure 3.2a, the misidentified area caused by glaciers and mountain shadows is still included even after the Otsu-thresholding step. To further reduce errors attributed to glaciers and mountain shadows, a simple non-iterative clustering (SNIC) segmentation (Achanta and Susstrunk, 2017) was used for each waterbody identified in the Otsu-thresholding step. The SNIC segmentation method clusters similar pixels, separating lake from the neighboring mountain shadows with two given seeds, one seed for water and one seed for mountain shadow.

For water seed, it will better represent water region when it is placed at the middle of the lake. To avoid the seed being placed at the edge of the object, a 3*3 square kernel is applied on the NDWI image to convolve the image, in this case, the boundary pixels will have a relatively low NDWI value, thus reducing the possibility of being chosen as water seed. Then the pixels with the highest NDWI value on the convolved image are chosen as water seed.

Conversely, mountain shadow normally falls near the edge of the object, The slope seed should be placed near the edge of the object. So first, the slope outside of classified water pixels is set to 0, then a 3*3 Gaussian kernel is applied on the slope map, the pixel with the highest slope is chosen as the slope seed. The values of a 3*3 square kernel and a Gaussian kernel are shown in Figure 3.3.

| | | |
|---|---|---|
| 1 | 1 | 1 |
| 1 | 1 | 1 |
| 1 | 1 | 1 |

(a)

| | | |
|---|---|---|
| 0.075 | 0.124 | 0.075 |
| 0.124 | 0.204 | 0.124 |
| 0.075 | 0.124 | 0.075 |

(b)

**Figure 3.3** (a) 3*3 square kernel; (b) 3*3 Gaussian kernel.

Each waterbody was divided into two sub-regions which are represented in different colors in Figure 3.2b, with criteria defining a sub-region as a waterbody if its average temperature exceeds 272.15 K (Shugar et al., 2020) and its slope is under 20°. The temperature was derived from the average of two thermal bands in the Landsat image, while the slope was calculated using the SRTM DEM. Pixels residing within a waterbody in more than five images were classified as water pixels. Finally, all water pixels adhering to the eight-connected rule were united into individual objects. Following established methodologies (Mitkari et al., 2017; Nie et al., 2017), objects larger than 0.0081 $km^2$ (equivalent to 9 Landsat pixels) were identified as lakes and incorporated into the lake inventory after manually comparing with high-resolution satellite images from Google Earth and ESRI using QGIS 3.28.

To better understand the diverse patterns in temporal area changes of lakes and the factors influencing lake dynamics, we calculated stream map and glacierized catchments using the SRTM DEM and GLIMS datasets within ArcGIS Pro 3.2. Information on human activities was gathered through several approaches: analysis of dam records available in OSM; examination of lakes affected by mining activities, as documented in the literature (Alvizuri-Tintaya et al., 2022; Caballero et al., 2004); and visual observations using recent high-resolution images from Google Earth to observe lakes displaying noticeable alterations, such as discernible human-built structures.

### 3.2.2. Lake delineation

For lake delineation, the cloud cover rate threshold was loosened to 40% for acquired lake data as much as possible. A total of 213 images (153 Landsat-5 images and 60 Landsat-8 images) (Figure 3.4 and Table A2) were filtered out.

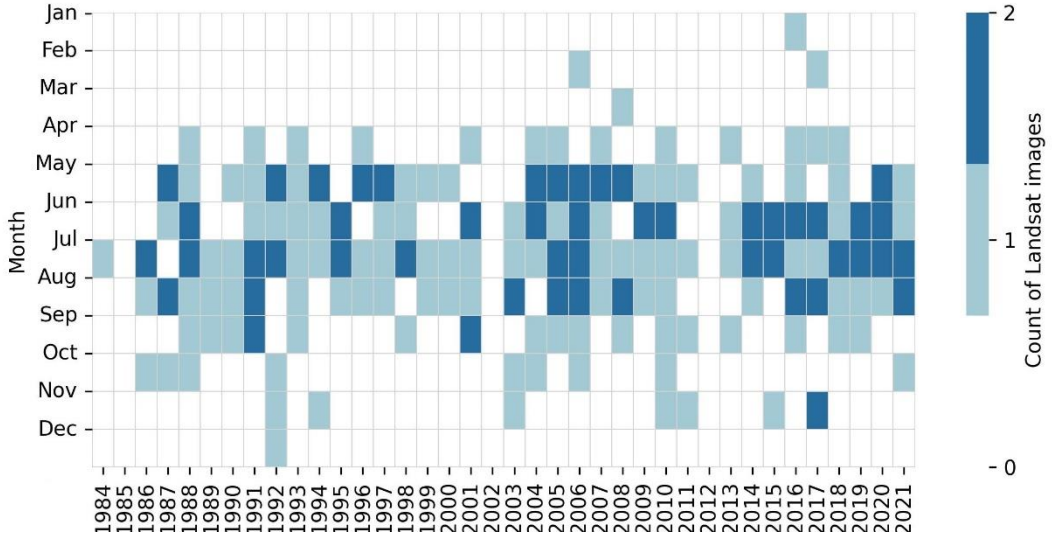


**Figure 3.4** Temporal distribution of Landsat images with cloud cover threshold less than 40%.

While glacier mapping necessitates clear scenes across the entire study area, lake delineation primarily requires clear views over the lake area. Therefore, to maximize the utilization of Landsat images, the cloud cover threshold in the study area was adjusted to 40%. This adjustment enables the inclusion of clear portions of the images, even if some areas are partially affected by cloud cover. This approach is highly effective because lake areas tend to vary depending on the season (usually decreasing during the dry season from April to October), while glacier areas remain relatively stable over a short period. By utilizing partially cloudy images, we obtained three times more lake area data compared to utilizing only clear scenes, thereby reducing the seasonal bias. This analysis was performed on the Google Colab cloud platform to ensure a swift and efficient processing workflow for each individual lake object.

The extent of each lake object was derived from the resulting lake inventory in Section 3.2.1. The region of interest (ROI) is defined as the area extending 10 pixels from each lake object. A sample lake can be seen in Figure 3.2b. The cloud cover rate over the ROI was calculated, applying a 10% threshold to ensure that the lake area

remains unaffected directly by cloud interference. The precise delineation of each lake employed the watershed segmentation method (Vincent and Soille, 1991).

The watershed segmentation method is a classical algorithm used for segmentation, it starts from user-defined markers, the watershed algorithm treats pixel values as a local topography. The algorithm floods basins from the markers until basins attributed to different markers meet on watershed lines.

Utilizing the area within 3 pixels from each lake object that was mapped in Section 3.2.1, the outermost pixels were designated as background (land) seeds, while the top 12% NDWI-value pixels were marked as water seeds. This approach divides the area into water and land sections, defining the lake region delineated by watershed segmentation. Given that watershed segmentation methods might occasionally misidentify narrow parts of the lakes, potentially omitting certain portions, we compared the delineation result with high-resolution satellite images from Google Earth. If omission happens, the area of those lakes is extracted using the Otsu method. To minimize errors from glaciers and mountain shadows, the SNIC segmentation method, configured as in the previous section, was once again applied to each lake object, alongside the temperature and slope filter.

### 3.2.3. Post process of lake area data

Outliers (points that are out of the green parts in the Figure 3.2b “IQR outlier removal” step) identified by the Interquartile Range (IQR) outlier detection method (as defined by Equations (3.2)–(3.4)) were automatically excluded from the obtained lake area data.

$$\mathrm{IQR} = \mathrm{Q}_3 - \mathrm{Q}_1 \tag{3.2}$$

$$\mathrm{Outlier} < \mathrm{Q}_1 - 3 \times \mathrm{IQR} \tag{3.3}$$

$$\mathrm{Outlier} > \mathrm{Q}_3 + 3 \times \mathrm{IQR} \tag{3.4}$$

where $\mathrm{Q}_1$ and $\mathrm{Q}_3$ represent the first quartile and the third quartile of the dataset, respectively.

Finally, all lake delineation results are manually reviewed and cross-checked with the RGB images from the corresponding Landsat images. In areas with glaciers, the presence of ice can obstruct the delineation of glacial lakes which were initially either

entirely or partially covered by ice during their formation, occurring in areas where glaciers have retreated. However, they were not counted as lakes because they were smaller than the lake area threshold of 8100 $m^2$ at the time. For larger lakes that were sometimes partially covered by ice or snow, the boundary between lake and land cannot be observed by optical satellite because they are all beneath the ice surface. Such area data are not included in the final statistics. Out of all the area records, a small portion (4.6% of the total data, approximately 0.5% of the total lake area) was removed due to the following reasons: (1) partial coverage of the lake by snow or ice; (2) partial coverage of the lake by clouds; (3) misidentification of glaciers as lakes; or (4) difficulty in distinguishing the boundary between the lake and mountain shadows through visual assessment.

The monthly average areas of each lake were calculated from the obtained results. Consistent decline in monthly water levels and lake areas for five large lakes (Tuni, Incachaca, Milluni, Ajuankhota, and Chiarkota) in the study region were recorded by EPSAS (https://www.epsas.com.bo/web/, accessed on 9 October 2022) during the dry season. Thus, a linear decrease in the lake areas was assumed, and linear interpolation was applied to the monthly average lake areas during the dry season (from April to October). Finally, the average lake areas during the dry season were divided into the temporal divisions consistent with those used for glacier mapping.

If a lake appears before 2015 and then continues to exist is categorized as an appear lake. If a lake disappears after 1990 is categorized as a disappeared lake. If a lake can not be detected for longer than 5 years, after confirming with historical Google Earth images, is categorized as an unstable lake. To find these lakes, the average lake area during the dry season every five years of each lake was calculated, and the lakes that have any void record were then checked with the historical Google Earth images and categorized.

### 3.2.4. Error estimation

Since this research generates both lake inventory and lake area datasets, each was validated using different methods.

#### 3.2.4.1. Validation of lake inventory

To evaluate the performance of lake detection of the method proposed in this study, the lake inventory result was compared with two datasets, OSM and JRC.

In this study, OSM data is extracted using a QGIS plugin called QuickOSM (Etienne, 2024), the plugin automatically fetches all the polygons defined as water in the natural column, and the polygons that are lake, reservoir and basin in the water column. Then the area of each polygon is calculated, and there are 292 water areas larger than 8100 $m^2$, including 125 polygons that are defined as water in the natural column and 123, 41, and 3 polygons defined as lake, reservoir, and basin in the water term respectively.

To convert this pixel-based dataset JRC into object-based dataset, all the pixels that has been classified as permanent water is classified as water. Connected clusters of water pixels were identified, and clusters containing over 9 connected pixels were defined as water objects. This process resulted in the identification of 289 water objects.

A confusion matrix is a table used to evaluate the performance of a classification model by displaying the counts of true positive, true negative, false positive, and false negative predictions. A standard confusion matrix is as follows:

Table 3.2 A standard confusion matrix.

| **Confusion Matrix** | **Actual Positive** | **Actual Negative** |
|---|---|---|
| **Predicted Positive** | TP | FP |
| **Predicted Negative** | FN | TN |

where TP stands for true positive, in this study it represents lakes that is correctly identified as a lake; FP stands for false positive, which is the object that is not a lake but misidentified as a lake; FN stands for false negative, which is a lake that did not successfully being detected as a lake. TN stands for true negative, it is not applicable in this study because datasets only look for lake objects.

After manually inspect all the lake area identified by three methods using high resolution Google Earth and ESRI satellite images, three datasets combined has found

total of 339 lakes in the study area. The confusion matrix of each dataset is shown in Table 3.3.

Table 3.3 Confusion matrix datasets (a) This study; (b) JRC; (c) OSM.

| **(a) This study** | **Actual Positive** | **Actual Negative** |
|---|---|---|
| **Predicted Positive** | 272 | 9 |
| **Predicted Negative** | 67 | |
| **(b) JRC** | **Actual Positive** | **Actual Negative** |
| **Predicted Positive** | 234 | 47 |
| **Predicted Negative** | 105 | |
| **(c) OSM** | **Actual Positive** | **Actual Negative** |
| **Predicted Positive** | 271 | 21 |
| **Predicted Negative** | 68 | |

To evaluate the performance of lake identification among three datasets, recall, precision, accuracy and F-score of each dataset were calculated based on the following equations:

$$\text{Recall} = \frac{TP}{(TP + FN)} \tag{3.5}$$

$$\text{Precision} = \frac{TP}{(TP + FP)} \tag{3.6}$$

$$\text{F} - \text{score} = \frac{2 * Recall * Precision}{(Recall + Precision)} \tag{3.7}$$

Recall is used to explain how many has the method predicted correctly. Precision is used to explain how many actually positive whining all the predicted positive. F-score helps to measure Recall and Precision at the same time. It uses Harmonic Mean in place of Arithmetic Mean by punishing the extreme values more. The results are shown in Table 3.4.

Table 3.4 Evaluation results of the performance of the three datasets.

| | **This study** | **JRC** | **OSM** |
|---|---|---|---|
| **Recall** | 0.8024 | 0.6903 | 0.7994 |
| **Precision** | 0.9680 | 0.8327 | 0.9281 |
| **F-score** | 0.8774 | 0.7548 | 0.8590 |

The error of commission (false positive) of this study and the JRC dataset mainly comes from mountain shadows. This occurs because the NDWI values of mountain shadows are similar to those of water bodies due to their low reflectance. Despite the application of a slope filter, commission errors remain unavoidable. Additionally, shallow water objects, where the exposed lake bottom or emergent plants are visible in Google Earth or Bing satellite images, should be classified as wetlands or ponds rather than lakes. This misclassification is a significant source of commission error in both the OSM and JRC datasets.

The error of omission of the OSM dataset is mainly from high altitude and inaccessible locations, it also fails to capture the lakes that appear and disappear within two or three years. While JRC and the result of this study mainly missed small lakes, especially those smaller than 15,000 $m^2$ and those with irregular, non-circular shapes. Some shallow lakes, which were not detected by either the JRC dataset or this study, likely have reflections influenced by the lake bottom. This results in lower NDWI values, causing these lakes to be unrecognized as water bodies by both models.

3.2.4.2. Error estimation of lake area delineation

The accuracy of the lake area delineation results was evaluated using 11 Sentinel-2 images (Table A3) captured concurrently with the Landsat 8 images. A subset of 101 lakes was randomly selected from these images to ensure a representative distribution of lake sizes across the entire study region. The 10 m resolution of the Sentinel-2 images facilitated the manual delineation of water boundaries using the RGB image.

The uncertainty of our analysis was quantified using the root mean square error (RMSE), a statistically significant indicator of accuracy (Jawak and Luis, 2014), represented by:

$$\mathrm{RMSE} = \sqrt{\frac{1}{n}\sum_{i-1}^{n}(\mathrm{Ar_i} - \mathrm{Am_i})^2} \tag{3.4}$$

where, $\mathrm{Ar_i}$ and $\mathrm{Am_i}$ are the area ($km^2$) of the $i^{th}$ lake derived from the Sentinel-2 RGB image and the proposed method, respectively, and n is the number of sampled lakes (=101).

Bias, the difference between the reference area (Ar) and the measured area (Am), was calculated. Additionally, the misclassified area (M), total underestimated area (U), and total overestimated area (O) were calculated as percentages relative to the total reference area using the following equations:

$$\text{Bias} = \text{Ar} - \text{Am} \tag{3.5}$$

$$\text{M}\ (\%) = \frac{\sum_1^n \text{Abs(Bias)}}{\sum_1^n \text{Ar}_\text{i}} \times 100 \tag{3.6}$$

$$\text{U}\ (\%) = \frac{\sum \text{Positive Bias}}{\sum_1^n \text{Ar}_\text{i}} \times 100 \tag{3.7}$$

$$\text{O}\ (\%) = \frac{\sum \text{Abs (Negative Bias)}}{\sum_1^n \text{Ar}_\text{i}} \times 100 \tag{3.8}$$

From the randomly selected lakes covering a total area of 10.6931 $km^2$, the RMSE between the proposed method and the Sentinel-2-derived area is 0.008182 $km^2$.The bias is 2.75%, with an underestimated area of 0.16% and an overestimated area of 2.59%

### 3.3. Lake inventory

This study delivered a comprehensive inventory of lakes situated above 4300 m.a.s.l. Within the study region, a total of 272 lakes were identified. Figure 3.5 displays the average area of each lake during the study period, with over two-thirds of the lakes being smaller than 0.05 $km^2$ in size. The lakes were categorized into four types based on their dependency on glaciers and direct human influences (reservoir construction).

For human effected lakes, OSM record 33 dams, one is built on a stream, 4 are built on 3 water ponds that are smaller than 0.0081 $km^2$, and some are built on the same lake. So, there are totally 27 lakes that have water dams recorded in OSM. And adding Milluni Grande Lagoon and Milluni Chico Lagoon which are influenced by mining activities (Alvizuri-Tintaya et al., 2022; Caballero et al., 2004). There are also 16 lakes that suddenly appear/disappear/expansion and obvious human build structures can be seen from recent Google Earth high-resolution images. When there's water dam on the lakes upstream, all the lakes downstream are considered influenced by human activity. Thus, adding another 11 lakes. So, there's total 54 lakes that effected by human activity.

There are total 183 lakes located in the catchment that receive glacier-melting water. And after manual visual inspection against the stream map, 129 lakes were fed by glacier-melting water.

This classification resulted in 100 natural glacier-fed lakes, 118 natural non-glacier-fed lakes, 29 human-affected glacier-fed lakes, and 25 human-affected non-glacier-fed lakes. Their average areas during the study period were found to be 9.92, 3.47, 11.34, and 2.34 $km^2$, respectively, indicating a tendency for glacier-fed lakes to be larger in size, potentially containing greater water volumes. The detailed lake size (dry season average area during the study period) and elevation distribution of the four categories of lakes are shown in Figure 3.6 and 3.7. While higher elevation zones (above 5000 m.a.s.l.) are home to a considerable number of natural glacier-fed lakes, most human-affected lakes are limited to elevation zones below 4800 m.a.s.l. and nearly 20 human-affected lakes, including glacier-fed and non-glacier-fed ones, are located within 20 km of La Paz, Bolivia's capital city. The storage capacity of glacier-fed and non-glacier-fed lakes is likely to have been augmented effectively by human influences to serve as water reservoirs for urban water supply and hydropower generation (Figure 3.6).

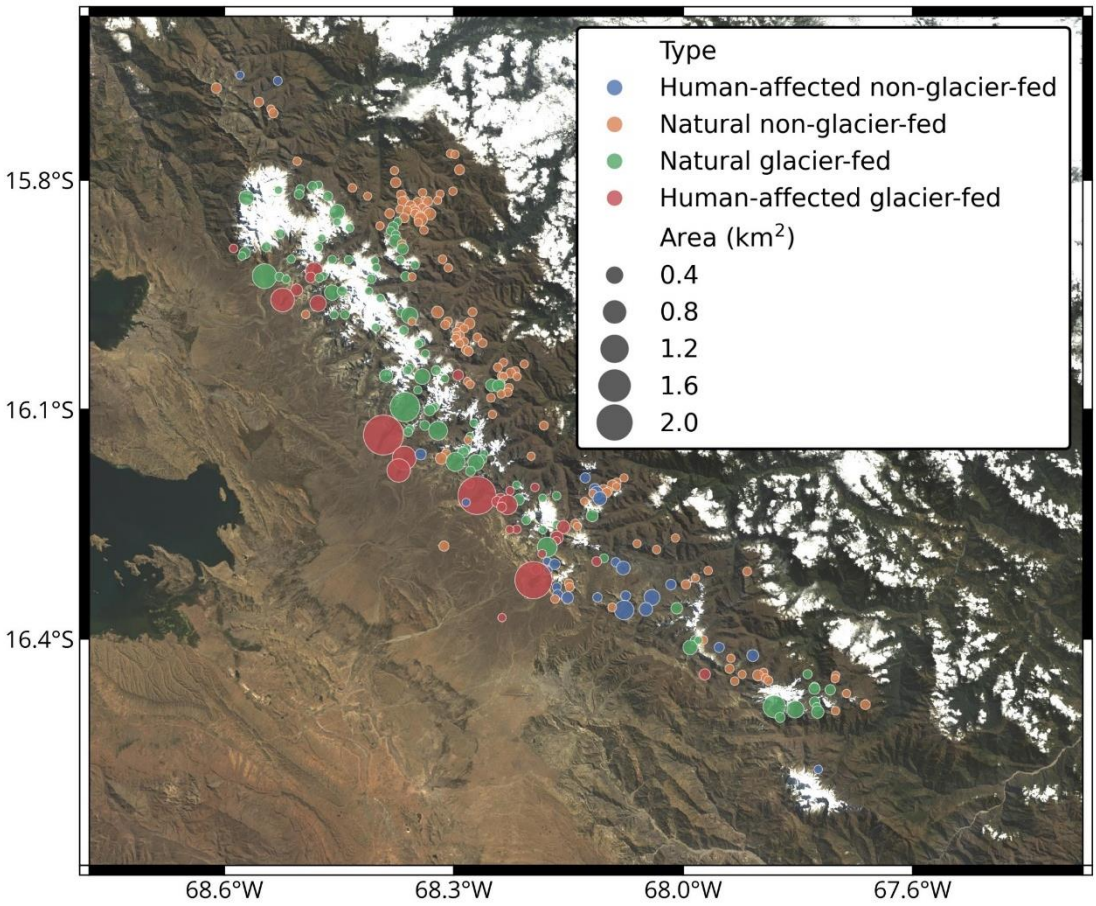


**Figure 3.5** Lake classification and average area during the study period.

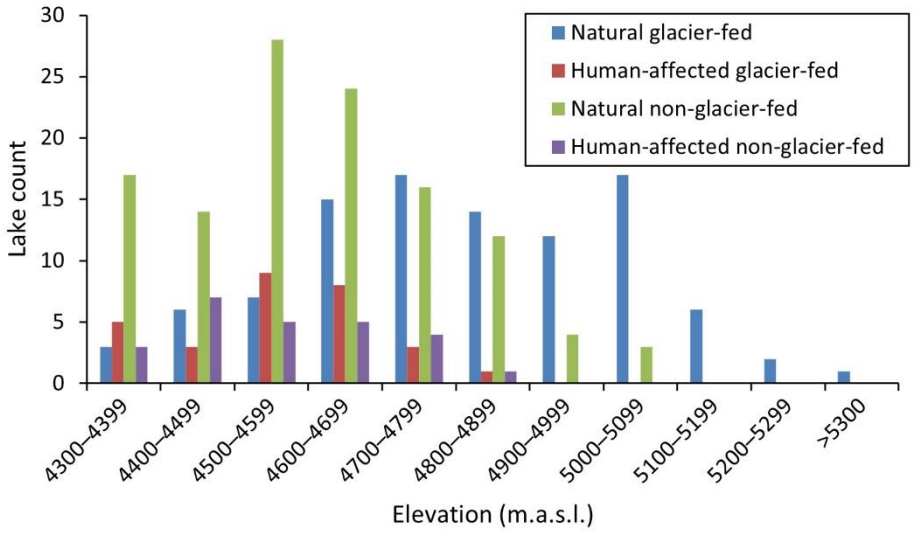


**Figure 3.6** Number of lakes by altitude zone and lake type. This figure was created for all lakes that existed during the study period.

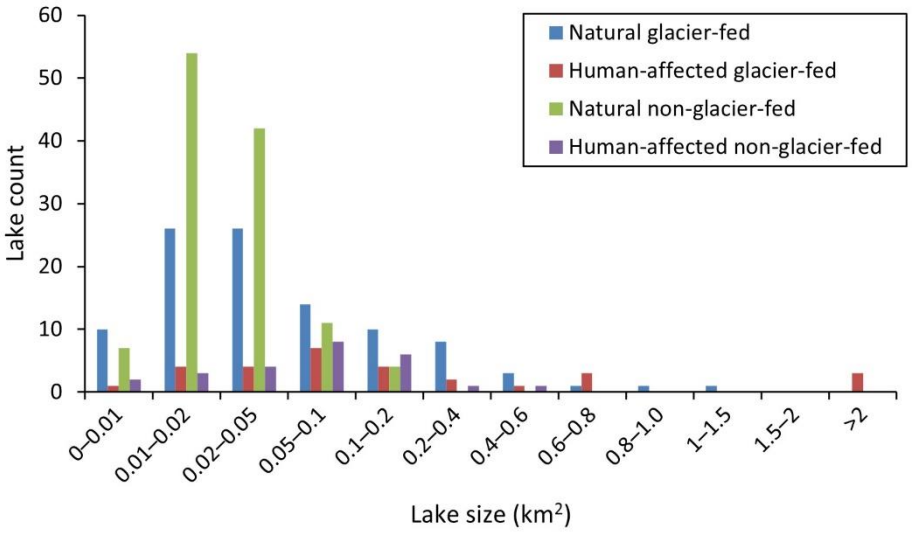


**Figure 3.7** Number of lakes by the lake area during the dry season and lake type. The area values are based on the average during the periods when the lakes were present throughout the study period.

Over the study period, 25 lakes appeared, 3 disappeared, and 1 briefly emerged from 1990 to 2010 (Figure 3.8). Naturally occurring lakes were predominantly located in the northern part of the Cordillera Real, often adjacent to retreating glacier edges. No new lakes formed without glacier feeding or human intervention. Out of the 25 appearing lakes, 22 are fed by glaciers, of which 4 are human-built reservoirs, and 18 lakes that are not intervened by humans are all located in the glacier retreated area. Three human-built, non-glacier-fed lakes (Embalse Represa de Chacaltaya, Embalse Represa Alpaquita, and Embalse Represa Hampaturi Alto), appeared during 2018–2019. Among 20 lakes appearing before 2015, only 2 were human-built reservoirs. Subsequent lakes emerging after 2016 were human-built reservoirs in the southern part of the Cordillera Real, primarily intended to supply water to nearby major cities. Of the three disappearing lakes, one was drained due to human activities, while the other two, fed by glaciers, naturally vanished, which could be a result of the declining net freshwater inflow or sedimentation. The briefly appearing lake followed a similar pattern of lakes being glacier-fed and naturally disappearing.

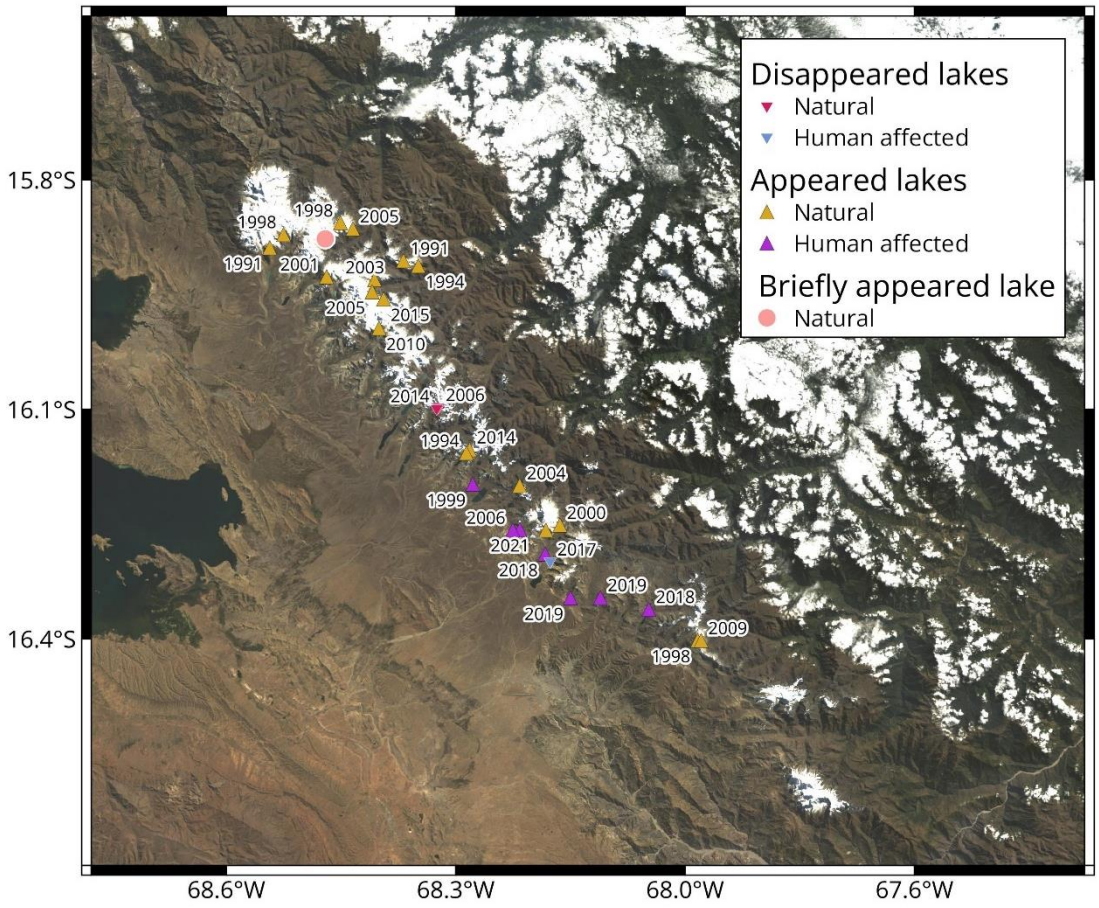


(a)

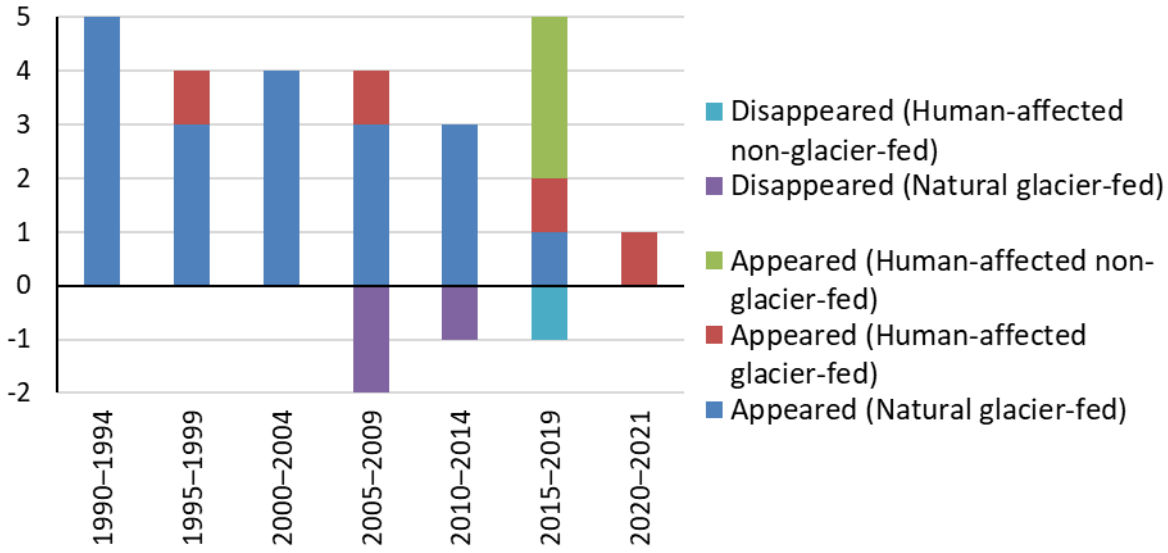


(b)

**Figure 3.8** (a) Spatial distribution of appeared, disappeared, and briefly appeared lakes; (b) Temporal distribution of appeared, disappeared, and briefly appeared lake.

## 3.4. Lake area changes

### 3.4.1. Comparison of lake area with observed lake volume of big lakes

As shown in Figure 3.9, the volume of the four large lakes recorded by EPSAS (https://www.epsas.com.bo/web/, accessed on 9 October 2022) exhibits a cyclical pattern in both lake volume and area over the years, indicating seasonal variations. During the dry season from April to October, the water volume in these lakes consistently declines. Consequently, a linear decrease in lake areas was assumed. The monthly average lake areas after linear interpolation during the dry season fit well with the water volume data. The second-order polynomial regression reveals a very strong correlation between lake area and volume. In lakes Milluni, Incachaca, and Ajuan Khota, maximum volumes occur repeatedly, likely due to overflow, which reduces the $R^2$ value. Nevertheless, it is reasonable to assume that changes in lake area can accurately represent the water storage in the lakes.

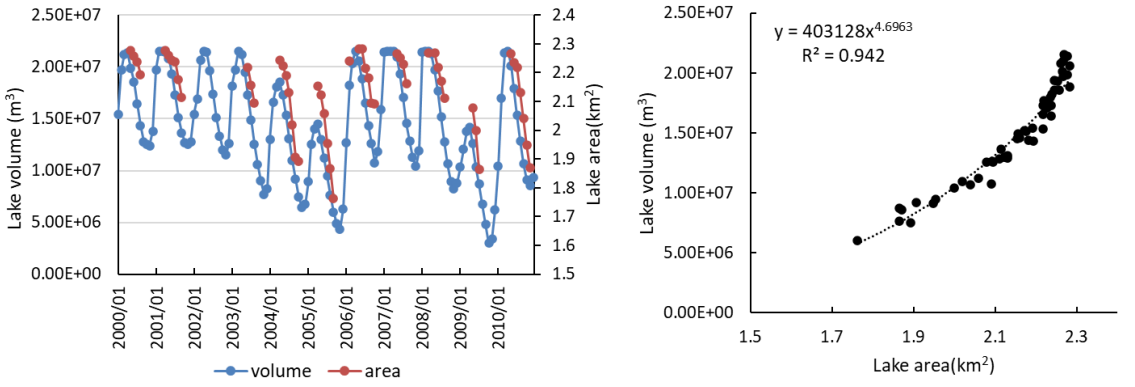


(a)

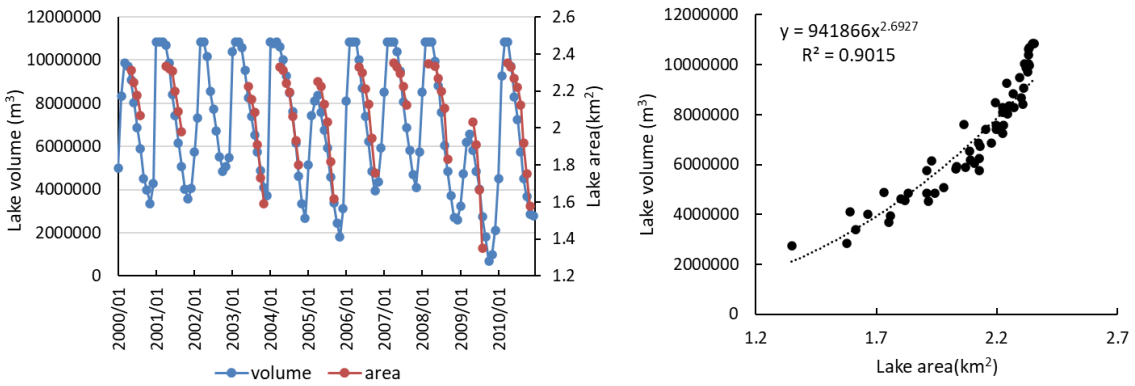


(b)

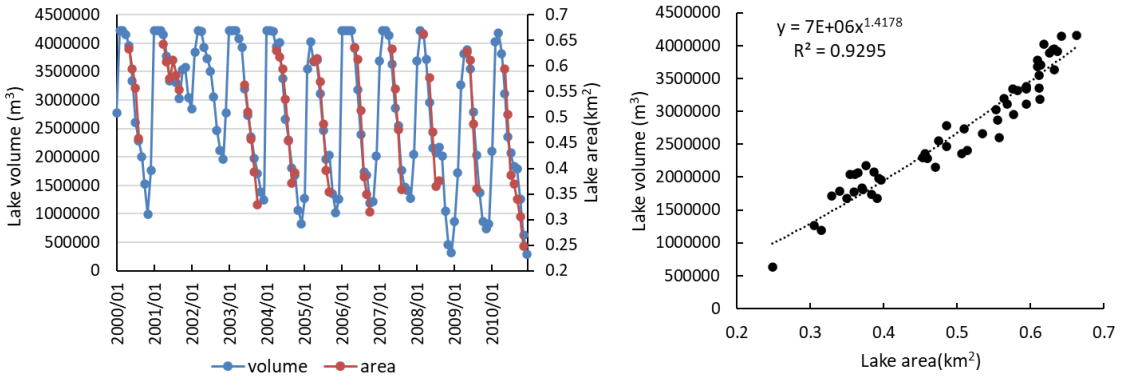


(c)

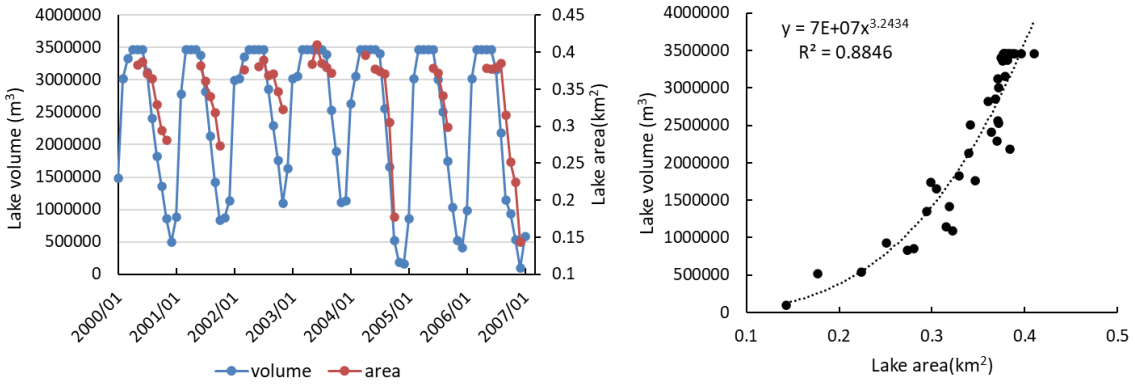


(d)

**Figure 3.9** Comparison between observed lake volume and lake area data from this study (a) Lake Tuni; (b) Lake Milluni; (c) Lake Incachaca; (d) Lake Ajuan Khota.

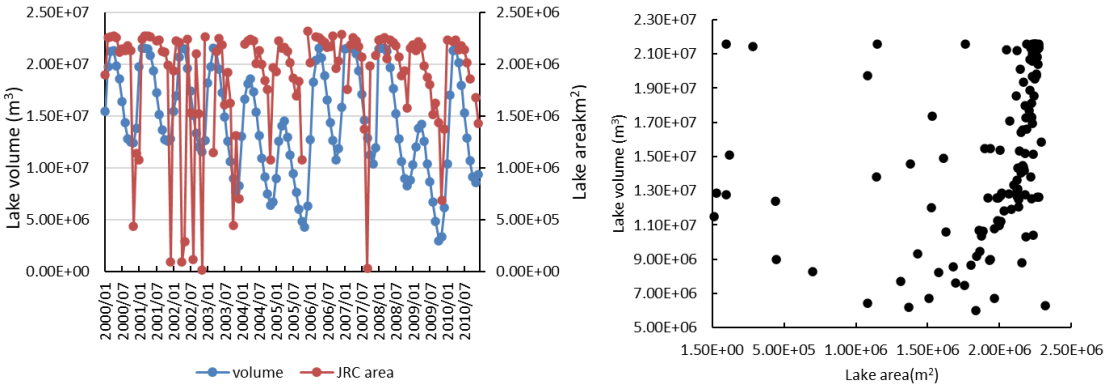


**Figure 3.10** Comparison between observed lake volume of Lake Tuni and lake area data from JRC

On the other hand, the lake volume of Lake Tuni is compared with the monthly area data from JRC, which is extracted using GEE. Even though JRC dataset almost

covered every month during the observation period, it contains a lot of missing area, which makes it difficult to construct the relationship between the area and volume or capture the seasonal or yearly variation of lakes (Figure 3.10).

### 3.4.2. Lake area and lake count changes in four categories

The total lake area in the study region (Figure 3.11) has steadily increased throughout the study period, with notable expansions during 1985–1994 and 2015–2021. Lakes receiving glacier meltwater, whether natural or human-affected, have shown varying growth patterns. Natural glacier-fed lakes showed continuous growth until 2014, expanding by 10.8% from 1985–1989 to 2010–2014. However, the lake area stabilized at approximately 10.3 $km^2$ after 2010, showing no further increase since then. Human-affected glacier-fed lakes demonstrated a consistent upward trend over the years, except for slight decreases of less than 0.1 $km^2$ in 1995–1999 and 2005–2009, with notably accelerated growth post-2005, increasing by 0.87 $km^2$. Similarly, human-affected non-glacier-fed lakes also exhibit an upward trend, with significant expansion during 1985−1999 and 2010−2021. A considerable area increase of around 0.55 $km^2$ during 2015–2021 aligns with the construction of three new water reservoirs (0.55 $km^2$) in 2018–2019. In contrast, natural non-glacier-fed lakes remained almost unchanged. Apart from a minor increase during 1990–1994, their area remained largely unchanged, fluctuating within 5%.

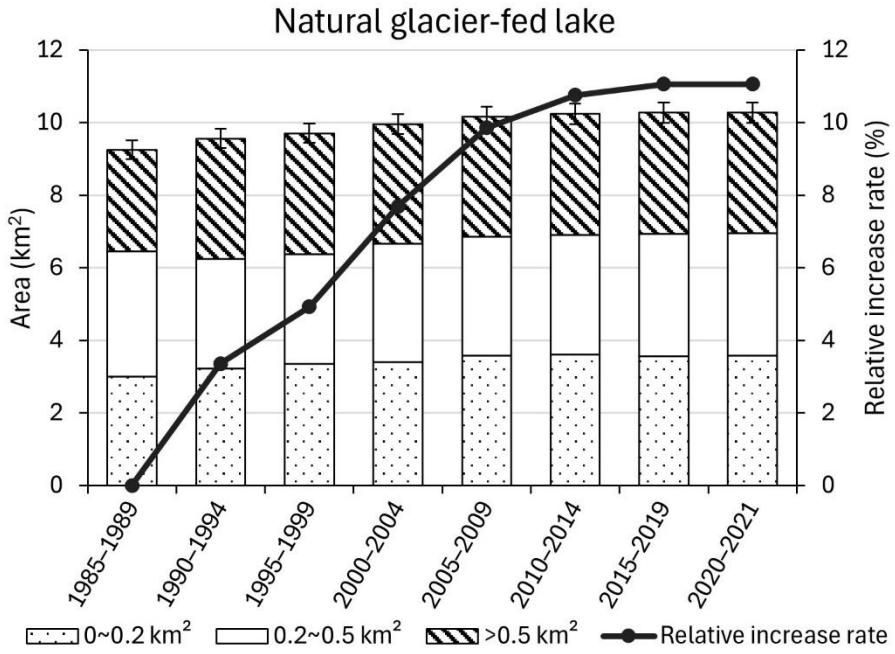
Natural glacier-fed lake
Area (km²)
Relative increase rate (%)
0
2
4
6
8
10
12
1985–1989
1990–1994
1995–1999
2000–2004
2005–2009
2010–2014
2015–2019
2020–2021
0~0.2 km²
0.2~0.5 km²
>0.5 km²
Relative increase rate

(a)

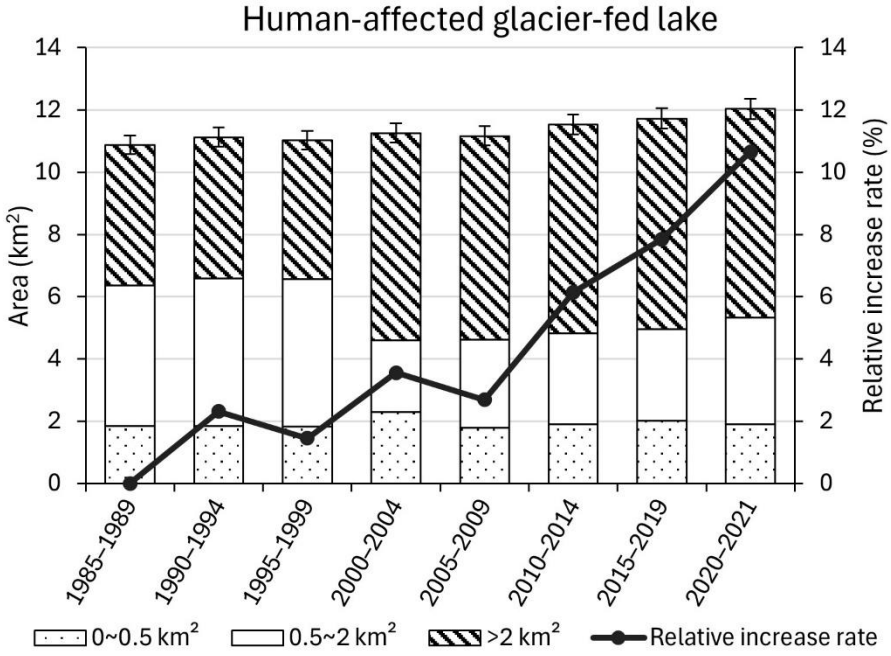
Human-affected glacier-fed lake
Area (km²)
Relative increase rate (%)
0
2
4
6
8
10
12
14
1985–1989
1990–1994
1995–1999
2000–2004
2005–2009
2010–2014
2015–2019
2020–2021
0~0.5 km²
0.5~2 km²
>2 km²
Relative increase rate

(b)

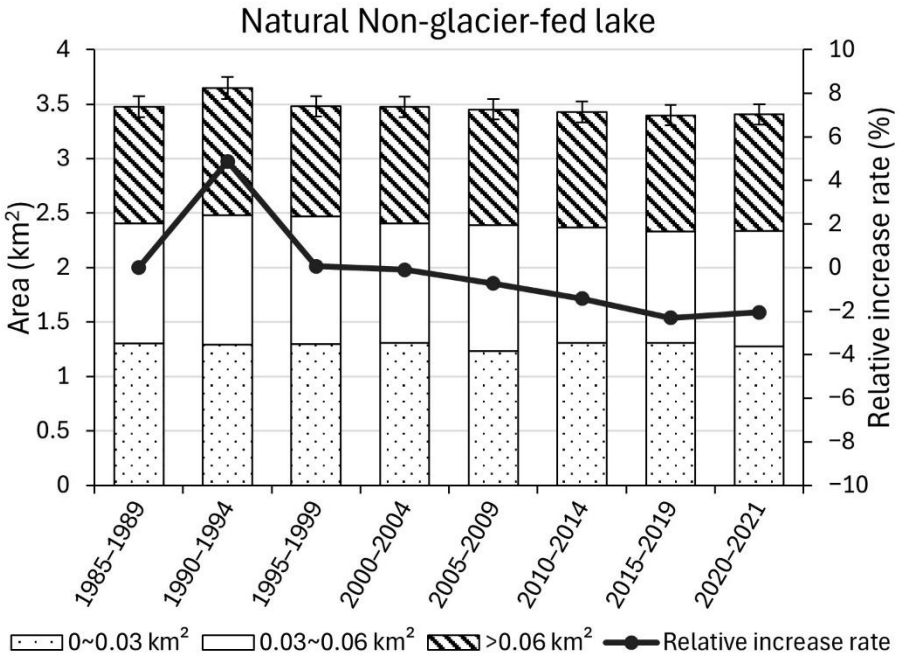
Natural Non-glacier-fed lake
Area (km²)
Relative increase rate (%)
4
3.5
3
2.5
2
1.5
1
0.5
0
10
8
6
4
2
0
−2
−4
−6
−8
−10
1985–1989
1990–1994
1995–1999
2000–2004
2005–2009
2010–2014
2015–2019
2020–2021
0~0.03 km²
0.03~0.06 km²
>0.06 km²
Relative increase rate

(c)

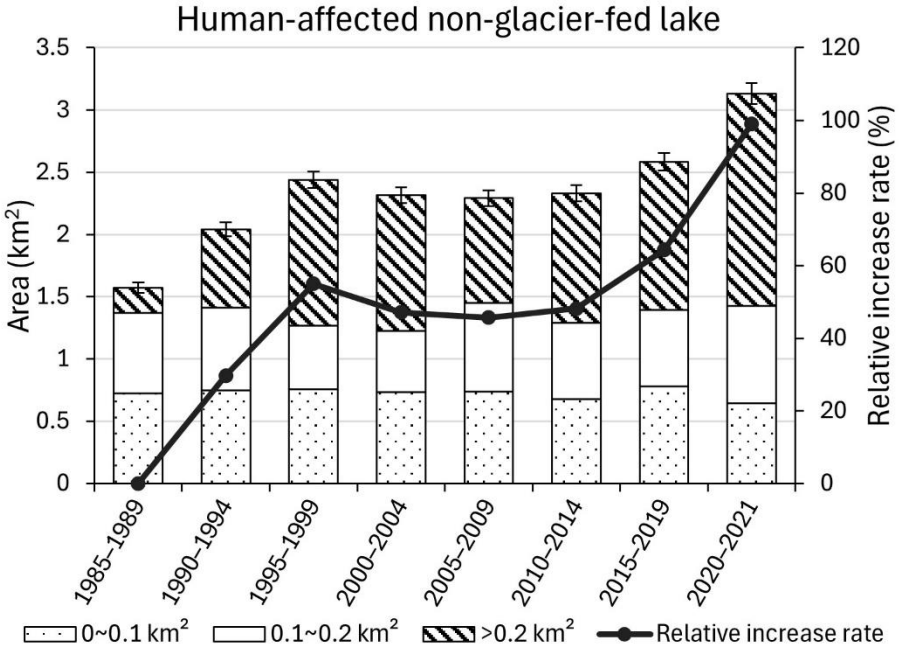
Human-affected non-glacier-fed lake
Area (km²)
Relative increase rate (%)
3.5
3
2.5
2
1.5
1
0.5
0
120
100
80
60
40
20
0
1985–1989
1990–1994
1995–1999
2000–2004
2005–2009
2010–2014
2015–2019
2020–2021
0~0.1 km²
0.1~0.2 km²
>0.2 km²
Relative increase rate

(d)

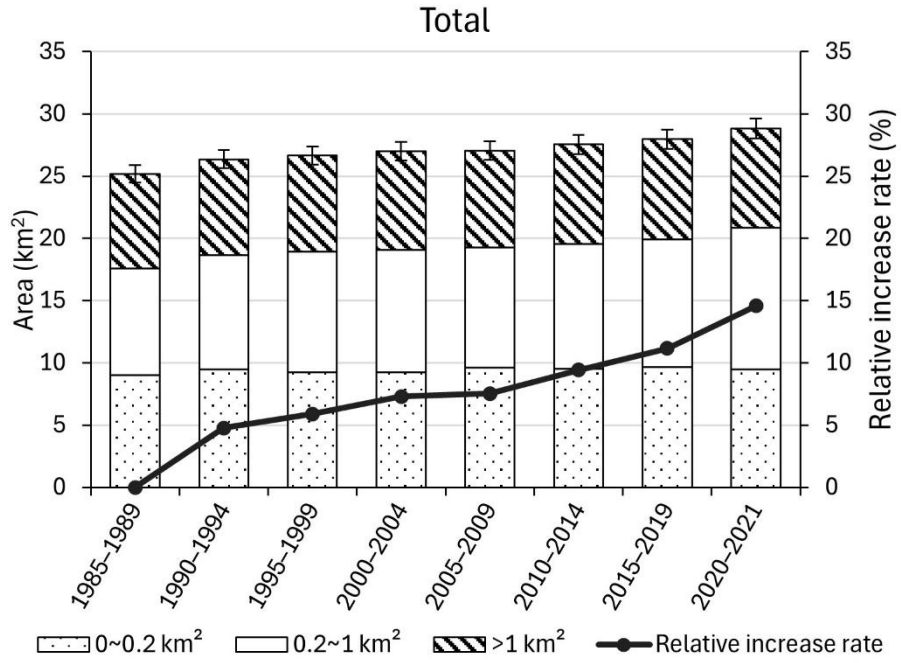


(e)

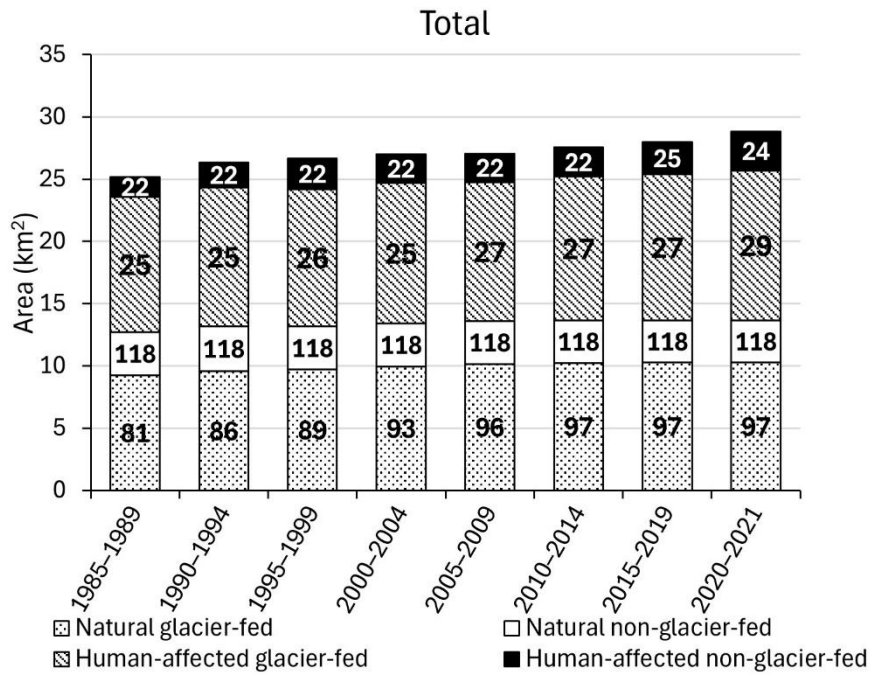


(f)

**Figure 3.11** Temporal changes in the area of (a–d) each lake type and (e) all types by area classification, and (f) the total area and number of each lake type

### 3.4.3. Comparison of glacier-fed lakes and non-glacier-fed lakes

To better understand the area change of each natural lake, the average lake area during dry months (May to September) for the period after 2014 and that before 1991 are compared.

It is evident from Figure 3.12 that the size of lakes decreased in most non-glacier-fed lakes, while there are more glacier-fed lakes that experienced an increase in area. Excluding newly formed lakes, those with an area greater than 0.03 $km^2$ before 1991 contributed nearly 85% of the remaining area growth in glacier-fed lakes. Lakes smaller than approximately 0.01 $km^2$ show a similar size distribution between glacier-fed and non-glacier-fed lakes. The total area for each type is significantly dominated by the top 40% of lakes.

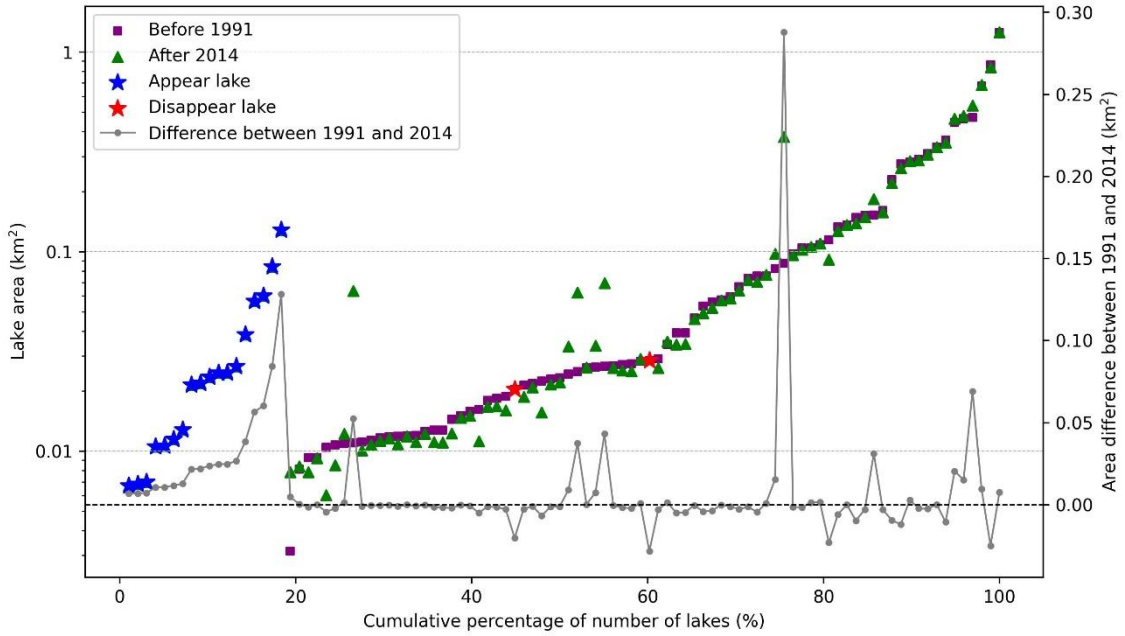


(a)

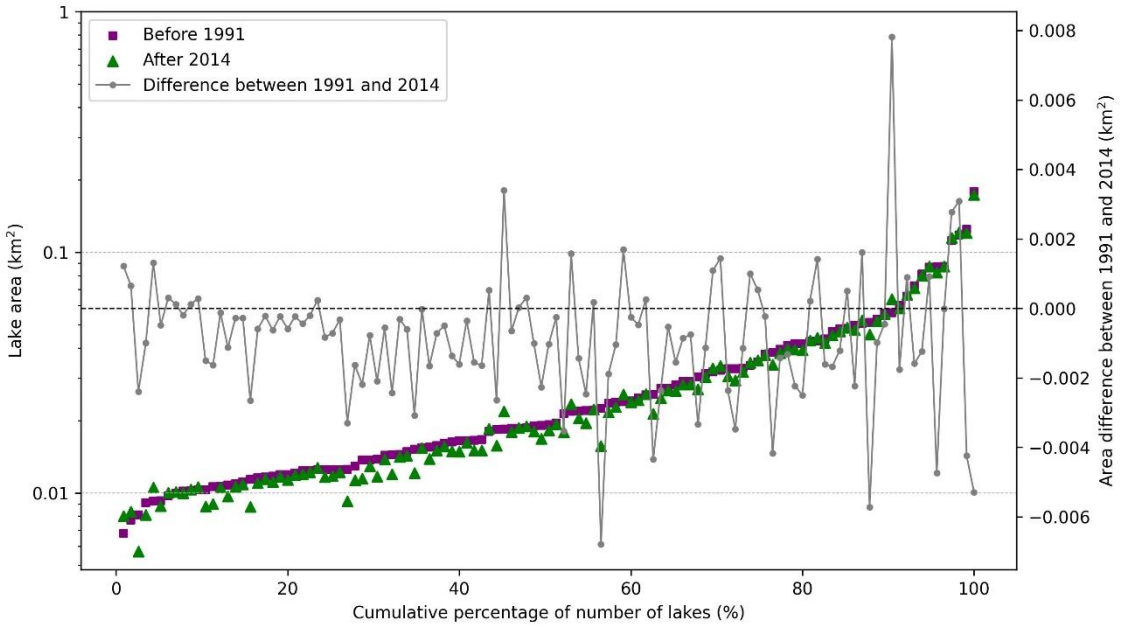


(b)

**Figure 3.12** Each lake area changes during the dry months (May to September) for the periods before 1991 and after 2014. (a) Glacier-fed lakes; (b) Non-glacier-fed Lakes. Lakes are sorted in ascending order based on their area during the period before1991.

The ratio of the average lake area during dry months (May to September) for the period after 2014 to that before 1991 is compared against the average lake area after 2014 (Figure 3.13). Lakes less than 0.01 $km^2$ were excluded considering detection errors. Also, for both periods before 1994 and after 2014, lakes for which the monthly average value could not be obtained for even one month are excluded from calculating the lake area ratio.

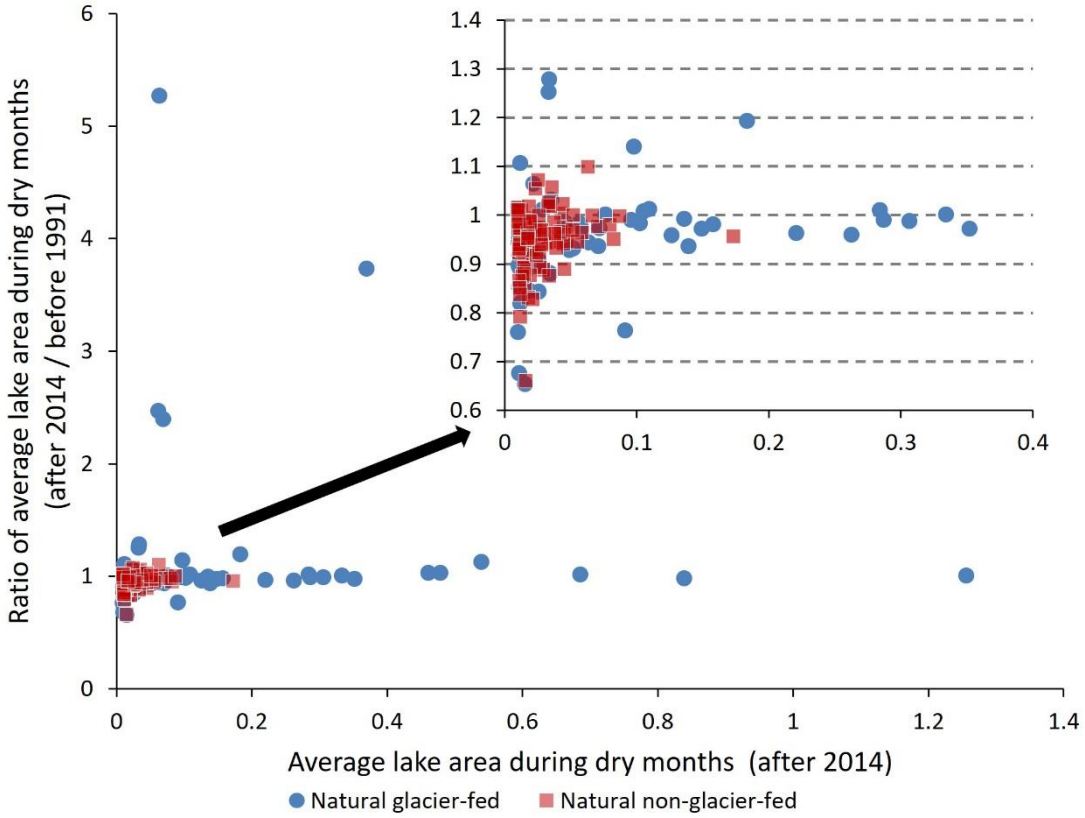


**Figure 3.13** The ratio of the average lake area during dry months (May to September) for the period after 2014 to that before 1991 compared against the average lake area after 2014.

Non-glacier-fed lakes tend to show a ratio less than 1, especially for lakes smaller than 0.05 km$^2$. Glacier-fed lakes experienced less change in lake area and a limited number of lakes show a ratio of less than 1.0, while a certain number of lakes exhibit large expansion (11 glacier-fed lakes show a ratio larger than 1.1).

The coefficient of variation (CV) of the mean monthly lake area during the dry months after 2014, calculated as the standard deviation of the mean monthly lake area divided by the mean monthly lake area, is determined for natural lakes. The histogram of CV for natural lakes indicates that non-glacier-fed lakes have a relatively higher CV, while many glacier-fed lakes show low values of CV (Figure 3.14). This result suggests that non-glacier-fed lakes are more susceptible to climate variability, leading to seasonal and inter-annual variations of inflow to the lake. The stability of inflow to glacier-fed lakes is reflected in their limited change in lake area, primarily due to smaller coefficients of variation in lake area (Figure 3.11 and 3.14)

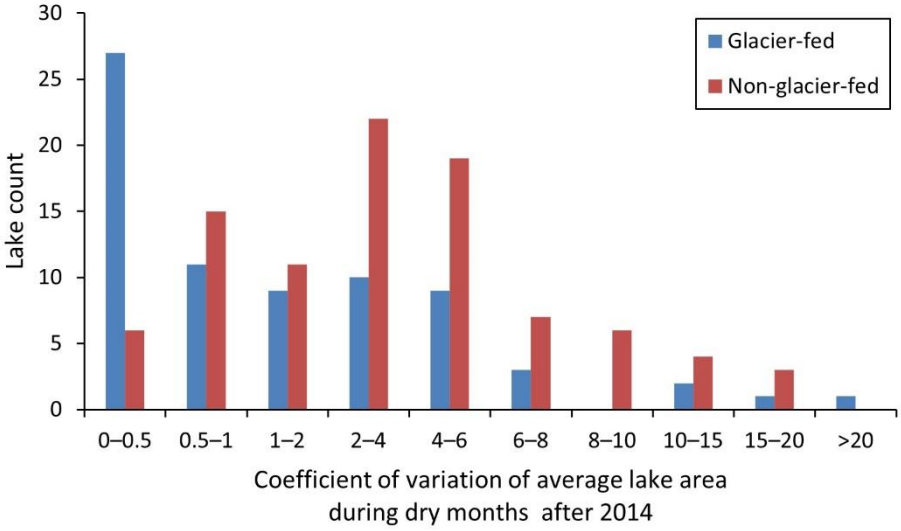


**Figure 3.14** Histogram of coefficient of variation of the average dry season area during dry months (May to September) after 2014.

### 3.5. Summary

This chapter has utilized 213 Landsat images to develop a semi-automated method for detail mapping the changes in lakes. In this study, several measurements and a careful validation process were carried out to map lakes comprehensively. To avoid missing newly formed lakes, especially those located in previous glacier regions with higher slopes, we carefully selected a slope threshold of 20°, which is higher than commonly used thresholds like 10° or 15°. Additionally, the slope was calculated for the entire lake object instead of a single pixel, further reducing the possibility of erroneously removing lakes. Manual visual inspections were conducted using high-resolution satellite images from Google Earth and ESRI to ensure that no such lakes were overlooked in the study region.

Although our study has detected a persistent increase in water surface area, the exclusion of human activity factors reveals the stable trend of natural glacier-fed lake area since 2010, which corresponds to the deceleration of glacier melting during the same period. Furthermore, no new naturally formed glacier-fed lakes have been found since 2015 while human activities have increasingly influenced the emergence of new lakes, reflecting the regional water resources development policies. Among the 25 new lakes that appeared during the study period, those appearing after 2015 were exclusively

human-built water reservoirs primarily serving nearby major cities in the southern Cordillera Real. These human-built reservoirs accounted for a water surface area 1.13 times larger than naturally occurring lakes.

# Chapter 4 Decadal climate change and its influence on glaciers and lakes

Chapter 4 begins with the selection of climate datasets focusing on temperature and precipitation. It provides a briefly overview of the spatial-temporal changes in climate factors within the study region. It investigates the correlation between glacier melting and changes in lake area under the influence of changing climate, examining both the entire study region and the catchment level. Finally, the chapter discusses the potential influence on water resources.

## 4.1. Selection of climate datasets

Temperature and precipitation play a pivotal role in glacier melting. To understand their influence on the long-term changes in glacier and glacier lake area (and volume), we compared our results of glaciers and glacier lakes with air temperature and precipitation within the study area. The area-averaged values of annual mean temperature and total precipitation for the study region were calculated for each hydrological year, i.e., from September in the preceding year to August in the present year. Based on the comparison with the observed data from specific sites, FLDAS and CHIRPS datasets were selected across various global datasets.

The information from the commonly used atmospheric reanalysis dataset and hydrological modeling system that contains precipitation and temperature data are summarized in Table 4.1. Considering the time coverage and spatial resolutions of the datasets, ERA5-Land and FLDAS are potential options for temperature data, as both started before the study period. For precipitation data, the possible datasets are ERA5, ERA5-Land, CHIRPS, FLDAS, TRMM, GPM, and GLDAS Noah.

To assess the reliability of these datasets, all of them were converted into monthly data. The Nash–Sutcliffe efficiency (NSE), RMSE-observations standard deviation ratio (RSR) and percent bias (PBIAS) were calculated using the observed data.

$$\mathrm{MSE} = \frac{\sum_{i=1}^{n}\left(X_{pre} - X_{obs}\right)^2}{N} \tag{4.1}$$

$$\mathrm{NSE} = 1 - \frac{\mathrm{MSE}}{\sigma_{\mathrm{obs}}^2} \tag{4.2}$$

$$\mathrm{RSR} = \frac{\sqrt{\mathrm{MSE}}}{\sigma_{\mathrm{obs}}} \tag{4.3}$$

$$\mathrm{PBIAS} = 100\frac{\sum_{i=1}^{n}(X_{\mathrm{pre}} - X_{\mathrm{obs}})}{\sum_{i=1}^{n} X_{\mathrm{obs}}} \tag{4.4}$$

where $X_{\mathrm{obs}}$ is monthly data from field observation, $X_{\mathrm{pre}}$ is the corresponding monthly data from the dataset that is being evaluated, and $\sigma_{\mathrm{obs}}$ is the standard deviation of the observation dataset.

NSE ranges between $-\infty$ and 1.0 (1 inclusive), with NSE = 1 being the optimal value. Values between 0.0 and 1.0 are generally viewed as acceptable levels of performance, whereas values <0.0 indicate that the mean observed value is a better predictor than the simulated value, which indicates unacceptable performance.

RSR varies from the optimal value of 0, which indicates zero RMSE or residual variation and therefore perfect model simulation, to a large positive value.

The optimal value of PBIAS is 0.0, with low-magnitude values indicating accurate model simulation. Positive values indicate overestimation bias, whereas negative values indicate model underestimation bias.

For temperature validation, daily average temperature data from El Alto International Airport (Lat: −16.510278, Lon: −68.198611) during 1980–2014 were obtained from the National Climate Data Center (https://www.ncei.noaa.gov/cdo-web/, accessed on 6 March 2023). The observation data was rescaled to the monthly average to allow the comparison with the ERA-5 Land and FLDAS datasets.

Monthly total precipitation data from eight sample sites in the study region during 2011–2017 was obtained from GRANDE/JSPS Bilateral Joint Research (http://grande.civil.tohoku.ac.jp/index_e.html, accessed on 12 June 2023) were used for precipitation validation. The average of the observation data was calculated and compared to the average of the three pixels that cover the eight locations. The comparison between observation data and the atmospheric reanalysis dataset and hydrological modeling system datasets are shown in Figure 4.1.

Table 4.1 Detailed information about atmospheric reanalysis dataset and hydrological modeling system datasets used in this study

| Full Name | Abbreviate | Domain | | Resolution | | Parameters | Data Types | Meteorological Inputs* | Institutional Sources | Reference | Data Access |
|---|---|---|---|---|---|---|---|---|---|---|---|
| | | Spatial | Temporal | Spatial | Temporal | | | | | | |
| ECMWF Reanalysis 5 | ERA5 | Global | 1979-2020 | 0.25o | Monthly | Temperature, precipitation | Reanalysis | — | ECMWF / Copernicus Climate Change Service | (Hersbach et al., 2020) | https://developers.google.com/earth-engine/datasets/catalog/ECMWF_ERA5_MONTHLY, accessed on 13 June 2023 |
| ECMWF Reanalysis 5-Land | ERA5-Land | Global | 1981-present | 0.1o | Monthly | Temperature, precipitation | Reanalysis | — | Google and Copernicus Climate Data Store | (Muñoz-Sabater et al., 2021) | https://developers.google.com/earth-engine/datasets/catalog/ECMWF_ERA5_LAND_MONTHLY_AGGR, accessed on 13 June 2023 |
| Climate Hazards group Infrared Precipitation with Stations (Version 2.0 Final) | CHIRPS | 50°S-50°N | 1981-present | 0.05o | Daily | Precipitation | Satellite | — | Climate Hazards Center UC SANTA BARBARA | (Funk et al., 2015) | https://chc.ucsb.edu/data/chirps, accessed on 12 July 2023 |
| Famine Early Warning Systems Network (FEWS NET) Land Data Assimilation System | FLDAS | 60°S-90°N | 1982-present | 0.1o | Monthly | Temperature, precipitation | Reanalysis | MERRA-2 & CHIRPS | NASA GES DISC at NASA Goddard Space Flight Center | (McNally et al., 2017) | https://developers.google.com/earth-engine/datasets/catalog/NASA_FLDAS_NOAH01_C_GL_M_V001, accessed on 13 June 2023 |
| Tropical Rainfall Measuring Mission 3B43 | TRMM 3B43 | 50°S-50°N | 1998-2019 | 0.25o | Monthly | Precipitation | Satellite | — | NASA GES DISC at NASA Goddard Space Flight Center | (Huffman et al., 2007) | https://developers.google.com/earth-engine/datasets/catalog/TRMM_3B43V7, accessed on 13 June 2023 |

(continued on next page)

Table 4.2 (continued)

| Full Name | Abbreviate | Domain | | Resolution | | Parameters | Data Types | Meteorological Inputs* | Institutional Sources | Reference | Data Access |
|---|---|---|---|---|---|---|---|---|---|---|---|
| | | Spatial | Temporal | Spatial | Temporal | | | | | | |
| Global Precipitation Measurement v6 | GPM | Global | 2000-2021 | 0.1o | Monthly | Precipitation | Satellite | — | NASA GES DISC at NASA Goddard Space Flight Center | (Precipitation Processing System (PPS) At NASA GSFC, 2019) | https://developers.google.com/earth-engine/datasets/catalog/NASA_GPM_L3_IMERG_MONTHLY_V06#bands, accessed on 13 June 2023 |
| Global Land Data Assimilation System Noah Land Surface Model L4 V2.1 | GLDAS Noah | 60°S-90°N | 2000-present | 0.25o | Monthly | Temperature, precipitation | Reanalysis | GDAS, GPCP, & AGRMET | Goddard Earth Sciences Data and Information Services Center (GES DISC) | (Rodell et al., 2004) | https://disc.gsfc.nasa.gov/datasets/GLDAS_NOAH025_M_2.1/summary, accessed on 13 June 2023 |

*Full name for meteorological inputs:
MERRA- 2: Modern-Era Retrospective analysis for Research and Applications version 2
GDAS: Global Data Assimilation System
GPCP: Global Precipitation Climatology Project
AGRMET: AGRicultural METeorological modeling system

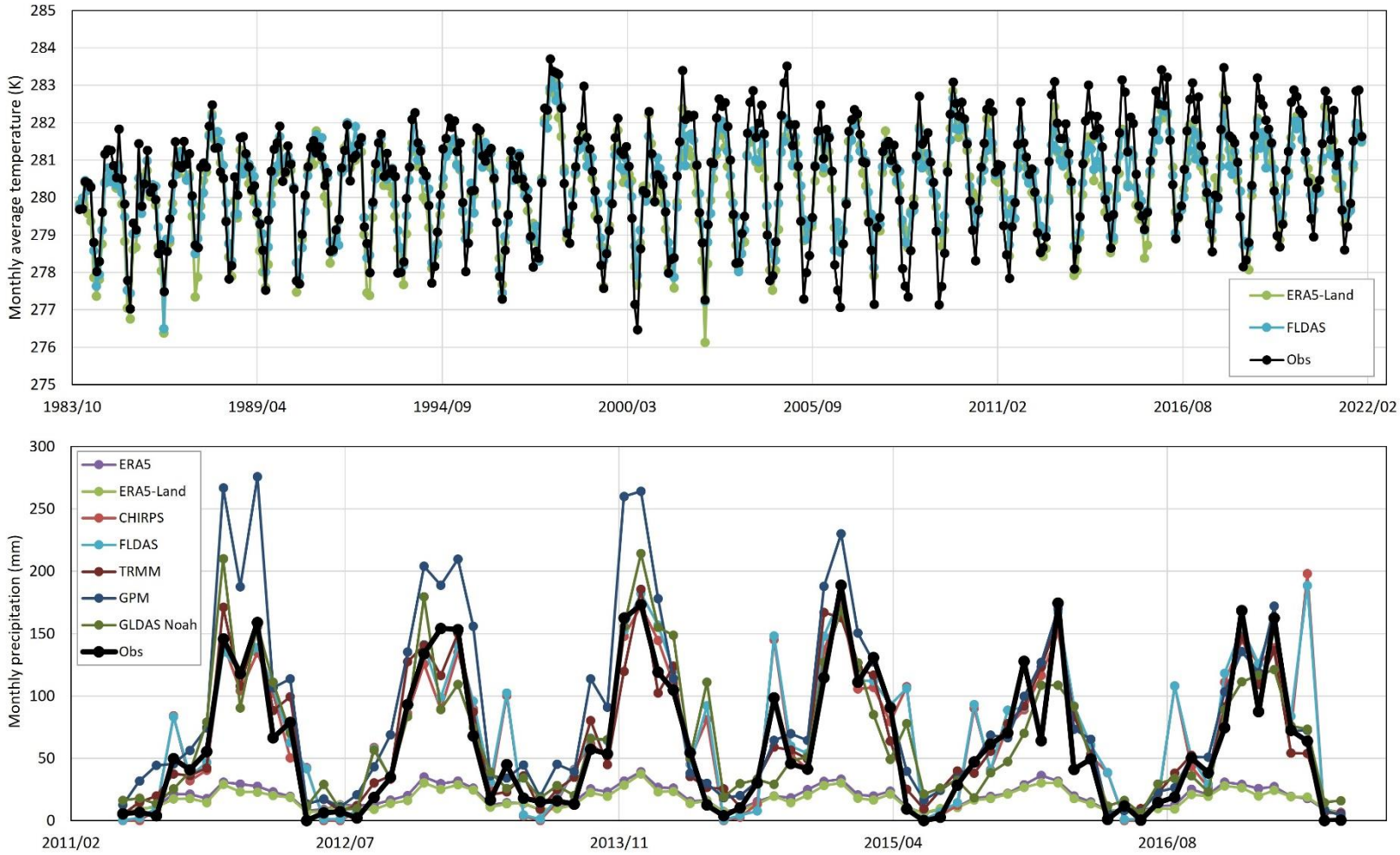


**Figure 4.1** Comparison between observation data and the atmospheric reanalysis dataset and hydrological modeling system datasets. Observed precipitation data are the average of precipitation measured at eight locations in the Tuni Lake catchment.

Table 4.3 Evaluation of climate datasets.

| | NSE | RSR | PBIAS |
|---|---|---|---|
| **Temperature** | | | |
| ERA5-Land | 0.815 | 0.430 | −0.106 |
| FLDAS | 0.821 | 0.423 | −0.052 |
| **Precipitation** | | | |
| ERA5 | −0.340 | 1.157 | −68.747 |
| ERA5-Land | −0.424 | 1.193 | −72.092 |
| CHIRPS | 0.651 | 0.590 | 11.020 |
| FLDAS | 0.648 | 0.593 | 18.569 |
| TRMM | 0.872 | 0.358 | 5.341 |
| GPM | 0.498 | 0.708 | 38.647 |
| GLDAS Noah | 0.674 | 0.571 | 6.769 |

While the temperature given in ERA5 Land represents the temperature of air at 2 m above the surface, FLDAS gives near-surface air temperature, but they did not show much difference. As can be seen from Figure 4.1, compared to observation data from El Alto airport, both datasets have relatively higher temperatures during the dry season. Based on NSE, RSR, and PBIAS, both datasets could be considered acceptable in predicting temperature, and FLDAS has slightly better performance than ERA5-Land.

As for precipitation data, TRMM 3B43 exhibits the best performance, followed by GLDAS Noah and CHIRPS. However, TRMM 3B43 and GLDAS Noah have shorter time coverage, starting from 1998 and 2000, respectively, making them unsuitable for comparing long-term lake changes. Therefore, CHIRPS precipitation data are utilized instead.

## 4.2. Spatiotemporal changes in climate factors in the study region

Based on FLDAS (Figure 4.2), the yearly average temperature is typically around 274.1K (0.95 °C), and an increasing trend can be seen, with notably higher temperatures observed in 1998, 2010, 2016, and 2019–2020. Torres-Batlló and Martí-Cardona (2020) also validated the CHIRPS precipitation dataset in the study region, observing a rise in precipitation during 1981–2018. According to CHIRPS, the yearly total precipitation is usually between 800 mm and 1000 mm. The lowest precipitation was recorded in 1992

and 2005, while relatively higher precipitation can be observed in recent years except for 2009, and the highest precipitation occurred from 2018 to 2019.

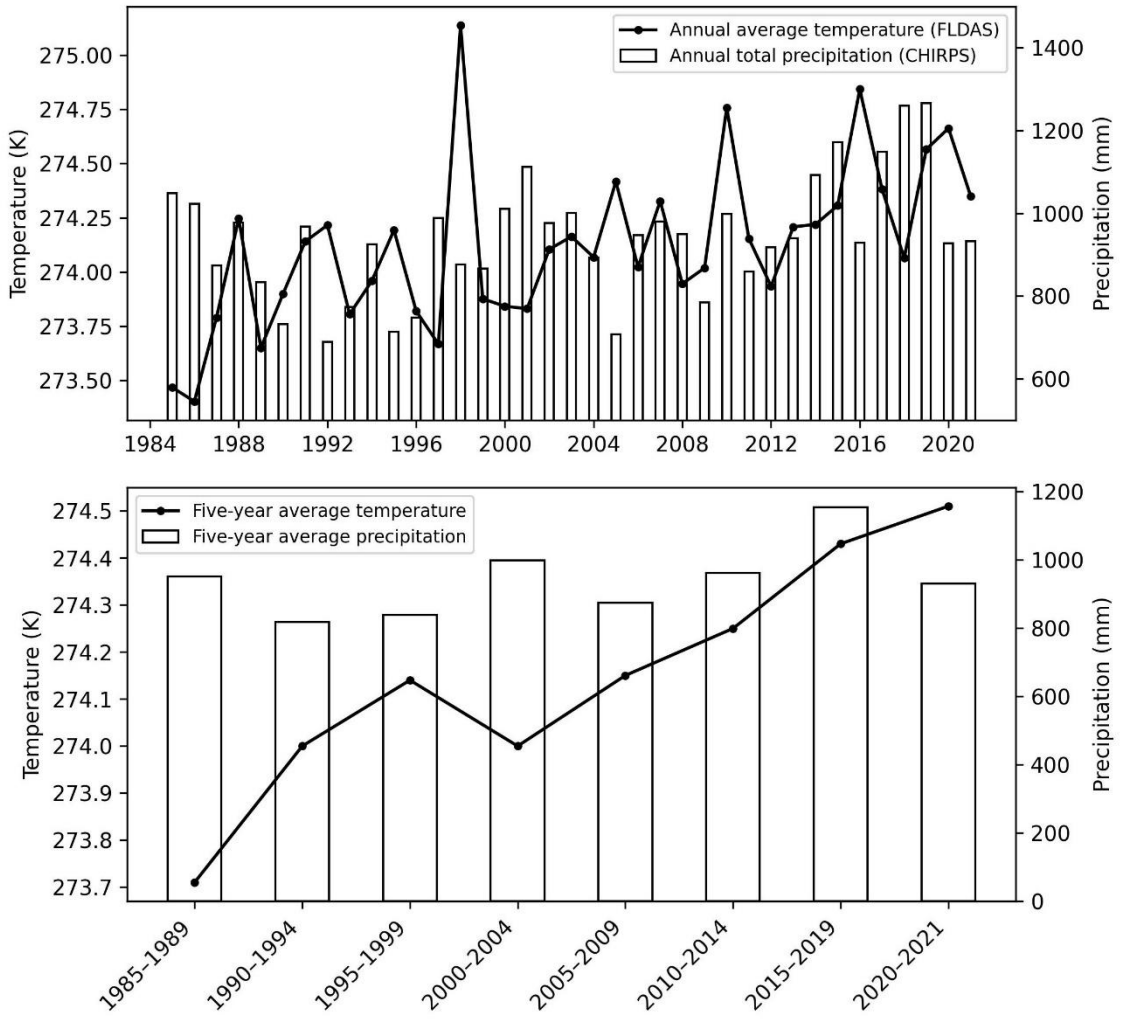


**Figure 4.2** Temperature data from FLDAS and precipitation data from CHIRPS in the study region. Above: annual data; Below: five-year average corresponding to the period for glacier and glacial lakes analysis.

The yearly average temperature in the Amazon basin on the eastern side of the Cordillera Real was higher than the western Altiplano plateau due to the lower elevation. From 1985 to 2021, a noticeable increase in temperature was observed, with the higher elevation regions experiencing more significant increases compared to the lower elevation Amazon basin (Figure 4.3).

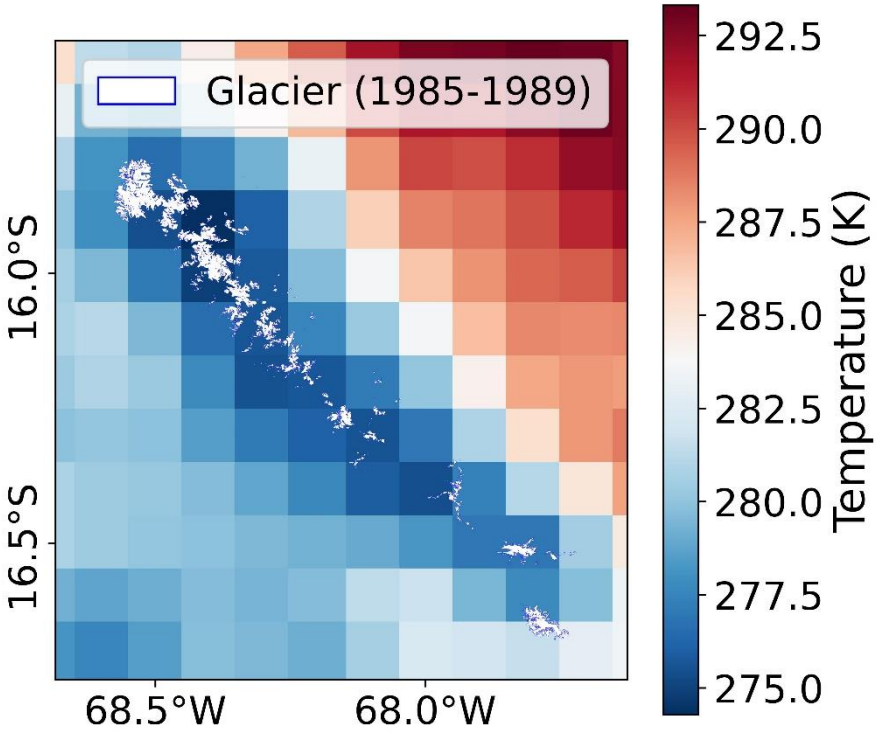
Glacier (1985-1989)
16.0°S
16.5°S
68.5°W
68.0°W
292.5
290.0
287.5
285.0
282.5
280.0
277.5
275.0
Temperature (K)

(a)

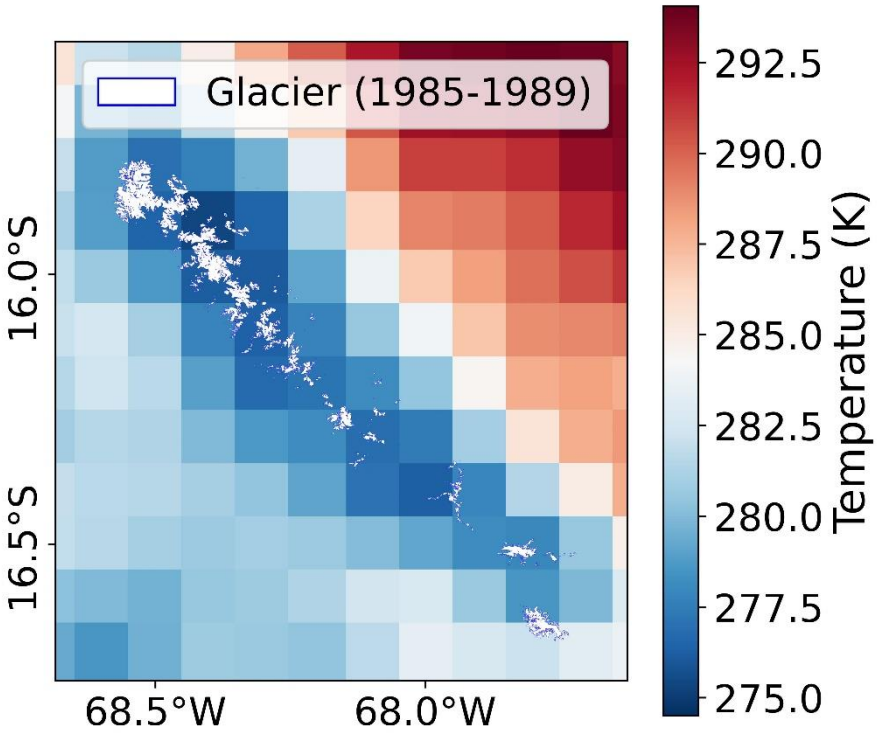
Glacier (1985-1989)
16.0°S
16.5°S
68.5°W
68.0°W
292.5
290.0
287.5
285.0
282.5
280.0
277.5
275.0
Temperature (K)

(b)

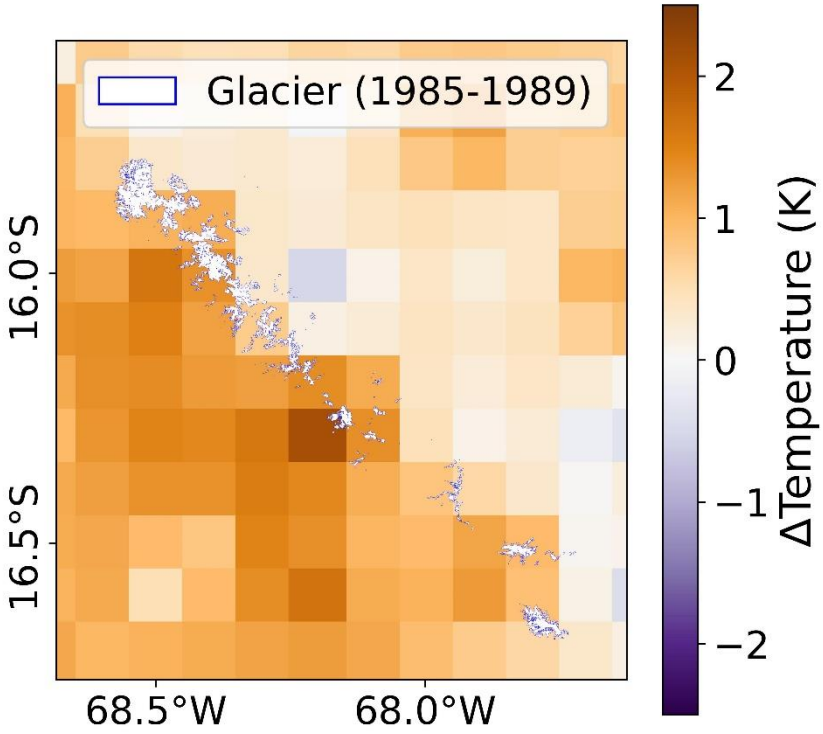


(c)

**Figure 4.3** (a) and (b) Yearly average temperatures in the research region from ERA5-Land for 1985 and 2021; (c) Difference in yearly average temperatures between 1985 and 2021 (temperature in 2021 minus temperature in 1985).

In contrast to temperature, yearly total evaporation exhibited a different spatial pattern. Evaporation rates were relatively higher on the eastern side of the Cordillera Real than on the western side. Unlike temperature, which tends to be lowest at the highest elevation mountain ranges, evaporation decreased from east to west across the study area. The changes in evaporation between 1985 and 2021 varied on both sides of the Cordillera Real, with an increase observed in the eastern Amazonia region and a decrease in the western region (Figure 4.4).

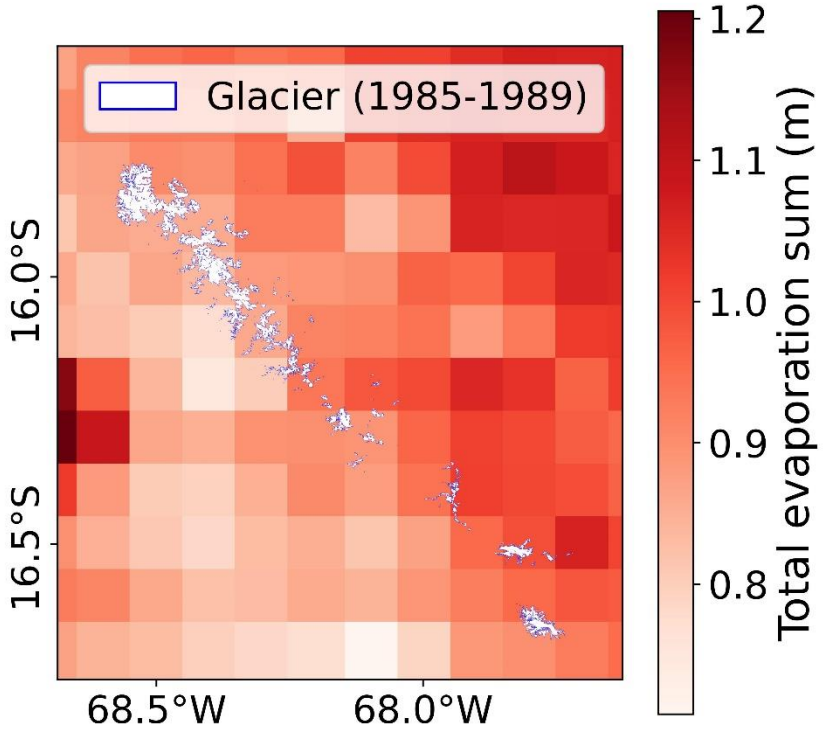
Glacier (1985-1989)
16.0°S
16.5°S
68.5°W
68.0°W
1.2
1.1
1.0
0.9
0.8
Total evaporation sum (m)

(a)

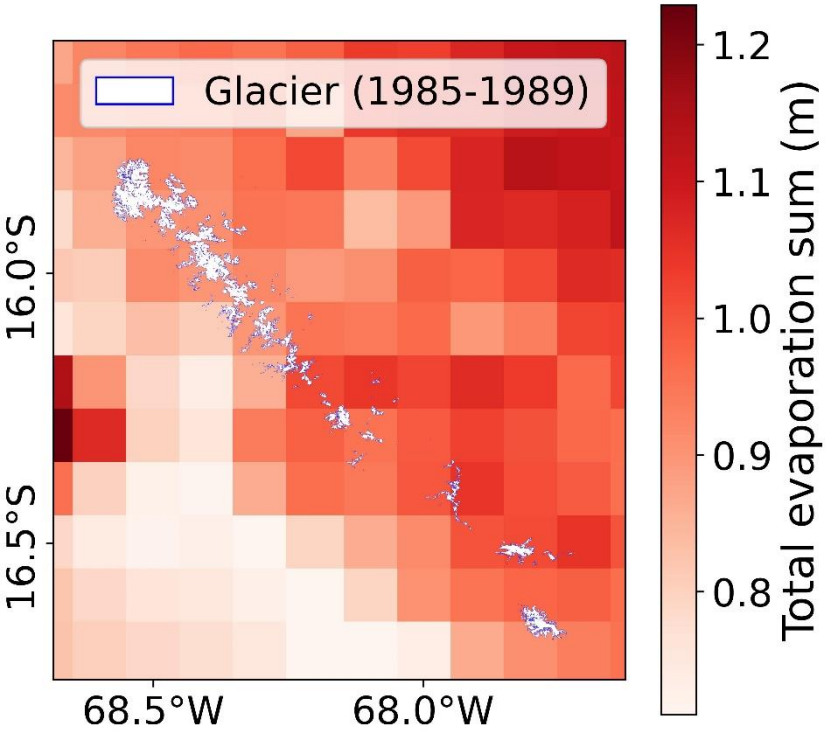
Glacier (1985-1989)
16.0°S
16.5°S
68.5°W
68.0°W
1.2
1.1
1.0
0.9
0.8
Total evaporation sum (m)

(b)

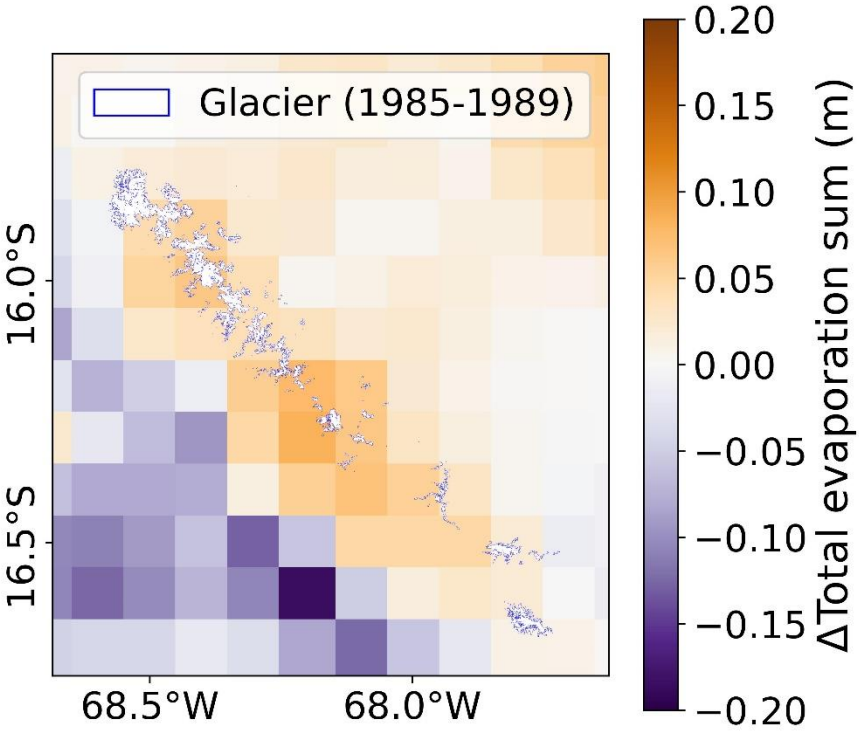


(c)

**Figure 4.4** (a) and (b) Yearly total evaporation in the research region from ERA5-Land for 1985 and 2021; (c) Difference in yearly total evaporation between 1985 and 2021 (total evaporation in 2021 minus total evaporation in 1985).

Precipitation data from CHIRPS showed significant differences between the eastern and western sides of the Cordillera Real, with much higher precipitation on the eastern side. Over the years, the western side experienced greater precipitation increases, while relatively high-elevation regions on the eastern side showed slight decreases despite an overall regional increase (Figure 4.5).

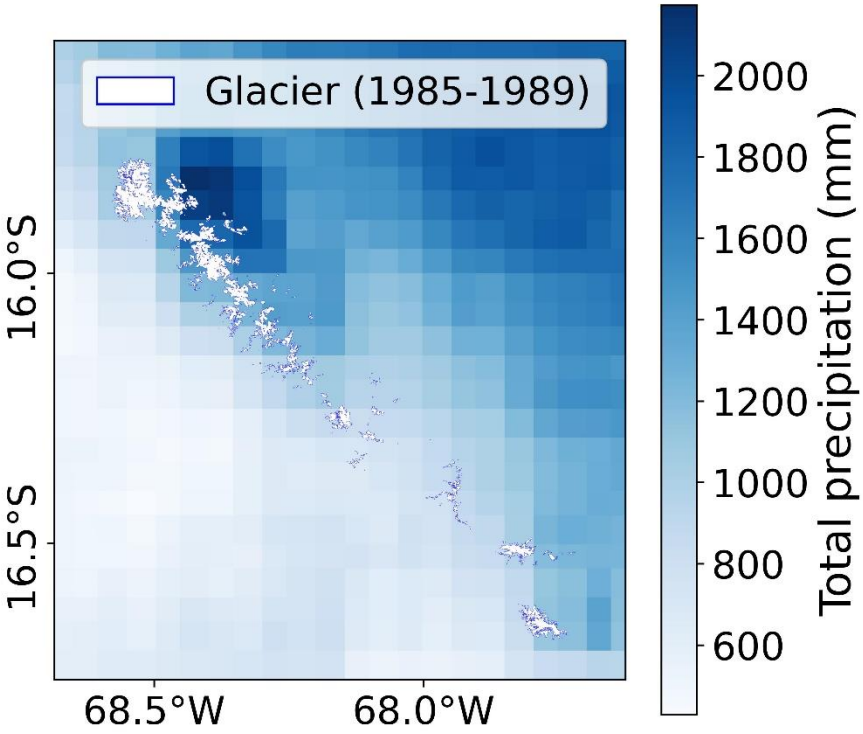
Glacier (1985-1989)
16.0°S
16.5°S
68.5°W
68.0°W
2000
1800
1600
1400
1200
1000
800
600
Total precipitation (mm)

(a)

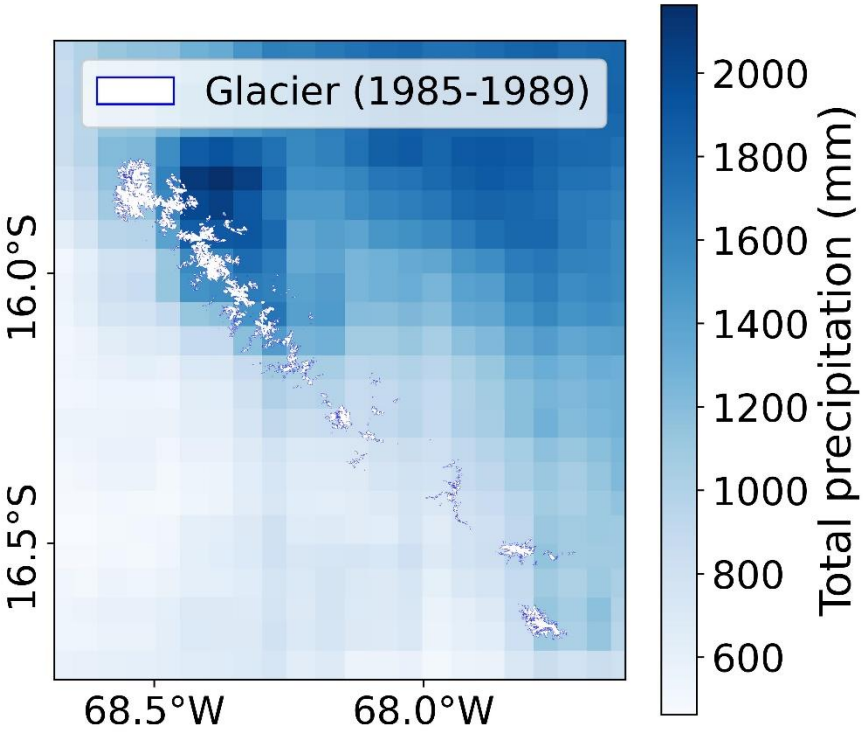
Glacier (1985-1989)
16.0°S
16.5°S
68.5°W
68.0°W
2000
1800
1600
1400
1200
1000
800
600
Total precipitation (mm)

(b)

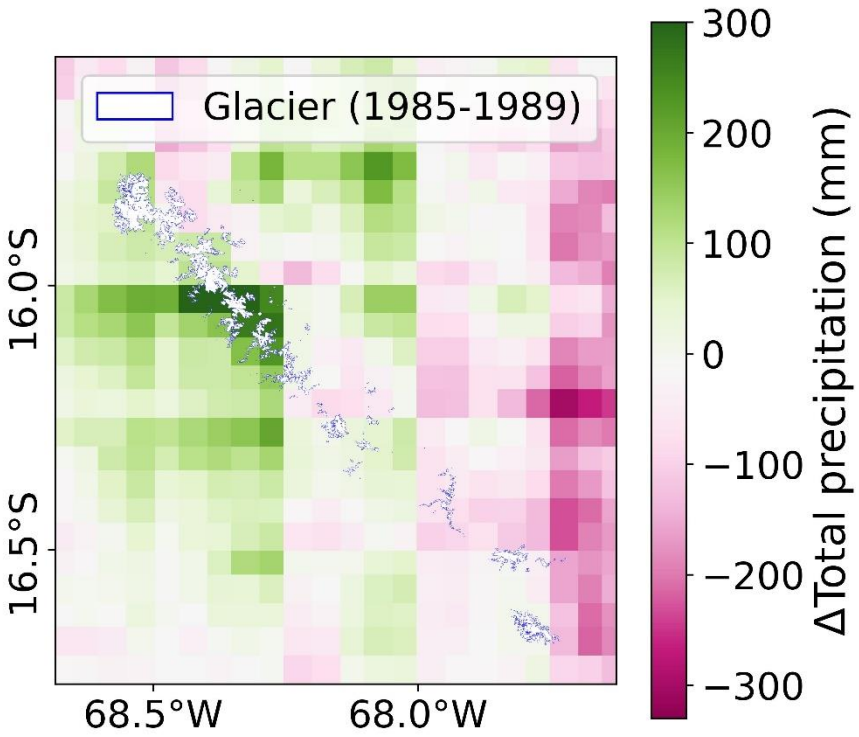


(c)

**Figure 4.5** (a) and (b) Yearly total precipitation in the research region from CHIRPS for 1985 and 2021; (c) Difference in yearly total precipitation between 1985 and 2021 (total precipitation in 2021 minus total precipitation in 1985).

### 4.3. The impact of temperature and precipitation on glacier and glacial lakes

Rising temperatures play an essential part in accelerating the melting of glaciers (Zhang et al., 2019). This warming effect is particularly evident at lower elevations, where precipitation falls as rain under relatively high temperatures at low altitudes. The combination of higher temperatures and rainfall enhances the melting of glaciers (Woo, 1990). In contrast to previous studies that exclusively utilized satellite images within specific years, this study has employed all the Landsat images devoid of cloud interference and short-term snow cover. Combining the glacier information at a uniform five-year interval, we have clarified the trend in glacier melting, enabling confirmation of the influence from global warming. During the period of 2015–2019, despite higher total precipitation, the glacier area decreased compared to the preceding period. This suggests a stronger impact from unprecedented high temperatures, notably in the years 2016 and 2020.

Precipitation has a mixed effect on glacier dynamics. At higher elevations or during colder periods, precipitation occurs as snowfall, contributing to glacier accumulation (Mott et al., 2019). A notable example is the period between 2000 and 2004, characterized by lower temperatures and abundant precipitation, resulting in increased or almost stable glacier area above 5200 m.a.s.l. However, glaciers at lower elevations continued their decreasing trend, underscoring the complex interplay between temperature and precipitation in affecting the dynamics of glaciers at different elevations.

Rising temperatures directly escalate lake evaporation, while precipitation augments lake inflow, providing direct water resources. This is particularly evident in non-glacier-fed lakes unaffected by human water management (Figure 3.11c). The total area of these lakes remained nearly constant throughout the study period, even post-2015 when precipitation surpassed the levels of previous years. The heightened evaporation due to the warming climate is likely the underlying cause.

With the anticipated increase in precipitation (CMIP5) (Taylor et al., 2012), along with the resilience of remaining glaciers at higher elevations, the deceleration in glacier melting shall continue. However, temperature will continue to be the predominant factor, with ongoing global warming, glaciers are inevitably destined to melt further.

## 4.4. The inherent connection between glacier melting and lake area under the changing climate

Glacial erosion creates deep depressions or overdeepenings in the landscape as glaciers move and carve through the underlying bedrock. When glaciers retreat or melt, these depressions may become filled with water, forming glacial lakes. Sediment accumulation, which includes rocks, gravel, sand, and clay carried by glaciers, can also contribute to the formation of natural barriers or dams that trap water in these depressions. During the research period, the formation of 18 natural glacial lakes was observed, all of which were located in areas where glaciers have retreated, indicating the contribution of glacial erosion as well as sedimentation. However, the sustainable formation of glacial lakes is not solely dependent on these processes. Factors such as

meltwater from glaciers, inflows from precipitation and snowmelt, as well as water loss through evaporation, can all influence the size and depth of the lakes.

### 4.4.1. Analysis on the whole study region

Glacial lakes are closely connected to the runoff from melting glaciers, contributing significantly to their water storage, and supporting lake expansion (Bajracharya and Mool, 2009). Moreover, the exacerbation of ongoing global climate change has notably fortified this correlation. In this study, to find out the inherent connection between glacier melting and lake area under the changing climate, the $R^2$ of the linear relationship between the area of the glacier, area of natural lakes, average temperature, and precipitation during the corresponding time period was calculated (Figure 4.6). Currently, many studies have proved that the increased precipitation intensity not only directly increases the inflow to lakes (Qiao and Zhu, 2019) but also mitigates glacier melting through snowfall by reducing surface albedo (Yue et al., 2022), thereby inhibiting the replenishment of water resources by glacial meltwater. This complex interaction between lake area and precipitation cannot be merely characterized by a positive or negative linear relationship. The anticipated increase in temperature in the Cordillera Real adds an additional layer of complexity.

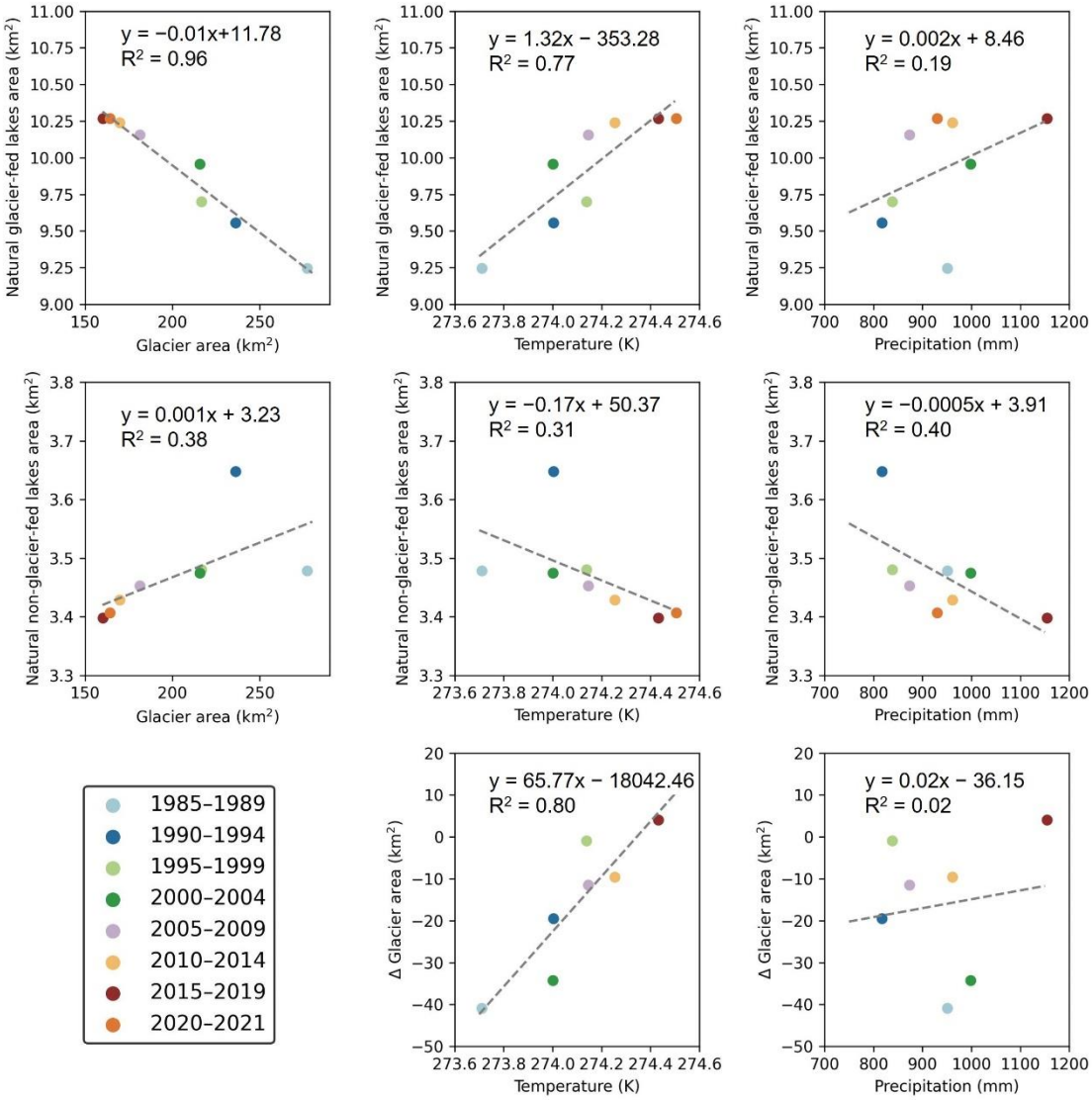


**Figure 4.6** Correlation between glacier area, natural glacier-fed and non-glacier-fed lake area, average temperature, and average yearly precipitation of the corresponding period, and correlation between glacier area change from the previous period and the temperature and precipitation.

Rising temperatures have led to an increase in the annual flow of glacial meltwater from glaciers to lakes (Zhang et al., 2019). In Figure 4.6, glacier area has shown a significant negative relationship with temperature, and the area of glaciers also shows a linear relationship with the area of natural glacier-fed lakes, with R2 being as high as 0.96. As rising temperatures accelerate the melting of glaciers, the annual glacier runoff volume generally rises until it peaks. Beyond this point, runoff decreases as glaciers become unable to sustain previous meltwater volumes (Jansson et al., 2003).

Consequently, rising temperatures do not consistently contribute to the expansion of lakes. The halt in natural glacial lake expansion observed in our research may serve as evidence supporting the projections made by Huss and Hock (Huss and Hock, 2018) in their global-scale study, indicating that Bolivian glaciers are either near or have already reached their maximum runoff. Even though lakes categorized as receiving glacier meltwater exhibit a linear correlation with temperature, $R^2$ was as high as 0.77 during the study period. Due to the diminishment of glaciers, a future temperature increase would be insufficient to yield a commensurate supply of glacial meltwater. Instead, it could promote evaporation from the lake water surface, ultimately leading to a reduction in the area of glacial lakes.

### 4.4.2. Analysis on catchment-level

To comprehensively evaluate the impact of long-term climate change on these glaciers and their downstream effects, continuous and up-to-date monitoring of glacier dynamics and their associated glacial lakes is crucial, an aspect that has been lacking in previous research. Through the calculation of streams and catchments, we establish hydrological connections between glaciers and lakes, enabling an analysis of the correlation between glacier-fed lakes and their source glaciers while considering the influence of multiple climate factors, including temperature, precipitation, and evaporation.

#### 4.4.2.1. Catchment delineation

To analyze the hydrological connections between glaciers and lakes, the study region was divided into sub-catchments based on a stream map calculated from the SRTM DEM using ArcGIS Pro 3.2. Sinks in the DEM were removed using the Fill function, and flow direction and accumulation were calculated.

Streams were defined as pixels receiving flow from more than 10,000 pixels, and their confluences were defined as pour points (outlets) for calculating watersheds.

Watersheds that contained glaciers or lakes located higher than 4300 m.a.s.l during the study period were defined as target watersheds and numbered (Figure 4.7). Glacier areas were extracted from the glacier map, and the summed area of lakes receiving glacier meltwater was defined as the water surface area for each watershed.

For detailed analysis of lakes and their glacier meltwater sources, the watershed feeding each lake was calculated, with the outlet defined as the lowest-elevation pixel in the lake.

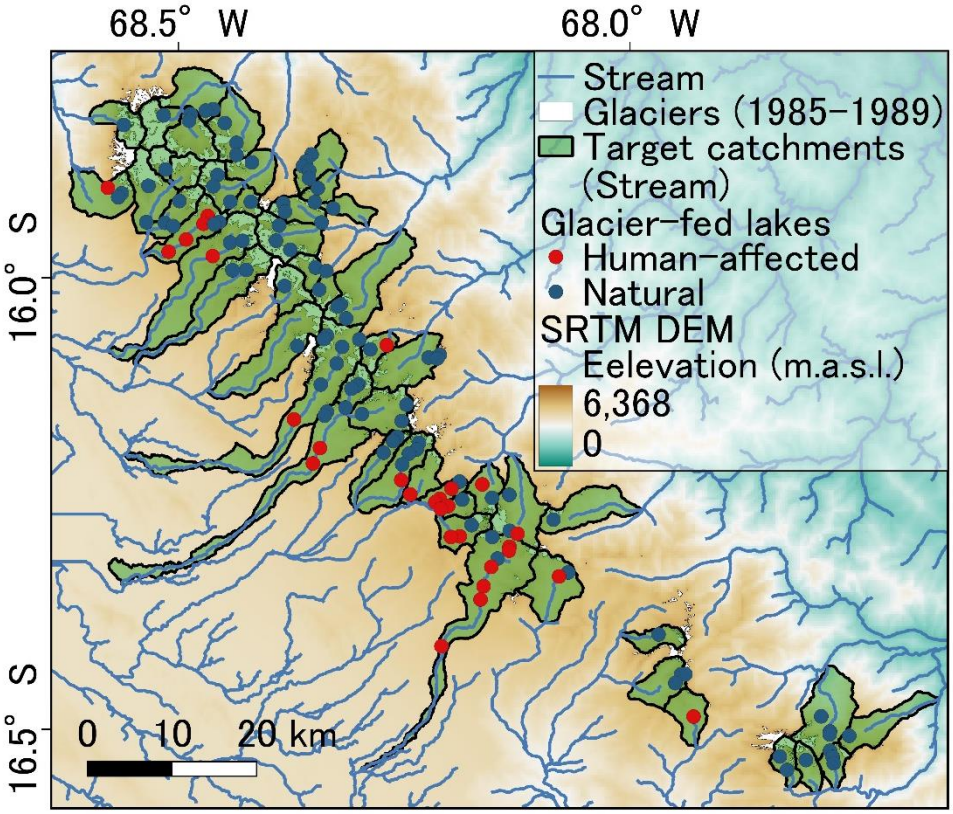


**Figure 4.7** Target catchments calculated from stream (n=28) and the distribution of glacier-fed lakes in the catchments.

Temperature and evaporation datasets were extracted from the ERA-5 Land, and precipitation data from CHIRPS. Both datasets were acquired from the GEE platform, and area-weigh averages were calculated using built-in GEE functions. For CHIRPS which is originally daily datasets, the monthly and yearly data were summed using Python Pandas.

4.4.2.2. Catchment of streams

There were a total of 77 catchments have contained both glaciers and lakes during the study period from 1984 to 2021. Based on the stream map, we confirmed that glacier meltwater flows into the lakes in 52 catchments. To allow a comparison between glaciers and lakes in different size, the area was first normalized to 0-100% following equation:

$$A_i(\%) = \frac{A_i - A_{min}}{A_{max} - A_{min}} \tag{4.5}$$

where $A_i$ represents the area in $i$ period, $A_{min}$ and $A_{max}$ are the maximum and minimum area during the whole study period.

Although glacier decline was observed in all catchments, with most experiencing rapid retreat during 1985-2014 followed by a slower trend in the recent decade (Figure 4.8), the change in water surface area did not always increase correspondingly.

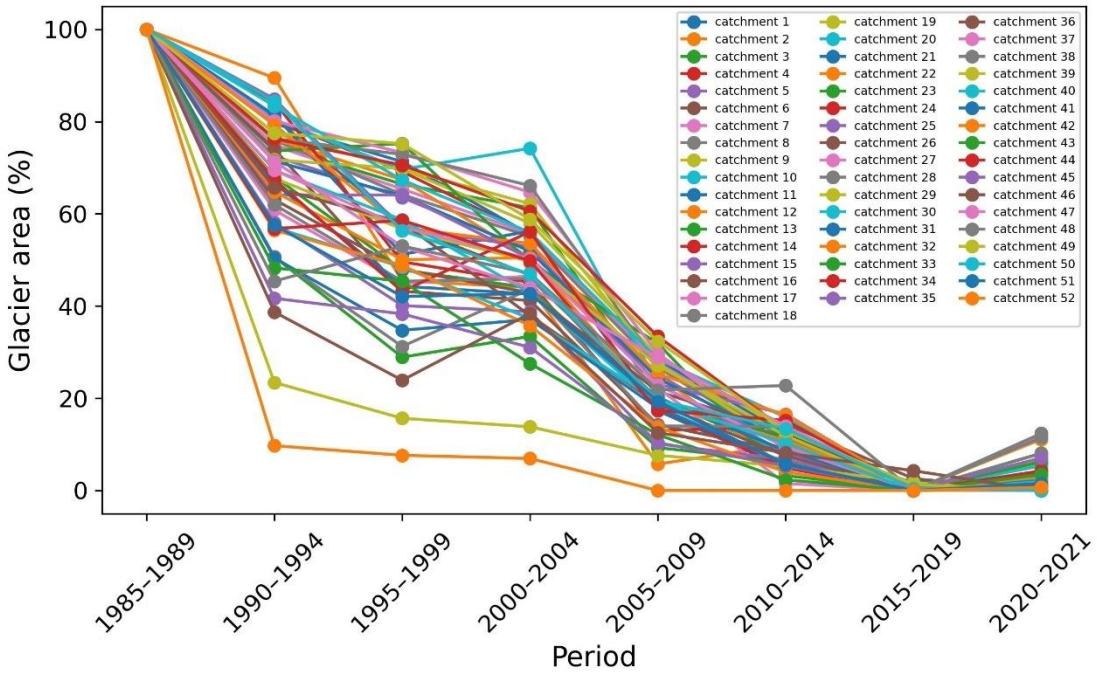


**Figure 4.8** Glacier area change in 52 catchments from 1985 to 2021.

To analyze the changes in water surface area in each catchment, catchments with a difference between maximum and minimum water surface area less than 9,000 m² were excluded from the analysis, as geometric constraints can limit a lake's ability to reflect changes in water resources. Additionally, lakes influenced by human-built water dams were excluded from the total water surface area calculations of the catchments. This exclusion left 28 catchments with changes larger than 9,000 m².

Given that the glacier areas were relatively similar during the periods from 1990 to 2004 and from 2010 to 2021, the average water surface and glacier areas for these two periods were calculated. The changes in the areas of glaciers and lakes in the same

catchments, shown in Figure 4.9, were determined by subtracting the average area from 1990 to 2004 from the average area from 2010 to 2021.

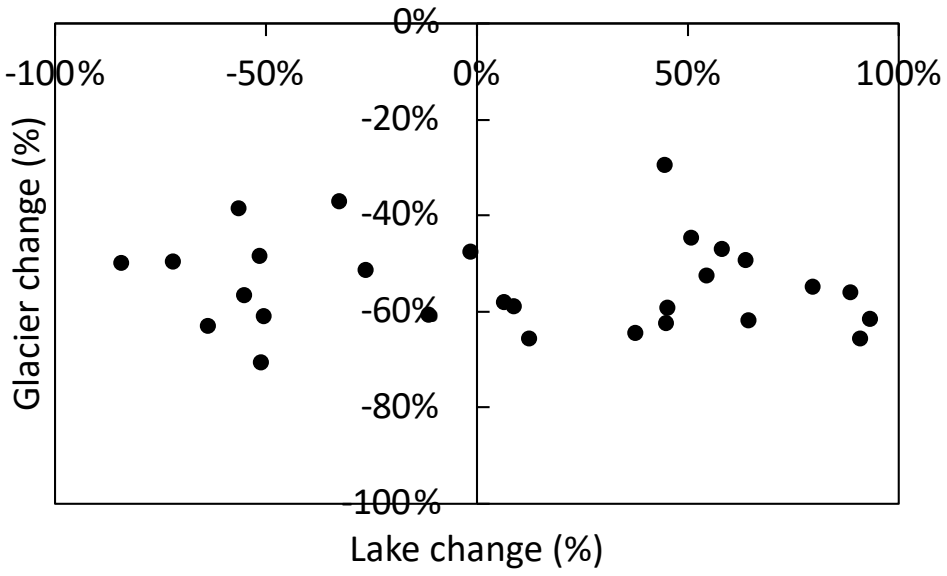


**Figure 4.9** Lake and glacier area change in the same catchment between 2010 – 2021 and 1990 – 2004.

If glacier meltwater solely contributed to lake expansion, water surface area should increase as glaciers decline. Considering the inherent uncertainties due to the 30 m spatial resolution of Landsat images, area changes larger than 5,000 m² were regarded as significant to mitigate the influence of minor inaccuracies. As a result, only 13 catchments showed an increase in water surface area. These catchments all contained glacial lakes located on or next to glaciers, suggesting that meltwater contributes significantly to the water surface increases. The ratio between glacier loss and lake area increase varied across catchments. Seven catchments had stable water surface changes (< 5000 $m^2$), and eight experienced obvious decreases despite glacier melting, indicating that in some catchments, glacier meltwater might no longer be the primary contributor, and climate factors like temperature, precipitation, and evaporation could impact lake water resources.

To better assess the impact of glacier meltwater on lake water resources, the catchment of individual lakes was calculated to investigate the relationships between lake area, its source glacier area, and their interplay.

4.4.2.3. Catchments of individual lakes

Focusing on lakes primarily influenced by glacier melting, lake catchments with maximum glacier cover less than 20% or non-glacier areas larger than 10 km² were excluded, as were lakes with maximum areas no more than 6 pixels larger than their minimum areas due to geometric constraints.

Similar to the above analysis of stream catchments, the average lake and glacier areas during the two periods, from 1990 to 2004 and from 2010 to 2021, were calculated. The area change of each lake during these two periods was compared with the area change of the glaciers providing meltwater. Additionally, the distance of each lake to its nearest glacier was calculated to provide more information. A total of 47 lake catchments remained (Figure 4.10), with 20 lakes having smaller average area during 2010-2021 than in 1990-2004, and 27 lakes showing increased area.

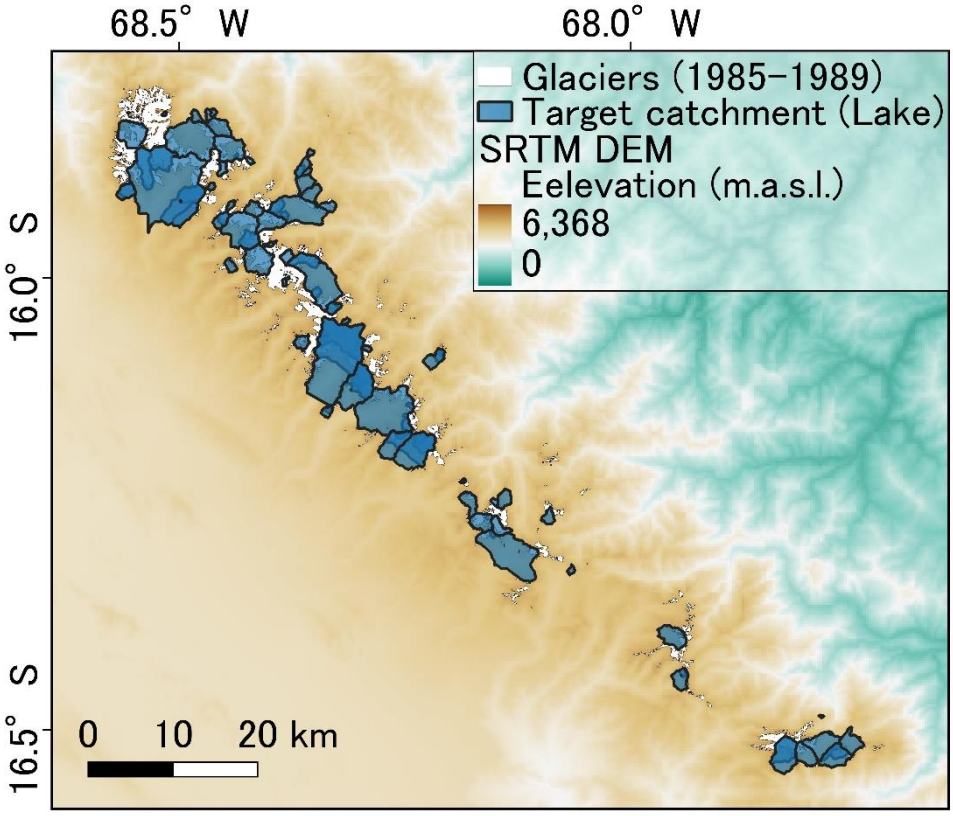


**Figure 4.10** Target catchments calculated from natural glacier-fed lakes (n=47).

For lakes very close to or even on the glaciers (distance less than 0.4 km), lake area was primarily influenced by glacier meltwater, increasing as glaciers retreated (Figure 4.11).

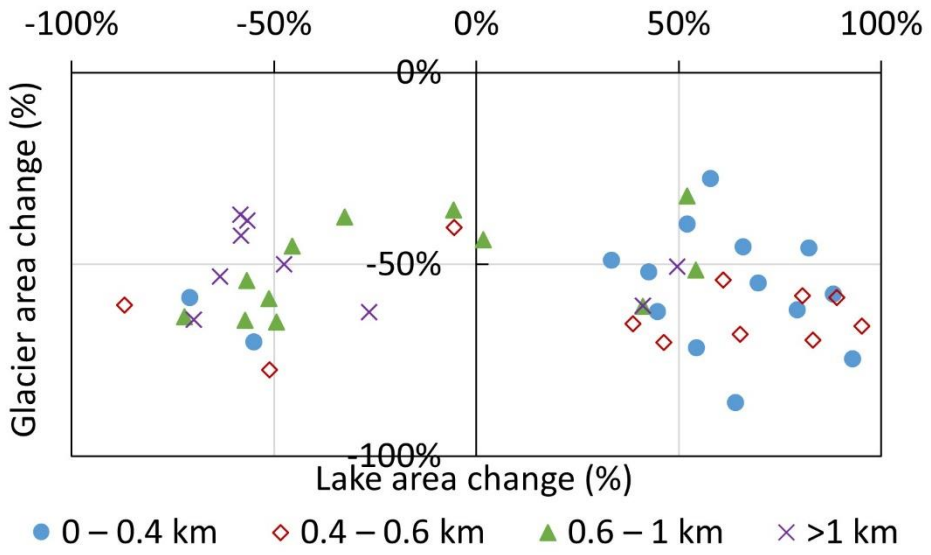


**Figure 4.11** Area change of Lake and its source glacier between 2010 – 2021 and 1990 – 2004. Different colors represent different distances from the lake to its nearest glaciers

Also from Figure 4.12, we observe that for lakes close to their source glaciers (distance < 600 m), the efficiency of glacier decline in contributing to lake area increase is higher. In contrast, lakes located further from their source glaciers (> 1 km) are more likely to decrease in area, suggesting meltwater loss during transportation. As the distance between lakes and glaciers increases, the proportion of glaciers within the lake catchments decreases. The reduction in lake areas, despite glacier decline, indicates that in these catchments, non-glacial factors have become the primary influence on lake area, rather than meltwater from glaciers.

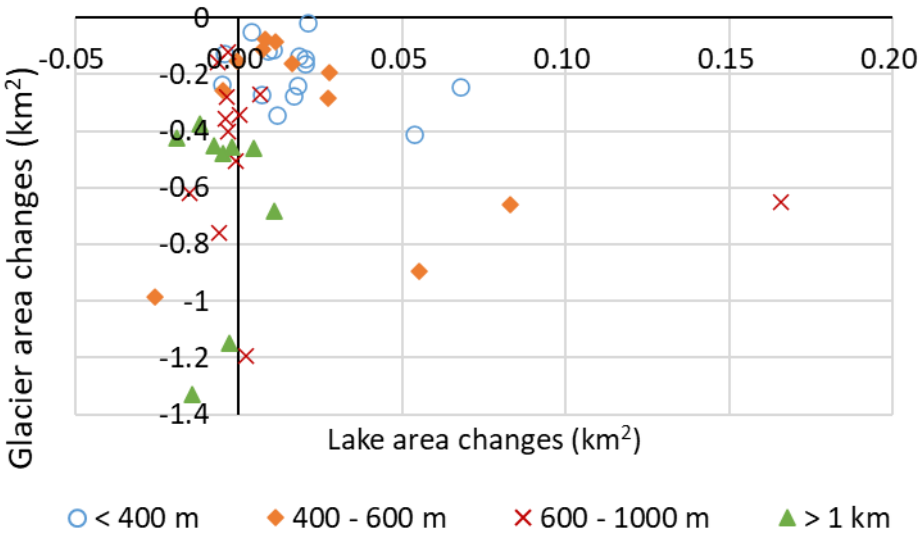


**Figure 4.12** Area change of Lake and its source glacier between 2010 – 2021 and 1990 – 2004 in units of $km^2$. Different colors represent different distances from the lake to its nearest glaciers

The relationship between lake area changes and the elevation of lake itself and their source glaciers was also investigated as shown in Figure 4.13 and 4.14. From Figure 4.13, it can be seen that lakes at relatively lower elevations are more likely to decrease in area, while many lakes above 5000 m are increasing. This suggests that glacier decline at higher elevations contributes to the growth of these lakes.

Figure 4.14 shows a similar trend, where lakes fed by glaciers at higher elevations are more likely to increase in area. However, this trend is less pronounced, likely because the average elevation of glaciers is less sensitive in representing glacier retreat compared to the shortest distance from glaciers to lakes.

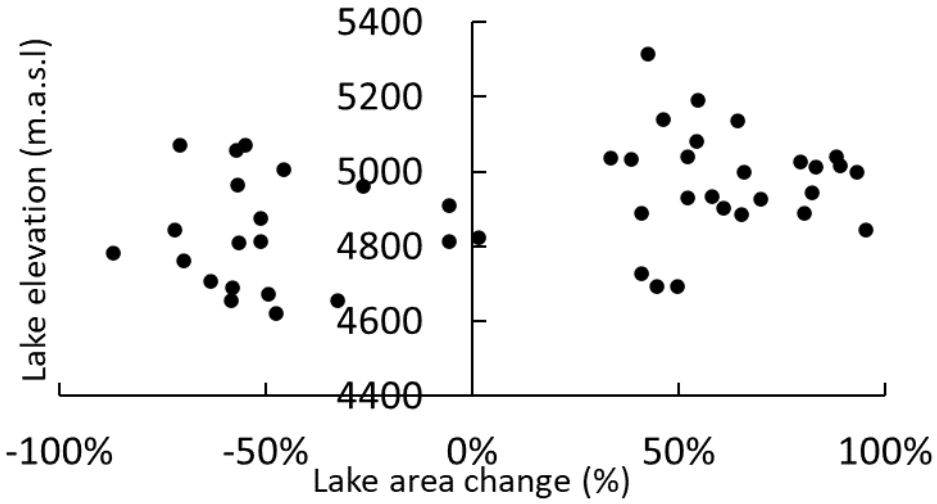


**Figure 4.13** Area change of lakes and their elevation between 2010–2021 and 1990–2004. Elevation is defined as the central point of a lake.

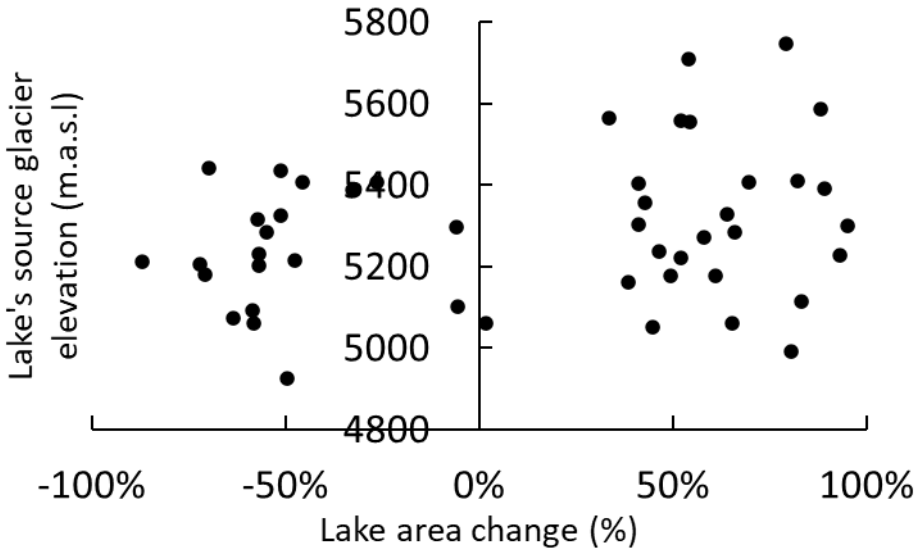


**Figure 4.14** Area change of lakes between 2010–2021 and 1990–2004, and the average elevation of their source glaciers in 1990–1994.

In Fig. 4.15, It can be observed that nearly all lakes with an elevation difference of less than 200 m from their source glaciers are increasing in area. In our study, we have also observed 18 newly appeared lakes, which all located at the retreated glacier edge.

However, as the elevation difference increases, no clear trend can be observed. This may be due to the same issue observed in the analysis in 4.14, average elevation of glaciers is less sensitive in representing glacier retreat compared to the shortest distance from glaciers to lakes.

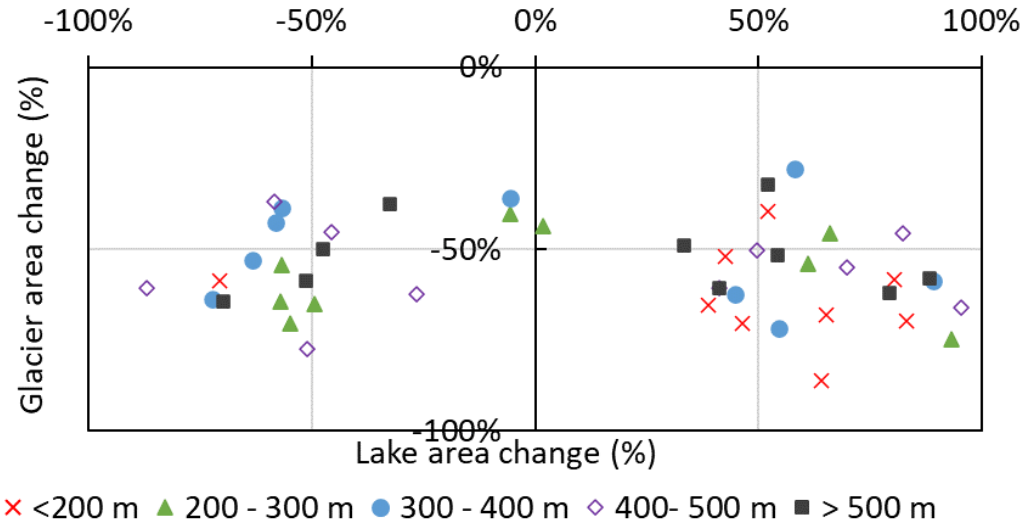


**Figure 4.15** Area change of lakes and their source glaciers between 2010–2021 and 1990–2004. Different colors and symbols represent the elevation difference between the lake and its source glaciers. The elevation of a lake is defined as the central point of the lake, and the average elevation of the source glaciers is defined based on glacier map from 1990–1994.

4.4.2.4. Influence of climate factors on lakes at the catchment level

To allow comparative analysis considering the spatial differences in climate factors (temperature, precipitation, and evaporation) on both sides of the Cordillera Real, catchments of lakes on the same stream were analyzed as an example to observe the influence of non-glacier areas. The chosen catchments are shown in Figure 4.16.

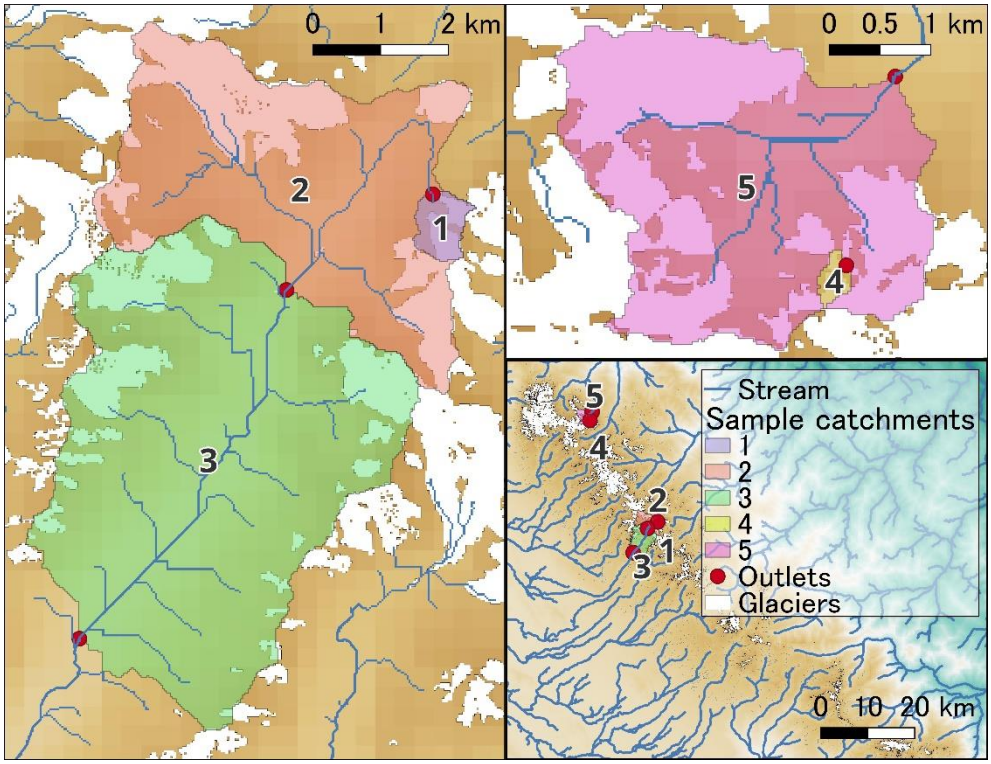


**Figure 4.16** Location of sample catchments.

Although all five catchments received glacier meltwater and the source glaciers experienced significant area loss, the correlation between lake area and its source glacier area is only evident in Lake 1 and Lake 4, which are very close to glacier (<500 m). For Lake 2, Lake 3, and Lake 5, despite large decreases in glacier area within the catchments, these lakes did not show an obvious relationship with glacier decline (Figure 4.17).

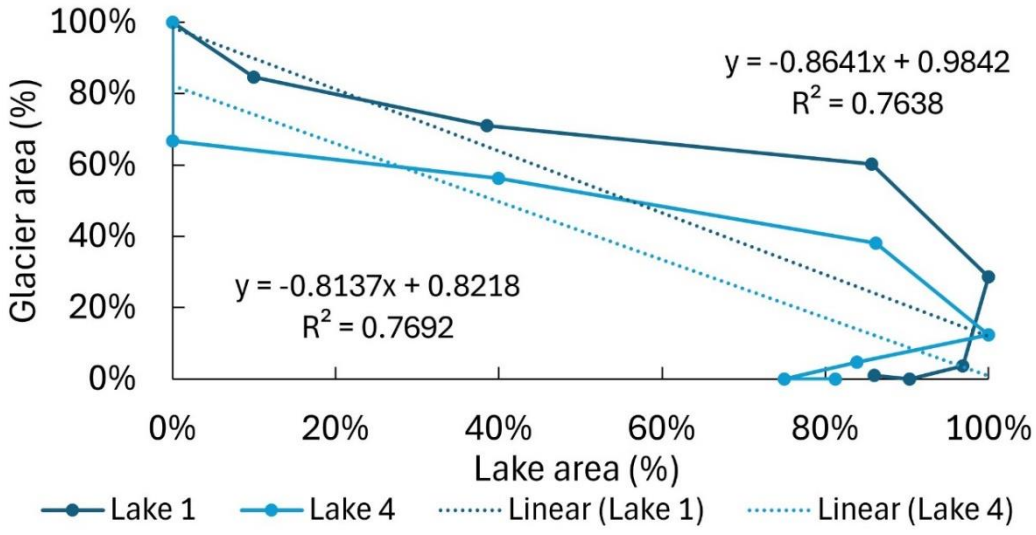

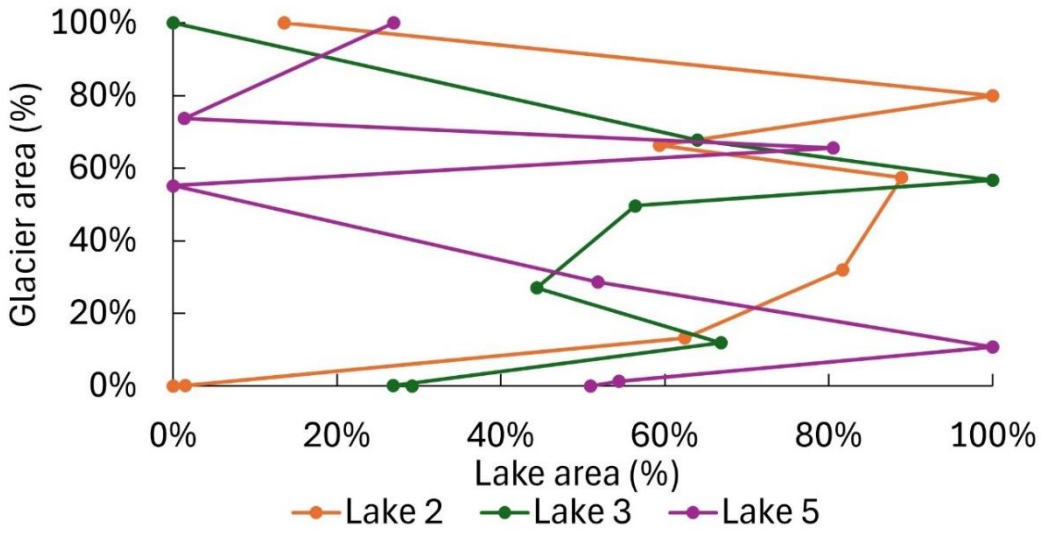


**Figure 4.17** Area of lakes and their source glaciers, normalized using the five-year average (except the last period of 2020-2021), data points are connected chronologically

The yearly area of each lake was calculated by averaging the lake area during the dry season (May to September). To allow comparison of lakes of different sizes, the areas were normalized (Figure 4.18). Lake 1 and Lake 4 are newly formed glacial lakes during the study period. However, Lake 1 gradually increased over the years and reached a stable area of around 0.07 km². In contrast, Lake 4's area remained very small, around 0.008 km², and has even become smaller in recent years. Lake 2 and Lake 3, situated along the same stream, with one upstream and the other downstream, exhibit similar trends in area changes over the years, with minimal changes in size and shape. These two lakes, along with Lake 5, which is also far from the glaciers, did not show significant area increases despite the decline of upstream glaciers, which should have provided sufficient meltwater.

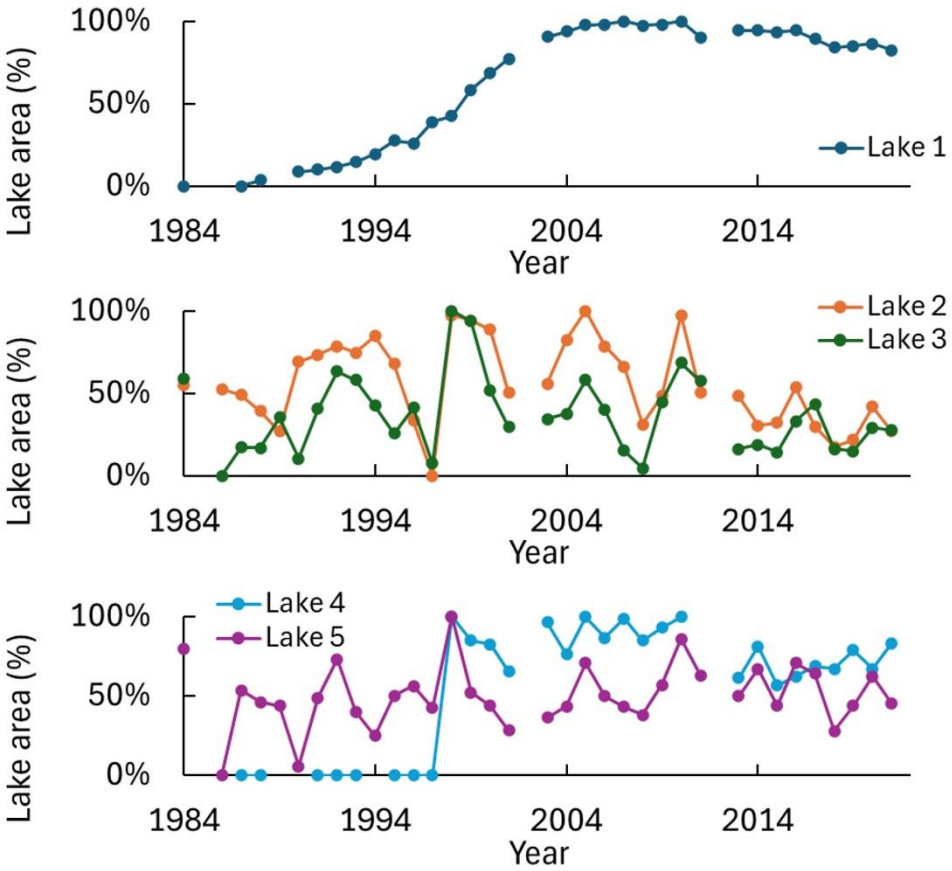


**Figure 4.18** Yearly average area of lakes during the dry season.

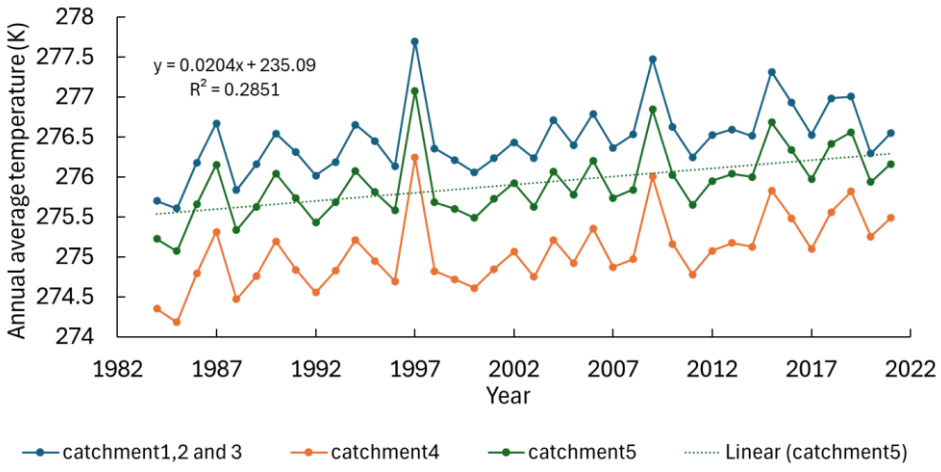

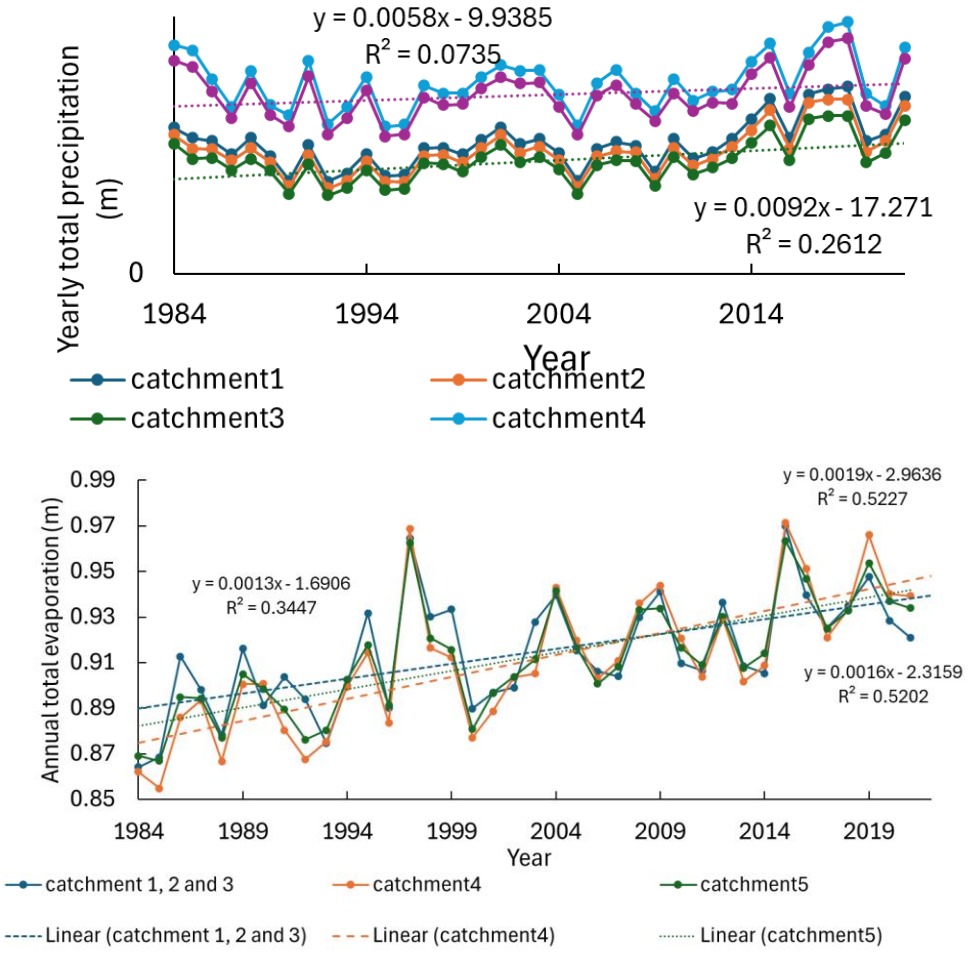


**Figure 4.19** Annual average temperature, total precipitation and total evaporation of catchments.

An evident increasing trend in temperature and evaporation in all catchments can be observed. For precipitation, the average area-weighted precipitation of Catchments 1, 2, and 3 was relatively lower than that of Catchments 4 and 5 due to their proximity to the arid Altiplano plateau (Figure 4.19). However, Catchments 1, 2, and 3 show a higher increasing rate in total precipitation, combined with a relatively lower rate in evaporation increasing compared to Catchment 4 and 5. This has reduced the difference in total precipitation minus total evaporation between these two area. It is worth noting that despite the relatively higher precipitation in the recent five years, none of the lakes has achieved its largest area. Specifically, Lakes 2, 3, and 5, whose catchments are relatively large and should be able to receive substantial precipitation, show an interesting pattern: their areas seem to increase when precipitation is high in a certain year, but the lake areas decrease rapidly the following year. This suggests that these

lakes are not able to capture or store precipitation effectively, even though maximum storage capacity is not reached. This could also be attributed to increased temperatures and enhanced evaporation, causing water loss during transportation or through evaporation.

These findings suggest that current glacier meltwater is insufficient to sustain lake water levels downstream. Moreover, increased precipitation alone is not adequate. Measures should be taken to mitigate the effects of increased temperature and evaporation to better preserve water resources.

### 4.4.3. Sample images of lakes' evolution

To better illustrate the evolution of glacier-fed lakes based on their proximity to glaciers, Figure 4.20 presents examples of lakes at varying distances from their source glaciers across different years. Lake A exemplifies a glacier that has transformed into a lake, with its edge still in contact with the glacier. Lake B formed after its source glaciers retreated, leaving a small gap between the lake and glaciers. Lake C, located 772 meters away from the glaciers, has shown little change in area over the years. Lake D, over 2 km from the glaciers, exhibits a slow decrease in area, likely due to rising temperatures and increased evaporation, with minimal influence from the distant glaciers.

| | A | B |
|---|---|---|
| Distance from its source glacier (m) | 0 | 530 |
| 1986 | 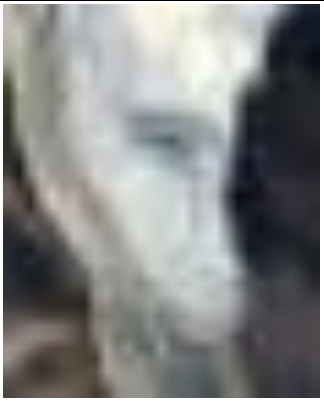 | 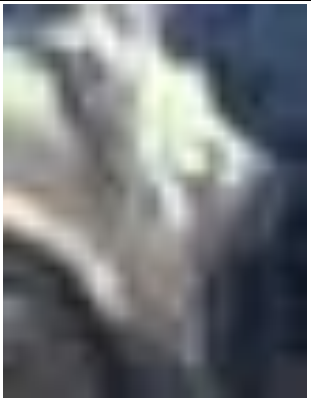 |
| 1995 | 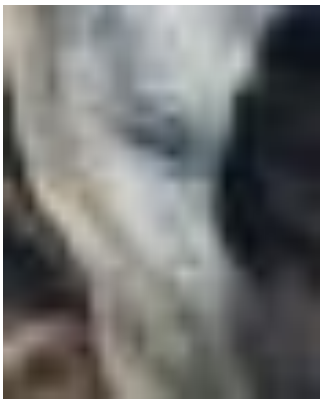 | 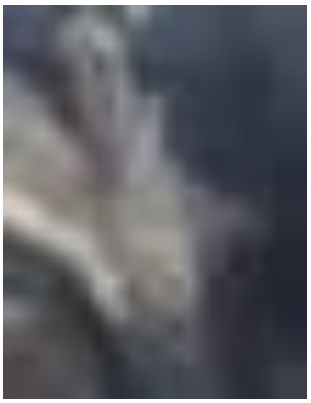 |
| 2005 | 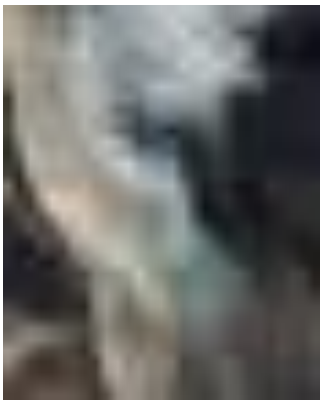 | 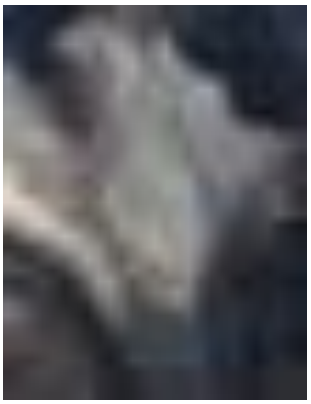 |
| 2015 | 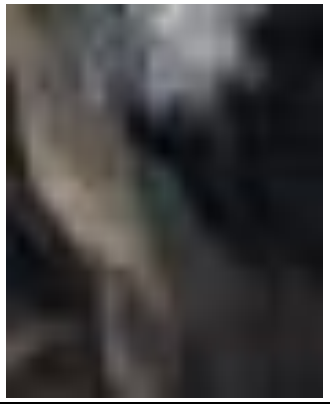 | 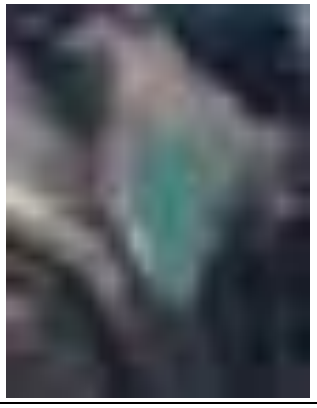 |

| | C | D |
|---|---|---|
| Distance from its source glacier (m) | 772 | 2179 |
| 1986 |  |  |
| 1995 |  |  |
| 2005 |  |  |
| 2015 | 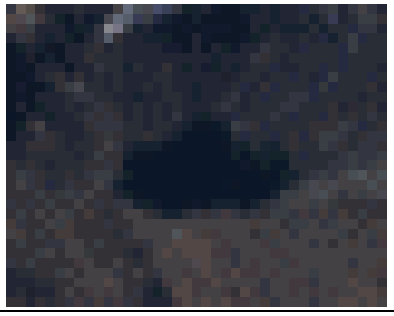 |  |

**Figure 4.20** Landsat images of sample lakes with different distances from their source glaciers across different years.

### 4.5. The potential influence on water resources

Changes in glacier and lake areas have potential impacts on basin water resources. However, previous studies have primarily focused on the mass balance and area changes of glaciers themselves (Cook et al., 2016; Kougkoulos, 2019; Sicart et al., 2011). This

study proposes that the upswing in glacier melting runoff instigated by climate change significantly influences glacial lakes, offering potential water resources in the Cordillera Real.

The static nature of both the number and area of natural lakes accentuates the growing importance of water resources provided by the construction of new water reservoirs and water management infrastructures. As documented by Kinouchi et al. (2019) and open map resources, many new water reservoirs and water management infrastructures were constructed in the Cordillera Real.

According to the Ministry of Environment and Water of Bolivia (MMAyA), they have invested 142 million US dollars in potable water and irrigation systems over the past decade (BNamericas). Many international organizations have financed the construction of drinking water supply and wastewater treatment facilities in Bolivia, including the Inter-American Development Bank (IDB) (2022), the European Investment Bank (EIB) (2018), and the Development Bank of Latin America and the Caribbean (CAF) (2024).

After the extreme drought period in 2015/2016, this study has identified five new lakes, all of which are human-constructed water reservoirs. However, not all of these new reservoirs were planned in response to the drought. Embalse Represa Hampaturi Alto was planned in 2014 (EPSAS, 2017) and brought online in 2017 (BNamericas, 2018), while Embalse Represa Alpaquita was proposed in 2013 (Buxton et al., 2013) and was scheduled for completion in 2019. Embalse Represa de Chacaltaya was started construction in 2017 and was inaugurated in 2019 (EPSAS, 2017).

Concurrently, pre-existing lakes, those significantly influenced by human activities, exhibit a sustained increase despite the rising temperature and the reduction in glacier areas. This countertrend suggests that human water management plays a pivotal role in sustaining waterbodies in the study region. Moreover, it serves as an example of the preservation of precipitation through strategic reservoir deployment and judicious water management techniques. This interaction between anthropogenic interventions and climatic variables underscores the dynamic nature of water resources with regard to glacial recession, stating the essential role of human activities in shaping the hydrological landscape in the Cordillera Real.

Based on the UN World Population Prospects (UNDP, 2008) medium growth scenario, Bolivia experienced a 20.6% population growth nationwide, with the capital city, La Paz, seeing a growth rate of 2.36% from 1993 to 2007. Combined population of La Paz and El Alto is projected to increase by 14.6% to 26.2% from 2012 to 2036 (Kinouchi et al., 2019). This growth, coupled with anticipated migration from rural areas to cities (Buytaert and De Bièvre, 2012), is expected to exacerbate water scarcity.

## 4.6. Summary

The first section of this chapter examines various climate datasets, including ERA5, ERA5-Land, CHIRPS, FLDAS, TRMM, GPM, and GLDAS Noah. It finds that FLDAS temperature data shows minor differences and is acceptable for temperature prediction, and CHIRPS precipitation data is preferred over other datasets despite its better performance. The spatiotemporal analysis reveals significant warming, especially at higher elevations, with increased evaporation rates, and regional differences in precipitation. The study demonstrates a significant negative relationship between glacier area and temperature, and a linear correlation between glacier area and natural glacier-fed lakes. Catchment-level analysis shows mixed results: some catchments experienced lake area increases with glacier retreat, while others saw stable or decreasing water surface areas. Lakes near glaciers showed a strong positive correlation with glacier retreat, whereas those farther away were influenced more by non-glacial factors. The final section emphasizes the crucial role of human-constructed reservoirs and water management in sustaining waterbodies in the Cordillera Real, particularly as population growth is expected to intensify water scarcity.

# Chapter 5 Conclusions

## 5.1. Summary of the research results and contributions

This study utilized over 200 Landsat images on the cloud platform GEE to develop a semi-automated method for detail mapping the changes of glaciers and glacial lakes. The method proposed in our study is efficient and significantly reduces manual work. Through the establishment of this semi-automated processing method, the study not only created a comprehensive lake inventory but also obtained a thorough observation of the spatiotemporal changes in lake surface areas. The glaciers in the Cordillera Real have undergone severe loss during the study period. The study updated the glacier area data in the Cordillera Real and clarified the trend in glacier melting with a uniform five-year interval. The application of this method revealed that a significant portion of glaciers shrank before 2010, especially those situated below 5400 m.a.s.l. However, as the distribution of glaciers is more concentrated at high elevations, and thus more resilient to the rising temperature of recent years, the rate of glacier recession has slowed down in recent years. Similarly, after a consistent increase since 1985, the area of natural glacier-fed lakes stabilized after 2010. Catchment-level analysis confirmed that glacial meltwater has contributed to the expansion of downstream lakes, particularly those proximal to source glaciers. As these lakes are still receiving melting waters from glaciers, their seasonal variations are lower than lakes that are not fed by glaciers. Even though the overall area of lakes shows a continuous increase over the years, the increase almost entirely comes from the contribution of human-affected lakes. The analysis of changes in glaciers and glacial lakes over 38 years indicated a strong influence of climate change on glacier retreat and lake expansion. Strong temperature increases were observed throughout the study period, with more significant increases in higher elevation regions. In contrast to temperature, evaporation enhanced in the eastern Amazonia region while decreasing in the western region. Overall, precipitation exhibited a variable pattern with relatively higher precipitation in recent years. However, the stabilized natural lake area could indicate that the increased precipitation in recent

years appears insufficient to compensate for water loss due to increased temperatures and enhanced evaporation.

The method developed in this study can be further employed for future glacier and glacial lake monitoring in this region and other mountain glacier areas. Its object-based algorithm and auto-adjusted threshold model design allow for continued monitoring. Due to its high temporal resolution, this method successfully captures lakes that appear for short periods or exhibit sudden expansion, which can contribute to the prevention of glacial lake outburst flood disasters. The findings of this study serve as a valuable resource for assessing the impact of climate change on water resources.

## 5.2. Limitations and future perspectives

Despite the contributions made, future work can be improved in the following ways: (1) Observations of glaciers and lakes can be enhanced by incorporating higher temporal or spatial resolution satellite imagery; (2) The effects of climatic factors on glacier melting and lake evolution, and their impact on local water resources and society, could be further explored if on-site climate datasets or high-resolution models become available. Alternatively, downscaling existing climate models and constructing water equilibrium models could provide more accurate estimates of future water resources, helping local populations prepare for impending climate changes.

# References

Achanta, R., Susstrunk, S., 2017. Superpixels and Polygons Using Simple Non-iterative Clustering, in: 2017 IEEE Conference on Computer Vision and Pattern Recognition (CVPR). Presented at the 2017 IEEE Conference on Computer Vision and Pattern Recognition (CVPR), IEEE, Honolulu, HI, pp. 4895–4904. https://doi.org/10.1109/CVPR.2017.520

Alvizuri-Tintaya, P.A., Rios-Ruiz, M., Lora-Garcia, J., Torregrosa-López, J.I., Lo-Iacono-Ferreira, V.G., 2022. Study and Evaluation of Surface Water Resources Affected by Ancient and Illegal Mining in the Upper Part of the Milluni Micro-Basin, Bolivia. Resources 11, 36. https://doi.org/10.3390/resources11040036

Bajracharya, S.R., Mool, P., 2009. Glaciers, glacial lakes and glacial lake outburst floods in the Mount Everest region, Nepal. Ann. Glaciol. 50, 81–86. https://doi.org/10.3189/172756410790595895

BNamericas, 2018. Bolivia moving ahead with La Paz water projects, Available online: https://www.bnamericas.com/en/news/bolivia-moving-ahead-with-la-paz-water-projects (accessed 3.22.24).

BNamericas, Bolivia Invests in Water Projects to Ward of Drought, Available online: https://www.bnamericas.com/en/news/bolivia-invests-in-water-projects-to-ward-off-drought (accessed 3.22.24).

Bolch, T., Menounos, B., Wheate, R., 2010. Landsat-based inventory of glaciers in western Canada, 1985–2005. Remote Sensing of Environment 114, 127–137. https://doi.org/10.1016/j.rse.2009.08.015

Bradley, R.S., Vuille, M., Diaz, H.F., Vergara, W., 2006. Threats to Water Supplies in the Tropical Andes. Science 312, 1755–1756. https://doi.org/10.1126/science.1128087

Buxton, N., Escobar, M., Purkey, D., Lima, N., 2013. Water Scarcity, Climate Change and Bolivia: Planning for Climate Uncertainties; Discussion Brief.

Buytaert, W., De Bièvre, B., 2012. Water for cities: The impact of climate change and demographic growth in the tropical Andes. Water Resources Research 48, 2011WR011755. https://doi.org/10.1029/2011WR011755

Caballero, Y., Chevallier, P., Gallaire, R., Pillco, R., 2004. Flow modelling in a high mountain valley equipped with hydropower plants: Rio Zongo Valley, Cordillera Real, Bolivia. Hydrological Processes 18, 939–957. https://doi.org/10.1002/hyp.1339

Carey, M., 2005. Living and dying with glaciers: people's historical vulnerability to avalanches and outburst floods in Peru. Global and Planetary Change 47, 122–134. https://doi.org/10.1016/j.gloplacha.2004.10.007

Cook, S.J., Kougkoulos, I., Edwards, L.A., Dortch, J., Hoffmann, D., 2016. Glacier change and glacial lake outburst flood risk in the Bolivian Andes. The Cryosphere 10, 2399–2413. https://doi.org/10.5194/tc-10-2399-2016

Development Bank of Latin America and the Caribbean, 2024. CAF approves US$240 million to improve water security in Bolivia, Available online: https://www.caf.com/en/currently/news/2024/03/caf-approves-us-240-million-to-improve-water-security-in-bolivia/ (accessed 3.22.24).

Drenkhan, F., Guardamino, L., Huggel, C., Frey, H., 2018. Current and future glacier and lake assessment in the deglaciating Vilcanota-Urubamba basin, Peruvian Andes. Global and Planetary Change 169, 105–118. https://doi.org/10.1016/j.gloplacha.2018.07.005

Dussaillant, I., Berthier, E., Brun, F., Masiokas, M., Hugonnet, R., Favier, V., Rabatel, A., Pitte, P., Ruiz, L., 2019. Two decades of glacier mass loss along the Andes. Nat. Geosci. 12, 802–808. https://doi.org/10.1038/s41561-019-0432-5

EPSAS, 2017a. Audiencia Inicial Pública de Rendición de Cuentas Gestión, Available online: https://www.epsas.com.bo/web/wp-content/uploads/2020/06/InformeFinal2017.pdf (accessed 3.22.24)

EPSAS, 2017b. HAMPATURI ES UNA REALIDAD, Available online: https://www.epsas.com.bo/web/wp-content/uploads/2019/01/hampaturi17.pdf (accessed 3.22.24)

Etienne, T., 2024. QuickOSM. Available online: https://github.com/3liz/QuickOSM

European Investment Bank, 2018. BOLIVIA MI AGUA WATER AND SANITATION Summary sheet, Available online: https://www.eib.org/en/projects/all/20170789 (accessed 3.22.24).

Farr, T.G., Rosen, P.A., Caro, E., Crippen, R., Duren, R., Hensley, S., Kobrick, M., Paller, M., Rodriguez, E., Roth, L., Seal, D., Shaffer, S., Shimada, J., Umland, J., Werner, M., Oskin, M., Burbank, D., Alsdorf, D., 2007. The Shuttle Radar Topography Mission. Reviews of Geophysics 45, 2005RG000183. https://doi.org/10.1029/2005RG000183

Feyisa, G.L., Meilby, H., Fensholt, R., Proud, S.R., 2014. Automated Water Extraction Index: A new technique for surface water mapping using Landsat imagery. Remote Sensing of Environment 140, 23–35. https://doi.org/10.1016/j.rse.2013.08.029

Foga, S., Scaramuzza, P.L., Guo, S., Zhu, Z., Dilley, R.D., Beckmann, T., Schmidt, G.L., Dwyer, J.L., Joseph Hughes, M., Laue, B., 2017. Cloud detection algorithm comparison and validation for operational Landsat data products. Remote Sensing of Environment 194, 379–390. https://doi.org/10.1016/j.rse.2017.03.026

Francou, B., Ramirez, E., Cáceres, B., Mendoza, J., 2000. Glacier Evolution in the Tropical Andes during the Last Decades of the 20th Century: Chacaltaya, Bolivia, and Antizana, Ecuador. Ambio 29, 416–422. http://www.jstor.org/stable/4315067

Funk, C., Peterson, P., Landsfeld, M., Pedreros, D., Verdin, J., Shukla, S., Husak, G., Rowland, J., Harrison, L., Hoell, A., Michaelsen, J., 2015. The climate hazards infrared precipitation with stations—a new environmental record for monitoring extremes. Sci Data 2, 150066. https://doi.org/10.1038/sdata.2015.66

Gao, B., 1996. NDWI—A normalized difference water index for remote sensing of vegetation liquid water from space. Remote Sensing of Environment 58, 257–266. https://doi.org/10.1016/S0034-4257(96)00067-3

Hall, D.K., Riggs, G.A., Salomonson, V.V., DiGirolamo, N.E., Bayr, K.J., 2002. MODIS snow-cover products. Remote Sensing of Environment 83, 181–194. https://doi.org/10.1016/S0034-4257(02)00095-0

Hanshaw, M.N., Bookhagen, B., 2014. Glacial areas, lake areas, and snow lines from 1975 to 2012: status of the Cordillera Vilcanota, including the Quelccaya Ice Cap, northern central Andes, Peru. The Cryosphere 8, 359–376. https://doi.org/10.5194/tc-8-359-2014

Hersbach, H., Bell, B., Berrisford, P., Hirahara, S., Horányi, A., Muñoz-Sabater, J., Nicolas, J., Peubey, C., Radu, R., Schepers, D., Simmons, A., Soci, C., Abdalla, S.,

Abellan, X., Balsamo, G., Bechtold, P., Biavati, G., Bidlot, J., Bonavita, M., De Chiara, G., Dahlgren, P., Dee, D., Diamantakis, M., Dragani, R., Flemming, J., Forbes, R., Fuentes, M., Geer, A., Haimberger, L., Healy, S., Hogan, R.J., Hólm, E., Janisková, M., Keeley, S., Laloyaux, P., Lopez, P., Lupu, C., Radnoti, G., De Rosnay, P., Rozum, I., Vamborg, F., Villaume, S., Thépaut, J., 2020. The ERA5 global reanalysis. Quart J Royal Meteoro Soc 146, 1999–2049. https://doi.org/10.1002/qj.3803

Huffman, G.J., Bolvin, D.T., Nelkin, E.J., Wolff, D.B., Adler, R.F., Gu, G., Hong, Y., Bowman, K.P., Stocker, E.F., 2007. The TRMM Multisatellite Precipitation Analysis (TMPA): Quasi-Global, Multiyear, Combined-Sensor Precipitation Estimates at Fine Scales. Journal of Hydrometeorology 8, 38–55. https://doi.org/10.1175/JHM560.1

Huggel, C., Kääb, A., Haeberli, W., Teysseire, P., Paul, F., 2002. Remote sensing based assessment of hazards from glacier lake outbursts: a case study in the Swiss Alps. Can. Geotech. J. 39, 316–330. https://doi.org/10.1139/t01-099

Huss, M., Hock, R., 2018. Global-scale hydrological response to future glacier mass loss. Nature Clim Change 8, 135–140. https://doi.org/10.1038/s41558-017-0049-x

Immerzeel, W.W., Van Beek, L.P.H., Bierkens, M.F.P., 2010. Climate Change Will Affect the Asian Water Towers. Science 328, 1382–1385. https://doi.org/10.1126/science.1183188

Jansson, P., Hock, R., Schneider, T., 2003. The concept of glacier storage: a review. Journal of Hydrology 282, 116–129. https://doi.org/10.1016/S0022-1694(03)00258-0

Jawak, S.D., Luis, A.J., 2014. A Semiautomatic Extraction of Antarctic Lake Features Using Worldview-2 Imagery. photogramm eng remote sensing 80, 939–952. https://doi.org/10.14358/PERS.80.10.939

Jiang, S., Nie, Y., Liu, Q., Wang, J., Liu, L., Hassan, J., Liu, X., Xu, X., 2018. Glacier Change, Supraglacial Debris Expansion and Glacial Lake Evolution in the Gyirong River Basin, Central Himalayas, between 1988 and 2015. Remote Sensing 10, 986. https://doi.org/10.3390/rs10070986

Jordan, E., 1991. Die Gletscher der bolivianischen Anden: eine photogrammetrisch-kartographische Bestandsaufnahme der Gletscher Boliviens als Grundlage für klimatische Deutungen und Potential für die wirtschaftliche Nutzung. Steiner, Stuttgart, Germany, 1991; ISBN 978-3-515-04917-7.

Kaser, G., 1999. A review of the modern fluctuations of tropical glaciers. Global and Planetary Change 22, 93–103. https://doi.org/10.1016/S0921-8181(99)00028-4

Kinouchi, T., Nakajima, T., Mendoza, J., Fuchs, P., Asaoka, Y., 2019. Water security in high mountain cities of the Andes under a growing population and climate change: A case study of La Paz and El Alto, Bolivia. Water Security 6, 100025. https://doi.org/10.1016/j.wasec.2019.100025

Kougkoulos, I., 2019. Glacial lake outburst flood risk in the Bolivian Andes (PhD diss). Manchester Metropolitan University.

Lejeune, Y., 2009. Apports des modèles de neige CROCUS et de sol ISBA à l'étude du bilan glaciologique d'un glacier tropical et du bilan hydrologique de son bassin versant (PhD diss). Université Joseph-Fourier - Grenoble I, Français.

Li, J., Sheng, Y., 2012. An automated scheme for glacial lake dynamics mapping using Landsat imagery and digital elevation models: a case study in the Himalayas. International Journal of Remote Sensing 33, 5194–5213. https://doi.org/10.1080/01431161.2012.657370

Liu, K., Song, C., Zhao, S., Wang, J., Chen, T., Zhan, P., Fan, C., Zhu, J., 2024. Mapping inundated bathymetry for estimating lake water storage changes from SRTM DEM: A global investigation. Remote Sensing of Environment 301, 113960. https://doi.org/10.1016/j.rse.2023.113960

Liu, T., Kinouchi, T., Ledezma, F., 2013. Characterization of recent glacier decline in the Cordillera Real by LANDSAT, ALOS, and ASTER data. Remote Sensing of Environment 137, 158–172. https://doi.org/10.1016/j.rse.2013.06.010

McFEETERS, S.K., 1996. The use of the Normalized Difference Water Index (NDWI) in the delineation of open water features. International Journal of Remote Sensing 17, 1425–1432. https://doi.org/10.1080/01431169608948714

McNally, A., Arsenault, K., Kumar, S., Shukla, S., Peterson, P., Wang, S., Funk, C., Peters-Lidard, C.D., Verdin, J.P., 2017. A land data assimilation system for sub-

Saharan Africa food and water security applications. Sci Data 4, 170012. https://doi.org/10.1038/sdata.2017.12

Mitkari, K.V., Arora, M.K., Tiwari, R.K., 2017. Extraction of Glacial Lakes in Gangotri Glacier Using Object-Based Image Analysis. IEEE J. Sel. Top. Appl. Earth Observations Remote Sensing 1–9. https://doi.org/10.1109/JSTARS.2017.2727506

Mölg, N., Bolch, T., Rastner, P., Strozzi, T., Paul, F., 2018. A consistent glacier inventory for Karakoram and Pamir derived from Landsat data: distribution of debris cover and mapping challenges. Earth Syst. Sci. Data 10, 1807–1827. https://doi.org/10.5194/essd-10-1807-2018

Morizawa, K., Asaoka, Y., Kazama, S., Gunawardhana, L.N., 2013. Temporal glacier area changes correlated with the El Niño/La Niña Southern Oscillation using satellite imagery. Hydrological Research Letters 7, 18–22. https://doi.org/10.3178/hrl.7.18

Mott, R., Wolf, A., Kehl, M., Kunstmann, H., Warscher, M., Grünewald, T., 2019. Avalanches and micrometeorology driving mass and energy balance of the lowest perennial ice field of the Alps: a case study. The Cryosphere 13, 1247–1265. https://doi.org/10.5194/tc-13-1247-2019

Muñoz-Sabater, J., Dutra, E., Agustí-Panareda, A., Albergel, C., Arduini, G., Balsamo, G., Boussetta, S., Choulga, M., Harrigan, S., Hersbach, H., Martens, B., Miralles, D.G., Piles, M., Rodríguez-Fernández, N.J., Zsoter, E., Buontempo, C., Thépaut, J.-N., 2021. ERA5-Land: a state-of-the-art global reanalysis dataset for land applications. Earth Syst. Sci. Data 13, 4349–4383. https://doi.org/10.5194/essd-13-4349-2021

Nie, Y., Sheng, Y., Liu, Q., Liu, L., Liu, S., Zhang, Y., Song, C., 2017. A regional-scale assessment of Himalayan glacial lake changes using satellite observations from 1990 to 2015. Remote Sensing of Environment 189, 1–13. https://doi.org/10.1016/j.rse.2016.11.008

OpenStreetMap contributors, 2017. OpenStreetMap. Available online: https://www.openstreetmap.org (accessed 2.16.23)

Otsu, N., 1979. A Threshold Selection Method from Gray-Level Histograms. IEEE Trans. Syst., Man, Cybern. 9, 62–66. https://doi.org/10.1109/TSMC.1979.4310076

Paul, F., Andreassen, L.M., Winsvold, S.H., 2011. A new glacier inventory for the Jostedalsbreen region, Norway, from Landsat TM scenes of 2006 and changes since 1966. Ann. Glaciol. 52, 153–162. https://doi.org/10.3189/172756411799096169

Paul, F., Kääb, A., Maisch, M., Kellenberger, T., Haeberli, W., 2002. The new remote-sensing-derived Swiss glacier inventory: I. Methods. Ann. Glaciol. 34, 355–361. https://doi.org/10.3189/172756402781817941

Paul, F., Rastner, P., 2023. Glacier extents in Peru and Bolivia are overestimated in RGIv6 by 27%. https://doi.org/10.5194/egusphere-egu23-12724

Pekel, J.-F., Cottam, A., Gorelick, N., Belward, A.S., 2016. High-resolution mapping of global surface water and its long-term changes. Nature 540, 418–422. https://doi.org/10.1038/nature20584

Precipitation Processing System (PPS) At NASA GSFC, 2019. GPM IMERG Final Precipitation L3 1 month 0.1 degree x 0.1 degree V06. https://doi.org/10.5067/GPM/IMERG/3B-MONTH/06

Qiao, B., Zhu, L., 2019. Difference and cause analysis of water storage changes for glacier-fed and non-glacier-fed lakes on the Tibetan Plateau. Science of The Total Environment 693, 133399. https://doi.org/10.1016/j.scitotenv.2019.07.205

Rabatel, A., Francou, B., Soruco, A., Gomez, J., Cáceres, B., Ceballos, J.L., Basantes, R., Vuille, M., Sicart, J.-E., Huggel, C., Scheel, M., Lejeune, Y., Arnaud, Y., Collet, M., Condom, T., Consoli, G., Favier, V., Jomelli, V., Galarraga, R., Ginot, P., Maisincho, L., Mendoza, J., Ménégoz, M., Ramirez, E., Ribstein, P., Suarez, W., Villacis, M., Wagnon, P., 2013. Current state of glaciers in the tropical Andes: a multi-century perspective on glacier evolution and climate change. The Cryosphere 7, 81–102. https://doi.org/10.5194/tc-7-81-2013

Raup, B., Racoviteanu, A., Khalsa, S.J.S., Helm, C., Armstrong, R., Arnaud, Y., 2007. The GLIMS geospatial glacier database: A new tool for studying glacier change. Global and Planetary Change 56, 101–110. https://doi.org/10.1016/j.gloplacha.2006.07.018

Rodell, M., Houser, P.R., Jambor, U., Gottschalck, J., Mitchell, K., Meng, C.-J., Arsenault, K., Cosgrove, B., Radakovich, J., Bosilovich, M., Entin, J.K., Walker,

J.P., Lohmann, D., Toll, D., 2004. The Global Land Data Assimilation System. Bull. Amer. Meteor. Soc. 85, 381–394. https://doi.org/10.1175/BAMS-85-3-381

Rouse, J.W., Haas, R.H., Schell, J.A., Deering, D.W., 1974. Monitoring vegetation systems in the Great Plains with ERTS. https://ntrs.nasa.gov/citations/19740022614

Seehaus, T., Malz, P., Sommer, C., Soruco, A., Rabatel, A., Braun, M., 2020. Mass balance and area changes of glaciers in the Cordillera Real and Tres Cruces, Bolivia, between 2000 and 2016. J. Glaciol. 66, 124–136. https://doi.org/10.1017/jog.2019.94

Shen, L., Li, C., 2010. Water body extraction from Landsat ETM+ imagery using adaboost algorithm, in: 2010 18th International Conference on Geoinformatics. Presented at the 2010 18th International Conference on Geoinformatics, IEEE, Beijing, China, pp. 1–4. https://doi.org/10.1109/GEOINFORMATICS.2010.5567762

Shugar, D.H., Burr, A., Haritashya, U.K., Kargel, J.S., Watson, C.S., Kennedy, M.C., Bevington, A.R., Betts, R.A., Harrison, S., Strattman, K., 2020. Rapid worldwide growth of glacial lakes since 1990. Nat. Clim. Chang. 10, 939–945. https://doi.org/10.1038/s41558-020-0855-4

Sicart, J.E., Hock, R., Ribstein, P., Litt, M., Ramirez, E., 2011. Analysis of seasonal variations in mass balance and meltwater discharge of the tropical Zongo Glacier by application of a distributed energy balance model. J. Geophys. Res. 116, D13105. https://doi.org/10.1029/2010JD015105

Song, C., Sheng, Y., 2016. Contrasting evolution patterns between glacier-fed and non-glacier-fed lakes in the Tanggula Mountains and climate cause analysis. Climatic Change 135, 493–507. https://doi.org/10.1007/s10584-015-1578-9

Soruco, A., Vincent, C., Francou, B., Gonzalez, J.F., 2009. Glacier decline between 1963 and 2006 in the Cordillera Real, Bolivia. Geophysical Research Letters 36, 2008GL036238. https://doi.org/10.1029/2008GL036238

Taylor, K.E., Stouffer, R.J., Meehl, G.A., 2012. An Overview of CMIP5 and the Experiment Design. Bulletin of the American Meteorological Society 93, 485–498. https://doi.org/10.1175/BAMS-D-11-00094.1

The Inter-American Development Bank, The Inter-American Investment Corporation, 2022. IDB Country Strategy with Bolivia (2022–2025), Available online: https://idbinvest.org/sites/default/files/2022-04/Bolivia-Country-Strategy-IDB-Group-2022.pdf (accessed 3.22.24)

Torres-Batlló, J., Martí-Cardona, B., 2020. Precipitation trends over the southern Andean Altiplano from 1981 to 2018. Journal of Hydrology 590, 125485. https://doi.org/10.1016/j.jhydrol.2020.125485

United Nations Population Division (UNDP), 2008, World population prospects: The 2008 revision population database, technical report, New York.

U.S. Geological Survey, 2020. Landsat 8-9 Operational Land Imager (OLI) - Thermal Infrared Sensor (TIRS) Collection 2 Level 1 (L1) Data Format Control Book (DFCB), Available online: https://www.usgs.gov/media/files/landsat-8-9-olitirs-collection-2-level-1-data-format-control-book

Veettil, B.K., Kamp, U., 2021. Glacial Lakes in the Andes under a Changing Climate: A Review. J. Earth Sci. 32, 1575–1593. https://doi.org/10.1007/s12583-020-1118-z

Veettil, B.K., Simões, J.C., 2019. The 2015/16 El Niño-related glacier changes in the tropical Andes. Front. Earth Sci. 13, 422–429. https://doi.org/10.1007/s11707-018-0738-4

Veettil, B.K., Wang, S., Simões, J.C., Pereira, S.F.R., 2018. Glacier monitoring in the eastern mountain ranges of Bolivia from 1975 to 2016 using Landsat and Sentinel-2 data. Environ Earth Sci 77, 452. https://doi.org/10.1007/s12665-018-7640-y

Veettil, B.K., Wang, S., Florêncio De Souza, S., Bremer, U.F., Simões, J.C., 2017. Glacier monitoring and glacier-climate interactions in the tropical Andes: A review. Journal of South American Earth Sciences 77, 218–246. https://doi.org/10.1016/j.jsames.2017.04.009

Veh, G., Korup, O., Roessner, S., Walz, A., 2018. Detecting Himalayan glacial lake outburst floods from Landsat time series. Remote Sensing of Environment 207, 84–97. https://doi.org/10.1016/j.rse.2017.12.025

Vergara, W., Deeb, A., Valencia, A., Bradley, R., Francou, B., Zarzar, A., Grünwaldt, A., Haeussling, S., 2007. Economic impacts of rapid glacier retreat in the Andes. EoS Transactions 88, 261–264. https://doi.org/10.1029/2007EO250001

Vincent, L., Soille, P., 1991. Watersheds in digital spaces: an efficient algorithm based on immersion simulations. IEEE Trans. Pattern Anal. Machine Intell. 13, 583–598. https://doi.org/10.1109/34.87344

Vuille, M., Carey, M., Huggel, C., Buytaert, W., Rabatel, A., Jacobsen, D., Soruco, A., Villacis, M., Yarleque, C., Elison Timm, O., Condom, T., Salzmann, N., Sicart, J.-E., 2018. Rapid decline of snow and ice in the tropical Andes – Impacts, uncertainties and challenges ahead. Earth-Science Reviews 176, 195–213. https://doi.org/10.1016/j.earscirev.2017.09.019

Vuille, M., Francou, B., Wagnon, P., Juen, I., Kaser, G., Mark, B.G., Bradley, R.S., 2008. Climate change and tropical Andean glaciers: Past, present and future. Earth-Science Reviews 89, 79–96. https://doi.org/10.1016/j.earscirev.2008.04.002

Wang, X., Guo, X., Yang, C., Liu, Q., Wei, J., Zhang, Yong, Liu, S., Zhang, Yanlin, Jiang, Z., Tang, Z., 2020. Glacial lake inventory of high-mountain Asia in 1990 and 2018 derived from Landsat images. Earth Syst. Sci. Data 12, 2169–2182. https://doi.org/10.5194/essd-12-2169-2020

Woo, M., 1990. Consequences of Climatic Change for Hydrology in Permafrost Zones. J. Cold Reg. Eng. 4, 15–20. https://doi.org/10.1061/(ASCE)0887-381X(1990)4:1(15)

Xu, H., 2006. Modification of normalised difference water index (NDWI) to enhance open water features in remotely sensed imagery. International Journal of Remote Sensing 27, 3025–3033. https://doi.org/10.1080/01431160600589179

Yao, X., Liu, S., Han, L., Sun, M., Zhao, L., 2018. Definition and classification system of glacial lake for inventory and hazards study. J. Geogr. Sci. 28, 193–205. https://doi.org/10.1007/s11442-018-1467-z

Yarleque, C., Vuille, M., Hardy, D.R., Timm, O.E., De La Cruz, J., Ramos, H., Rabatel, A., 2018. Projections of the future disappearance of the Quelccaya Ice Cap in the Central Andes. Sci Rep 8, 15564. https://doi.org/10.1038/s41598-018-33698-z

Yue, X., Li, Z., Li, H., Wang, F., Jin, S., 2022. Multi-Temporal Variations in Surface Albedo on Urumqi Glacier No.1 in Tien Shan, under Arid and Semi-Arid Environment. Remote Sensing 14, 808. https://doi.org/10.3390/rs14040808

Zemp, M., Huss, M., Thibert, E., Eckert, N., McNabb, R., Huber, J., Barandun, M., Machguth, H., Nussbaumer, S.U., Gärtner-Roer, I., Thomson, L., Paul, F., Maussion, F., Kutuzov, S., Cogley, J.G., 2019. Global glacier mass changes and their contributions to sea-level rise from 1961 to 2016. Nature 568, 382–386. https://doi.org/10.1038/s41586-019-1071-0

Zhang, G., Chen, W., Xie, H., 2019. Tibetan Plateau's Lake Level and Volume Changes From NASA's ICESat/ICESat-2 and Landsat Missions. Geophysical Research Letters 46, 13107–13118. https://doi.org/10.1029/2019GL085032

Zhao, H., Chen, F., Zhang, M., 2018. A Systematic Extraction Approach for Mapping Glacial Lakes in High Mountain Regions of Asia. IEEE J. Sel. Top. Appl. Earth Observations Remote Sensing 11, 2788–2799. https://doi.org/10.1109/JSTARS.2018.2846551

# Appendices

Table A1 List of Landsat images with cloud cover rate smaller than 15%

| Date of image acquisition | Image ID | Date of image acquisition | Image ID |
|---|---|---|---|
| 1988/6/17 | LT05_L1TP_001071_19880617_20200917_02_T1 | 2009/5/26 | LT05_L1TP_001071_20090526_20200827_02_T1 |
| 1988/7/3 | LT05_L1TP_001071_19880703_20200917_02_T1 | 2009/6/11 | LT05_L1TP_001071_20090611_20200827_02_T1 |
| 1988/7/19 | LT05_L1TP_001071_19880719_20200917_02_T1 | 2009/6/27 | LT05_L1TP_001071_20090627_20200827_02_T1 |
| 1988/8/20 | LT05_L1TP_001071_19880820_20200917_02_T1 | 2010/5/13 | LT05_L1TP_001071_20100513_20200824_02_T1 |
| 1991/5/25 | LT05_L1TP_001071_19910525_20230519_02_T1 | 2010/6/14 | LT05_L1TP_001071_20100614_20200824_02_T1 |
| 1992/5/11 | LT05_L1TP_001071_19920511_20200914_02_T1 | 2010/8/17 | LT05_L1TP_001071_20100817_20200824_02_T1 |
| 1992/5/27 | LT05_L1TP_001071_19920527_20200914_02_T1 | 2010/10/4 | LT05_L1TP_001071_20101004_20200823_02_T1 |
| 1992/6/12 | LT05_L1TP_001071_19920612_20200914_02_T1 | 2011/5/16 | LT05_L1TP_001071_20110516_20200822_02_T1 |
| 1994/6/2 | LT05_L1TP_001071_19940602_20200913_02_T1 | 2014/7/11 | LC08_L1TP_001071_20140711_20200911_02_T1 |
| 1994/7/20 | LT05_L1TP_001071_19940720_20200913_02_T1 | 2015/6/28 | LC08_L1TP_001071_20150628_20200909_02_T1 |
| 1995/6/5 | LT05_L1TP_001071_19950605_20200912_02_T1 | 2015/7/30 | LC08_L1TP_001071_20150730_20200908_02_T1 |
| 1995/6/21 | LT05_L1TP_001071_19950621_20200913_02_T1 | 2016/5/29 | LC08_L1TP_001071_20160529_20200906_02_T1 |
| 1995/8/8 | LT05_L1TP_001071_19950808_20200912_02_T1 | 2016/8/1 | LC08_L1TP_001071_20160801_20200906_02_T1 |
| 1996/5/22 | LT05_L1TP_001071_19960522_20200911_02_T1 | 2017/7/19 | LC08_L1TP_001071_20170719_20200903_02_T1 |
| 1999/7/2 | LT05_L1TP_001071_19990702_20200907_02_T1 | 2017/8/4 | LC08_L1TP_001071_20170804_20200903_02_T1 |
| 2000/8/5 | LT05_L1TP_001071_20000805_20200906_02_T1 | 2017/8/20 | LC08_L1TP_001071_20170820_20200903_02_T1 |
| 2003/6/27 | LT05_L1TP_001071_20030627_20200905_02_T1 | 2019/6/7 | LC08_L1TP_001071_20190607_20200828_02_T1 |
| 2004/4/26 | LT05_L1TP_001071_20040426_20200903_02_T1 | 2019/6/23 | LC08_L1TP_001071_20190623_20200827_02_T1 |
| 2004/5/28 | LT05_L1TP_001071_20040528_20200903_02_T1 | 2019/7/9 | LC08_L1TP_001071_20190709_20200827_02_T1 |
| 2005/4/29 | LT05_L1TP_001071_20050429_20200902_02_T1 | 2020/5/24 | LC08_L1TP_001071_20200524_20200820_02_T1 |
| 2005/6/16 | LT05_L1TP_001071_20050616_20200902_02_T1 | 2020/6/9 | LC08_L1TP_001071_20200609_20200824_02_T1 |
| 2005/9/4 | LT05_L1TP_001071_20050904_20200901_02_T1 | 2020/6/25 | LC08_L1TP_001071_20200625_20200823_02_T1 |
| 2006/6/19 | LT05_L1TP_001071_20060619_20200831_02_T1 | 2020/7/11 | LC08_L1TP_001071_20200711_20200912_02_T1 |
| 2006/7/5 | LT05_L1TP_001071_20060705_20200831_02_T1 | 2020/7/27 | LC08_L1TP_001071_20200727_20200908_02_T1 |
| 2008/7/26 | LT05_L1TP_001071_20080726_20200829_02_T1 | 2021/7/14 | LC08_L1TP_001071_20210714_20210721_02_T1 |
| 2008/8/27 | LT05_L1TP_001071_20080827_20200829_02_T1 | | |

Table A2 List of Landsat images with cloud cover rate smaller than 40%

| Date of image acquisition | Image ID | Date of image acquisition | Image ID |
|---|---|---|---|
| 1984/7/8 | LT05_L1TP_001071_19840708_20200918_02_T1 | 2005/7/18 | LT05_L1TP_001071_20050718_20200902_02_T1 |
| 1986/7/14 | LT05_L1TP_001071_19860714_20200917_02_T1 | 2005/8/3 | LT05_L1TP_001071_20050803_20200902_02_T1 |
| 1986/7/30 | LT05_L1TP_001071_19860730_20200917_02_T1 | 2005/8/19 | LT05_L1TP_001071_20050819_20200902_02_T1 |
| 1986/8/15 | LT05_L1TP_001071_19860815_20200918_02_T1 | 2005/9/4 | LT05_L1TP_001071_20050904_20200901_02_T1 |
| 1986/10/2 | LT05_L1TP_001071_19861002_20200917_02_T1 | 2006/2/27 | LT05_L1TP_001071_20060227_20200901_02_T1 |
| 1987/5/14 | LT05_L1TP_001071_19870514_20201014_02_T1 | 2006/5/2 | LT05_L1TP_001071_20060502_20200901_02_T1 |
| 1987/5/30 | LT05_L1TP_001071_19870530_20201014_02_T1 | 2006/5/18 | LT05_L1TP_001071_20060518_20200901_02_T1 |
| 1987/6/15 | LT05_L1TP_001071_19870615_20201014_02_T1 | 2006/6/3 | LT05_L1TP_001071_20060603_20200831_02_T1 |
| 1987/8/2 | LT05_L1TP_001071_19870802_20201014_02_T1 | 2006/6/19 | LT05_L1TP_001071_20060619_20200831_02_T1 |
| 1987/8/18 | LT05_L1TP_001071_19870818_20201014_02_T1 | 2006/7/5 | LT05_L1TP_001071_20060705_20200831_02_T1 |
| 1987/10/21 | LT05_L1TP_001071_19871021_20201014_02_T1 | 2006/7/21 | LT05_L1TP_001071_20060721_20200831_02_T1 |
| 1988/4/30 | LT05_L1TP_001071_19880430_20200917_02_T1 | 2006/8/6 | LT05_L1TP_001071_20060806_20200831_02_T1 |
| 1988/5/16 | LT05_L1TP_001071_19880516_20200917_02_T1 | 2006/8/22 | LT05_L1TP_001071_20060822_20200831_02_T1 |
| 1988/6/1 | LT05_L1TP_001071_19880601_20200917_02_T1 | 2006/9/23 | LT05_L1TP_001071_20060923_20200831_02_T1 |
| 1988/6/17 | LT05_L1TP_001071_19880617_20200917_02_T1 | 2006/10/9 | LT05_L1TP_001071_20061009_20200831_02_T1 |
| 1988/7/3 | LT05_L1TP_001071_19880703_20200917_02_T1 | 2007/4/19 | LT05_L1TP_001071_20070419_20200830_02_T1 |
| 1988/7/19 | LT05_L1TP_001071_19880719_20200917_02_T1 | 2007/5/5 | LT05_L1TP_001071_20070505_20200830_02_T1 |
| 1988/8/20 | LT05_L1TP_001071_19880820_20200917_02_T1 | 2007/5/21 | LT05_L1TP_001071_20070521_20200830_02_T1 |
| 1988/9/5 | LT05_L1TP_001071_19880905_20200917_02_T1 | 2007/6/22 | LT05_L1TP_001071_20070622_20200830_02_T1 |
| 1988/10/23 | LT05_L1TP_001071_19881023_20200917_02_T1 | 2007/7/24 | LT05_L1TP_001071_20070724_20200829_02_T1 |
| 1989/7/6 | LT05_L1TP_001071_19890706_20200916_02_T1 | 2007/8/25 | LT05_L1TP_001071_20070825_20200829_02_T1 |
| 1989/8/23 | LT05_L1TP_001071_19890823_20200916_02_T1 | 2008/3/20 | LT05_L1TP_001071_20080320_20200829_02_T1 |
| 1989/9/8 | LT05_L1TP_001071_19890908_20200916_02_T1 | 2008/5/7 | LT05_L1TP_001071_20080507_20200829_02_T1 |
| 1990/5/22 | LT05_L1TP_001071_19900522_20200916_02_T1 | 2008/5/23 | LT05_L1TP_001071_20080523_20200829_02_T1 |
| 1990/7/25 | LT05_L1TP_001071_19900725_20200916_02_T1 | 2008/7/26 | LT05_L1TP_001071_20080726_20200829_02_T1 |
| 1990/8/10 | LT05_L1TP_001071_19900810_20200916_02_T1 | 2008/8/11 | LT05_L1TP_001071_20080811_20200829_02_T1 |
| 1990/9/11 | LT05_L1TP_001071_19900911_20200915_02_T1 | 2008/8/27 | LT05_L1TP_001071_20080827_20200829_02_T1 |
| 1991/4/23 | LT05_L1TP_001071_19910423_20230518_02_T1 | 2008/9/28 | LT05_L1TP_001071_20080928_20200829_02_T1 |
| 1991/5/25 | LT05_L1TP_001071_19910525_20230519_02_T1 | 2009/5/26 | LT05_L1TP_001071_20090526_20200827_02_T1 |
| 1991/6/26 | LT05_L1TP_001071_19910626_20230522_02_T1 | 2009/6/11 | LT05_L1TP_001071_20090611_20200827_02_T1 |
| 1991/7/12 | LT05_L1TP_001071_19910712_20230522_02_T1 | 2009/6/27 | LT05_L1TP_001071_20090627_20200827_02_T1 |
| 1991/7/28 | LT05_L1TP_001071_19910728_20200915_02_T1 | 2009/7/29 | LT05_L1TP_001071_20090729_20200827_02_T1 |
| 1991/8/13 | LT05_L1TP_001071_19910813_20230523_02_T1 | 2009/8/30 | LT05_L1TP_001071_20090830_20200825_02_T1 |
| 1991/8/29 | LT05_L1TP_001071_19910829_20200915_02_T1 | 2010/4/11 | LT05_L1TP_001071_20100411_20200824_02_T1 |
| 1991/9/14 | LT05_L1TP_001071_19910914_20230511_02_T1 | 2010/5/13 | LT05_L1TP_001071_20100513_20200824_02_T1 |

| | | | |
|---|---|---|---|
| 1991/9/30 | LT05_L1TP_001071_19910930_20230512_02_T1 | 2010/6/14 | LT05_L1TP_001071_20100614_20200824_02_T1 |
| 1992/5/11 | LT05_L1TP_001071_19920511_20200914_02_T1 | 2010/6/30 | LT05_L1TP_001071_20100630_20200823_02_T1 |
| 1992/5/27 | LT05_L1TP_001071_19920527_20200914_02_T1 | 2010/7/16 | LT05_L1TP_001071_20100716_20200824_02_T1 |
| 1992/6/12 | LT05_L1TP_001071_19920612_20200914_02_T1 | 2010/8/17 | LT05_L1TP_001071_20100817_20200824_02_T1 |
| 1992/7/14 | LT05_L1TP_001071_19920714_20200914_02_T1 | 2010/9/18 | LT05_L1TP_001071_20100918_20200823_02_T1 |
| 1992/7/30 | LT05_L1TP_001071_19920730_20200914_02_T1 | 2010/10/4 | LT05_L1TP_001071_20101004_20200823_02_T1 |
| 1992/10/2 | LT05_L1TP_001071_19921002_20200914_02_T1 | 2010/11/5 | LT05_L1TP_001071_20101105_20200823_02_T1 |
| 1992/11/3 | LT05_L1TP_001071_19921103_20200914_02_T1 | 2011/5/16 | LT05_L1TP_001071_20110516_20200822_02_T1 |
| 1992/12/21 | LT05_L1TP_001071_19921221_20200914_02_T1 | 2011/7/19 | LT05_L1TP_001071_20110719_20200822_02_T1 |
| 1993/4/12 | LT05_L1TP_001071_19930412_20200914_02_T1 | 2011/9/5 | LT05_L1TP_001071_20110905_20200820_02_T1 |
| 1993/5/30 | LT05_L1TP_001071_19930530_20200914_02_T1 | 2011/11/8 | LT05_L1TP_001071_20111108_20200820_02_T1 |
| 1993/6/15 | LT05_L1TP_001071_19930615_20200914_02_T1 | 2013/4/19 | LC08_L1TP_001071_20130419_20200913_02_T1 |
| 1993/7/1 | LT05_L1TP_001071_19930701_20200914_02_T1 | 2013/6/22 | LC08_L1TP_001071_20130622_20200912_02_T1 |
| 1993/8/2 | LT05_L1TP_001071_19930802_20200913_02_T1 | 2013/7/24 | LC08_L1TP_001071_20130724_20200912_02_T1 |
| 1993/9/19 | LT05_L1TP_001071_19930919_20200913_02_T1 | 2013/9/26 | LC08_L1TP_001071_20130926_20200913_02_T1 |
| 1994/5/1 | LT05_L1TP_001071_19940501_20200913_02_T1 | 2014/5/8 | LC08_L1TP_001071_20140508_20200911_02_T1 |
| 1994/5/17 | LT05_L1TP_001071_19940517_20200913_02_T1 | 2014/6/9 | LC08_L1TP_001071_20140609_20200911_02_T1 |
| 1994/6/2 | LT05_L1TP_001071_19940602_20200913_02_T1 | 2014/6/25 | LC08_L1TP_001071_20140625_20200911_02_T1 |
| 1994/7/20 | LT05_L1TP_001071_19940720_20200913_02_T1 | 2014/7/11 | LC08_L1TP_001071_20140711_20200911_02_T1 |
| 1994/11/25 | LT05_L1TP_001071_19941125_20200913_02_T1 | 2014/7/27 | LC08_L1TP_001071_20140727_20200911_02_T1 |
| 1995/6/5 | LT05_L1TP_001071_19950605_20200912_02_T1 | 2014/8/28 | LC08_L1TP_001071_20140828_20200911_02_T1 |
| 1995/6/21 | LT05_L1TP_001071_19950621_20200913_02_T1 | 2015/6/12 | LC08_L1TP_001071_20150612_20201015_02_T1 |
| 1995/7/7 | LT05_L1TP_001071_19950707_20200912_02_T1 | 2015/6/28 | LC08_L1TP_001071_20150628_20200909_02_T1 |
| 1995/7/23 | LT05_L1TP_001071_19950723_20200912_02_T1 | 2015/7/14 | LC08_L1TP_001071_20150714_20200908_02_T1 |
| 1995/8/8 | LT05_L1TP_001071_19950808_20200912_02_T1 | 2015/7/30 | LC08_L1TP_001071_20150730_20200908_02_T1 |
| 1996/4/20 | LT05_L1TP_001071_19960420_20200911_02_T1 | 2015/11/19 | LC08_L1TP_001071_20151119_20200908_02_T1 |
| 1996/5/6 | LT05_L1TP_001071_19960506_20200911_02_T1 | 2016/1/22 | LC08_L1TP_001071_20160122_20200907_02_T1 |
| 1996/5/22 | LT05_L1TP_001071_19960522_20200911_02_T1 | 2016/4/27 | LC08_L1TP_001071_20160427_20200907_02_T1 |
| 1996/7/25 | LT05_L1TP_001071_19960725_20200911_02_T1 | 2016/5/29 | LC08_L1TP_001071_20160529_20200906_02_T1 |
| 1996/8/10 | LT05_L1TP_001071_19960810_20200911_02_T1 | 2016/6/14 | LC08_L1TP_001071_20160614_20200906_02_T1 |
| 1997/5/9 | LT05_L1TP_001071_19970509_20200910_02_T1 | 2016/6/30 | LC08_L1TP_001071_20160630_20200906_02_T1 |
| 1997/5/25 | LT05_L1TP_001071_19970525_20200910_02_T1 | 2016/7/16 | LC08_L1TP_001071_20160716_20200906_02_T1 |
| 1997/6/10 | LT05_L1TP_001071_19970610_20200910_02_T1 | 2016/8/1 | LC08_L1TP_001071_20160801_20200906_02_T1 |
| 1997/7/12 | LT05_L1TP_001071_19970712_20200910_02_T1 | 2016/8/17 | LC08_L1TP_001071_20160817_20200906_02_T1 |
| 1997/8/29 | LT05_L1TP_001071_19970829_20200909_02_T1 | 2016/9/18 | LC08_L1TP_001071_20160918_20200906_02_T1 |
| 1998/5/12 | LT05_L1TP_001071_19980512_20200909_02_T1 | 2017/2/9 | LC08_L1TP_001071_20170209_20200905_02_T1 |
| 1998/6/13 | LT05_L1TP_001071_19980613_20200909_02_T1 | 2017/4/14 | LC08_L1TP_001071_20170414_20200904_02_T1 |
| 1998/7/15 | LT05_L1TP_001071_19980715_20200908_02_T1 | 2017/6/1 | LC08_L1TP_001071_20170601_20200903_02_T1 |
| 1998/7/31 | LT05_L1TP_001071_19980731_20200908_02_T1 | 2017/6/17 | LC08_L1TP_001071_20170617_20200903_02_T1 |

| | | | |
|---|---|---|---|
| 1998/9/17 | LT05_L1TP_001071_19980917_20200908_02_T1 | 2017/7/19 | LC08_L1TP_001071_20170719_20200903_02_T1 |
| 1999/5/15 | LT05_L1TP_001071_19990515_20200908_02_T1 | 2017/8/4 | LC08_L1TP_001071_20170804_20200903_02_T1 |
| 1999/7/2 | LT05_L1TP_001071_19990702_20200907_02_T1 | 2017/8/20 | LC08_L1TP_001071_20170820_20200903_02_T1 |
| 1999/8/19 | LT05_L1TP_001071_19990819_20200907_02_T1 | 2017/11/8 | LC08_L1TP_001071_20171108_20200902_02_T1 |
| 2000/5/1 | LT05_L1TP_001071_20000501_20200907_02_T1 | 2017/11/24 | LC08_L1TP_001071_20171124_20200902_02_T1 |
| 2000/7/4 | LT05_L1TP_001071_20000704_20200907_02_T1 | 2018/4/17 | LC08_L1TP_001071_20180417_20201015_02_T1 |
| 2000/8/5 | LT05_L1TP_001071_20000805_20200906_02_T1 | 2018/5/19 | LC08_L1TP_001071_20180519_20200901_02_T1 |
| 2001/4/18 | LT05_L1TP_001071_20010418_20200906_02_T1 | 2018/6/20 | LC08_L1TP_001071_20180620_20201015_02_T1 |
| 2001/6/5 | LT05_L1TP_001071_20010605_20200906_02_T1 | 2018/7/6 | LC08_L1TP_001071_20180706_20200831_02_T1 |
| 2001/6/21 | LT05_L1TP_001071_20010621_20230211_02_T1 | 2018/7/22 | LC08_L1TP_001071_20180722_20200831_02_T1 |
| 2001/7/23 | LT05_L1TP_001071_20010723_20200906_02_T1 | 2018/8/23 | LC08_L1TP_001071_20180823_20200831_02_T1 |
| 2001/8/24 | LT05_L1TP_001071_20010824_20200905_02_T1 | 2018/9/8 | LC08_L1TP_001071_20180908_20200831_02_T1 |
| 2001/9/9 | LT05_L1TP_001071_20010909_20200905_02_T1 | 2019/6/7 | LC08_L1TP_001071_20190607_20200828_02_T1 |
| 2001/9/25 | LT05_L1TP_001071_20010925_20200905_02_T1 | 2019/6/23 | LC08_L1TP_001071_20190623_20200827_02_T1 |
| 2003/6/27 | LT05_L1TP_001071_20030627_20200905_02_T1 | 2019/7/9 | LC08_L1TP_001071_20190709_20200827_02_T1 |
| 2003/7/13 | LT05_L1TP_001071_20030713_20200904_02_T1 | 2019/7/25 | LC08_L1TP_001071_20190725_20200827_02_T1 |
| 2003/8/14 | LT05_L1TP_001071_20030814_20200904_02_T1 | 2019/8/26 | LC08_L1TP_001071_20190826_20200826_02_T1 |
| 2003/8/30 | LT05_L1TP_001071_20030830_20200904_02_T1 | 2019/9/27 | LC08_L1TP_001071_20190927_20200825_02_T1 |
| 2003/10/17 | LT05_L1TP_001071_20031017_20200904_02_T1 | 2020/5/8 | LC08_L1TP_001071_20200508_20200820_02_T1 |
| 2003/11/18 | LT05_L1TP_001071_20031118_20200904_02_T1 | 2020/5/24 | LC08_L1TP_001071_20200524_20200820_02_T1 |
| 2004/4/26 | LT05_L1TP_001071_20040426_20200903_02_T1 | 2020/6/9 | LC08_L1TP_001071_20200609_20200824_02_T1 |
| 2004/5/12 | LT05_L1TP_001071_20040512_20200903_02_T1 | 2020/6/25 | LC08_L1TP_001071_20200625_20200823_02_T1 |
| 2004/5/28 | LT05_L1TP_001071_20040528_20200903_02_T1 | 2020/7/11 | LC08_L1TP_001071_20200711_20200912_02_T1 |
| 2004/6/13 | LT05_L1TP_001071_20040613_20200903_02_T1 | 2020/7/27 | LC08_L1TP_001071_20200727_20200908_02_T1 |
| 2004/6/29 | LT05_L1TP_001071_20040629_20200903_02_T1 | 2020/8/28 | LC08_L1TP_001071_20200828_20200906_02_T1 |
| 2004/7/15 | LT05_L1TP_001071_20040715_20200903_02_T1 | 2021/5/11 | LC08_L1TP_001071_20210511_20210524_02_T1 |
| 2004/9/17 | LT05_L1TP_001071_20040917_20200903_02_T1 | 2021/6/12 | LC08_L1TP_001071_20210612_20210622_02_T1 |
| 2004/10/3 | LT05_L1TP_001071_20041003_20200903_02_T1 | 2021/7/14 | LC08_L1TP_001071_20210714_20210721_02_T1 |
| 2005/4/29 | LT05_L1TP_001071_20050429_20200902_02_T1 | 2021/7/30 | LC08_L1TP_001071_20210730_20210804_02_T1 |
| 2005/5/15 | LT05_L1TP_001071_20050515_20230211_02_T1 | 2021/8/15 | LC08_L1TP_001071_20210815_20210826_02_T1 |
| 2005/5/31 | LT05_L1TP_001071_20050531_20200902_02_T1 | 2021/8/31 | LC08_L1TP_001071_20210831_20210909_02_T1 |
| 2005/6/16 | LT05_L1TP_001071_20050616_20200902_02_T1 | 2021/10/18 | LC08_L1TP_001071_20211018_20211026_02_T1 |
| 2005/7/2 | LT05_L1TP_001071_20050702_20200902_02_T1 | | |

Table A3 List of Sentinel-2 images used in validation

| **Date of image acquisition** | **Image ID** |
|---|---|
| 2016/4/27 | S2A_MSIL1C_20160427T145722_N0201_R139_T19LEC_20160427T145719 |
| 2016/7/16 | S2A_MSIL1C_20160716T144732_N0204_R139_T19LEC_20160716T145212 |
| 2017/6/1 | S2A_MSIL1C_20170601T144731_N0205_R139_T19LEC_20170601T144737 |
| 2017/8/20 | S2A_MSIL1C_20170820T144731_N0205_R139_T19LEC_20170820T145633 |
| 2017/11/8 | S2A_MSIL1C_20171108T144731_N0206_R139_T19LEC_20171108T181232 |
| 2018/4/17 | S2A_MSIL1C_20180417T144731_N0206_R139_T19LEC_20180417T200318 |
| 2018/7/6 | S2A_MSIL1C_20180706T144731_N0206_R139_T19LEC_20180706T181524 |
| 2020/6/25 | S2A_MSIL1C_20200625T144731_N0209_R139_T19LEC_20200625T181113 |
| 2021/5/11 | S2A_MSIL1C_20210511T144731_N0300_R139_T19LEC_20210512T140023 |
| 2021/7/30 | S2A_MSIL1C_20210730T144731_N0301_R139_T19LEC_20210730T181642 |
| 2021/10/18 | S2A_MSIL1C_20211018T144731_N0301_R139_T19LEC_20211018T181804 |